

# Numerical modelling of the human inner ear: associated pathologies and therapies



Bruno André Faria Areias

Supervisor: Prof. Marco Paulo Lages Parente  
Co-Supervisor: Prof.<sup>a</sup> Maria Fernanda Gentil Costa

Faculty of Engineering of the University of Porto

A thesis submitted for the degree of  
*Doctoral Degree in Mechanical Engineering*

November, 2021





**Numerical modelling of the human  
inner ear: associated pathologies  
and therapies**

Bruno André Faria Areias

Doctoral Degree in Mechanical Engineering

November, 2021



This thesis is dedicated to my family:

mother, father, brother and sister without whom it would be impossible to complete this thesis. Also a special dedication to my girlfriend, Raquel, who supported me during this entire journey.

Thank you!



## Acknowledgements

I would to thank you to all important people who have supported and helped me in this long journey.

First of all, I want to thank God, Who gave me a lot of strength and made me believe that there are no barriers that cannot be overcome.

I am gratefully to my supervisor, Prof. Dr. Marco Paulo Lages Parente for his guidance and encouragement. Thank you for sharing your knowledge about Abaqus. A special thanks to my co-supervisors, Prof.<sup>a</sup> Dra. Maria Fernanda Gentil Costa and Dr. Eurico Fernando Martins Gomes de Almeida for their insightful comments, and strong experience and knowledge in human ear area. My sincere thanks also goes to Prof. Dr. Renato Natal Jorge, Prof. Dr. Carlos António, Prof. Dr. José Rodrigues, Prof. Dr. João Tavares, Prof. Dr. António Augusto Fernandes and Prof.<sup>a</sup> Dra. Luisa Sousa, whom in some way has contributed to this work.

To the University of Porto and to the Institute of science and innovation in mechanical and industrial engineering, I would like to express my gratitude for providing material, logistical and great conditions, which allowed the development of this work.

I acknowledge the financial support provided by the Portuguese

Foundation for Science and Technology through the PhD fellowship SFRH/BD/129397/2017.

To my friends, Gaspar, Rúben and Sérgio, I express my gratitude for their support, patience and unconditional friendship.

I also thank to my LDPS partners, André, Edwin, João, Leonardo, Ana, Maria and Rita not only for the daily support, but also for the daily partnership and the essential distraction from science during lunch and coffee breaks.

Last, but not least, I would like to thank my family, mother, father, brother and sister, without their support and love would not be possible to complete this thesis. I'd like to give special thanks to my girlfriend, Raquel, who is always by my side pushing me further than I thought I could go.

## Abstract

We live in a world of sounds, some of which are essential and some of which are unnecessary noise. Such sounds are produced as a result of a vibrating object. The sound source causes the propagation of sound waves through some elastic medium, such as air, water, or even solids. The sound waves collected by the auricle travel through the external acoustic meatus towards the tympanic membrane, causing its vibration. The vibration of the tympanic membrane sets three ossicles into motion. The last small ossicle that connects the middle ear to the inner ear is responsible for developing the travelling wave inside the cochlea. The Reissner's membrane and the basilar membrane delimits three fluid-filled chambers within the cochlea: scala tympani, scala media, and scala vestibuli. Deflection of the basilar membrane shears the hair bundles of hair cells, that opens the mechanically sensitive ion channels and produces electrical responses in these cells. The cochlear nerve sends these impulses into the brain. Each location along the basilar membrane is associated with the reception of a given frequency, designated by characteristic frequency. This particular arrangement is called tonotopic organization and allows the perception of frequencies between 20Hz and 20kHz.

Hearing loss can be caused by the loss of the hair cells. The loss of these cells in mammals is irreversible which leads to permanent hearing

loss. Noise exposure is one of the main causes of sensorineural hearing loss that affects both the cochlear hair cells and the auditory neurons. However, other disorders like Ménière's disease can also lead to fluctuating sensorineural hearing loss.

Cochlear implants are electronic devices used in auditory rehabilitation of patients with sensory deafness. They restore the missing function of the inner hair cells by converting the acoustic signal into electrical stimuli, which activates the auditory nerve fibers.

This thesis intends to deepen the knowledge about the human ear using the finite element analysis tool, Abaqus. The coiled shape as well as the mechanical properties of the basilar membrane will be studied. The Ménière's disease that alters the functioning of the inner ear will also be discussed. Consequently, within the theme of cochlear implants, the influence of the insertion speed, the friction coefficient between the cochlear wall and the electrode array, and several configurations of the cochlear implant tip will be studied. Finally, three different arrangements in the platinum/iridium wires within the electrode array were investigated.

**Keywords:** cochlea; inner ear; basilar membrane; cochlear implant; hearing loss



## Resumo

Vivemos num mundo de sons, alguns dos quais são considerados essenciais enquanto outros desnecessários. Os sons são produzidos através da vibração dos objetos. Uma fonte sonora dá início à propagação de ondas sonoras num meio elástico tal como por exemplo o ar, água ou mesmo um sólido. Parte das ondas sonoras são captadas pelo pavilhão auditivo e encaminhadas até à membrana timpânica através do canal auditivo externo. O movimento oscilatório da membrana timpânica é então transmitido a três ossículos. O último ossículo conecta o ouvido médio ao ouvido interno e é responsável por gerar uma onda viajante no interior da cóclea. A membrana de Reissner e a membrana basilar delimitam três compartimentos no interior da cóclea: rampa timpânica, rampa média e rampa vestibular. A deflexão da membrana basilar provoca o deslocamento dos estereocílios das células ciliadas, que por sua vez induz a abertura dos canais iónicos mecano-sensíveis desencadeando respostas eléctricas nessas células. O nervo coclear é responsável por transportar esses impulsos eléctricos até ao cérebro onde são reconhecidos como sensações auditivas. Cada ponto ao longo da membrana basilar está associado a uma frequência, designada por frequência característica. Esta particular organização é designada por distribuição tonotópica e permite a percepção de sons com frequências entre 20Hz e 20kHz.

A hipoacusia pode ser causada pela perda das células ciliadas. A perda de tais células em mamíferos é permanente conduzindo assim a uma perda neurosensorial irreversível. A exposição a níveis sonoros elevados é uma das principais causas, afetando tanto as células ciliadas como o nervo auditivo. Contudo, outras doenças como por exemplo a doença de Ménière pode também conduzir à perda auditiva neurosensorial flutuante.

Implantes cocleares são dispositivos eletrônicos capazes de recuperar a capacidade auditiva. Estes dispositivos convertem o sinal acústico em sinal elétrico com a finalidade de estimular as fibras do nervo auditivo.

Esta dissertação pretende assim aprofundar o conhecimento sobre o ouvido humano utilizando a ferramenta de elementos finitos, Abaqus. A forma enrolada da cóclea assim como as propriedades mecânicas da membrana basilar serão tema do estudo. O estudo das alterações provocadas pela doença de Ménière no ouvido interno permitirão uma detecção antecipada da doença. Por conseguinte, dentro do tema dos implantes cocleares, a influência da velocidade de inserção, do coeficiente de atrito entre a parede coclear e o eletrodo, e de várias configurações da ponta do implante coclear serão abordadas. Por fim, três tipos de arranjos nos fios de platina/irídio no interior do eletrodo foram analisados.

**Palavras chave:** cóclea; ouvido interno; membrana basilar; implante coclear; perda auditiva

## Nomenclature

### Abbreviations

3D - Three dimensional

AAO-HNS - American academy of otolaryngology-head and neck surgery

ABR - Auditory brainstem response

BM - Basilar membrane

DPOAE - Distortion product otoacoustic emission

EABR - Electrically evoked auditory brainstem response

EOAE - Evoked otoacoustic emission

FE - Finite element

FEM - Finite element model

MAE - Mean absolute error

MRI - Magnetic resonance imaging

PEEK - Equivalent plastic strain

RMSE - Root mean-square error

SD - Standard deviation

SFOAE - Stimulus frequency otoacoustic emission

SOAE - Spontaneous otoacoustic emission

SPL - Sound pressure level

SSNHL - Sudden sensorineural hearing loss

TEOAE - Transient evoked otoacoustic emission

## Symbols

$\rho$	density
$E$	Young's modulus
$\nu$	Poisson's ratio
$G$	shear modulus
$C$	Rayleigh damping matrix
$\alpha, C_m$	mass proportional Rayleigh damping coefficient
$\beta, C_k$	stiffness proportional Rayleigh damping coefficient
$\mathbf{K}$	bulk modulus
$M$	mass matrix
$K$	stiffness matrix
$\Omega$	circular frequency
$u$	complex displacement
$\dot{u}$	velocity
$\ddot{u}$	acceleration
$P$	complex force
$p$	pressure
$x$	specific distance
$t$	time
$i$	increment
$I$	internal force vector
$\boldsymbol{\sigma}$	total stress
$S_{vM}$	von Mises stress
$\mathbf{D}$	elasticity tensor
$\boldsymbol{\varepsilon}$	total elastic strain
$\varepsilon_v$	volumetric strain
$\tau_{crit}$	critical shear stress
$\mu$	friction coefficient
$\sigma_{pl}$	plastic stress
$\varepsilon_{pl}$	plastic strain
$L_{min}$	smallest element dimension
$c_d$	dilatational wave speed
Ca	calcium
K	potassium

# Contents

<b>Acknowledgements</b>	<b>vii</b>
<b>Abstract</b>	<b>ix</b>
<b>Resumo</b>	<b>xi</b>
<b>Nomenclature</b>	<b>xiii</b>
Abbreviations . . . . .	xiii
Symbols . . . . .	xiv
<b>List of Figures</b>	<b>xxviii</b>
<b>List of Tables</b>	<b>xxv</b>
<b>1 Thesis Report</b>	<b>1</b>
1.1 Introduction . . . . .	3
1.1.1 The anatomy and physiology of the cochlea . . . . .	5
1.1.2 Passive cochlea . . . . .	9
1.1.3 Active cochlea . . . . .	10
1.1.4 Hair-cell mechanotransduction . . . . .	12
1.1.5 Otoacoustic emissions . . . . .	16
1.1.6 Auditory Brainstem Response . . . . .	18
	xv

1.1.7	Hearing disorders and pathologies . . . . .	21
1.1.8	Therapy . . . . .	25
1.2	Motivation and aim . . . . .	27
1.3	Thesis structure . . . . .	30
1.4	Scientific contribution . . . . .	31
1.4.1	Journal Articles and Book Chapters . . . . .	31
1.4.2	International Conference Presentations . . . . .	32
1.4.3	National Conference Presentations . . . . .	32
1.5	References . . . . .	34
<b>2</b>	<b>Influence of the basilar membrane shape and mechanical properties in the cochlear response: a numerical study</b>	<b>43</b>
2.1	Abstract . . . . .	47
2.2	Keywords . . . . .	47
2.3	Introduction . . . . .	48
2.4	Materials and Methods . . . . .	51
2.5	Results . . . . .	57
2.6	Conclusions . . . . .	64
2.7	Conflict of interest statement . . . . .	64
2.8	Acknowledgements . . . . .	65
2.9	References . . . . .	66
<b>3</b>	<b>A finite element model to predict the consequences of endolymphatic hydrops in the basilar membrane</b>	<b>73</b>
3.1	Abstract . . . . .	77

3.2	Keywords . . . . .	77
3.3	Introduction . . . . .	78
3.4	Materials and Methods . . . . .	81
3.5	Results . . . . .	87
3.6	Conclusions . . . . .	94
3.7	Conflict of interest statement . . . . .	97
3.8	Acknowledgements . . . . .	97
3.9	References . . . . .	98
<b>4</b>	<b>Finite element modelling of the surgical procedure for placement of a straight electrode array: mechanical and clinical consequences</b>	<b>105</b>
4.1	Abstract . . . . .	109
4.2	Keywords . . . . .	109
4.3	Introduction . . . . .	110
4.4	Materials and Methods . . . . .	115
4.5	Results . . . . .	118
4.6	Conclusions . . . . .	127
4.7	Conflict of interest statement . . . . .	129
4.8	Acknowledgements . . . . .	129
4.9	References . . . . .	130
<b>5</b>	<b>Insertion of a cochlear straight electrode array with different wires arrangements: a numerical study</b>	<b>137</b>
5.1	Abstract . . . . .	141
5.2	Keywords . . . . .	141

5.3	Introduction . . . . .	142
5.4	Materials and Methods . . . . .	143
5.5	Results . . . . .	147
5.6	Conclusions . . . . .	151
5.7	Conflict of interest statement . . . . .	152
5.8	Acknowledgements . . . . .	152
5.9	References . . . . .	153
<b>6</b>	<b>Thesis considerations</b>	<b>155</b>
6.1	Conclusions . . . . .	157
6.2	Future works . . . . .	158
	<b>Appendix A</b>	<b>161</b>
6.3	Permission 1 . . . . .	163
6.4	Permission 2 . . . . .	165
6.5	Permission 3 . . . . .	167
6.6	Permission 4 . . . . .	169



## List of Figures

1.1	The three parts of the human ear, adapted from [2]. . . . .	3
1.2	Traveling wave. Cochlea is represented as uncoiled. Adapted from [2].	5
1.3	Thresholds of the human hearing in decibels. Thresholds are based on the Handbook of Psychology, Experimental Psychology [6]. . . . .	6
1.4	Inner ear scalae (left); Scala media and organ of Corti (right). Adapt- ed from [8]. . . . .	7
1.5	Schematic model of the organ of Corti. Adapted from [2]. . . . .	9
1.6	Two mechanisms of force production on the outer hair cells. Adapted from [21]. . . . .	11
1.7	Schematic motion of the stereocilia. . . . .	13
1.8	Potential differences inside the cochlear partition. Adapted from [29].	14
1.9	A normal ABR waveform using a click stimulus. The stimulus was ap- plied at 0 ms. Adapted from Kramer and Brown [38]. . . . .	18
1.10	Electrically evoked auditory brainstem response reported from a child who was 3 years of age at the time of implant activation. EABR records were performed at 1 year, 6 months, 3 months and 1 day after implantation. Adapted from [47]. . . . .	20
1.11	Development of endolymphatic hydrops. . . . .	23

1.12	Electrode array types. . . . .	26
1.13	Prevalence of disabling hearing loss among regions, in 2018, adapted from the World Health Organization [66]. . . . .	28
1.14	Projections of number of people with disabling hearing loss among regions, adapted from the World Health Organization [66]. . . . .	29
2.1	Representation of the straight model (A), the spiral model (B), the basilar membrane of the straight model (C) and the basilar membrane of the spiral model (D). . . . .	52
2.2	Place of the maximum response on the basilar membrane vs frequency.	57
2.3	Basilar membrane displacement between the straight and isotropic model, and the spiral and transversely isotropic model for three frequencies (7713 Hz (A, D); 1847 Hz (B, E); 349 Hz (C, F)) and an 80 dB SPL. . . . .	60
2.4	Magnitude of the displacement of the basilar membrane at 12 mm from the stapes normalized with respect to the stapes displacement. . . . .	61
2.5	Phase of the displacement of the basilar membrane at 12 mm from the stapes normalized with respect to the stapes displacement. . . . .	62
2.6	Magnitude of the displacement of the basilar membrane at 12 mm from the stapes using 0.1 nm as reference. . . . .	63
3.1	Anatomy of the human inner ear, adapted from Neuroscience by Purves [4]. . . . .	78
3.2	3D finite model of the inner ear. Red arrows show the location and direction of the static and dynamic pressure. Finite element mesh	

characterization of all parts. . . . .	82
3.3 3D finite model of the inner ear. Detail of the scala vestibuli, the scala tympani, and the helicotrema. . . . .	83
3.4 Comparison and validation of the magnitude and phase of basilar membrane velocity relative to stapes footplate velocity with experimental results at 12 mm from the round window. . . . .	87
3.5 Cochlear map validation and comparison with different endolym- phatic hydrops stages. . . . .	88
3.6 Magnitude of the basilar membrane displacement at 600Hz, 1000Hz and 7000Hz for normal condition and two endolymphatic hydrops stages. . . . .	90
3.7 Magnitude and phase of the basilar membrane displacement at 19 mm from the apex of the cochlea. Basilar membrane illustrations correspond to the FE model normal, the displacement was amplified. . . . .	91
3.8 Magnitude and phase of the basilar membrane displacement at 15 mm from the apex of the cochlea. . . . .	92
3.9 Magnitude and phase of the basilar membrane displacement at 7 mm from the apex of the cochlea. . . . .	93
3.10 Maximum displacement of the basilar membrane imposed by the static pressure. . . . .	94
4.1 Position and orientation of the inner ear. . . . .	110
4.2 Illustration of the cochlear implant position with external and inter- nal part, adapted from Kral [7]. . . . .	111
4.3 Finite element model of the CI622 cochlear implant and the cochlear	

wall. Demonstration of the electrode tip length. . . . .	115
4.4 Relation between the insertion depth in millimetres vs in degrees ( $v_{\text{insertion}}=1 \text{ mm s}^{-1}$ , without friction). . . . .	119
4.5 Mean electrode tip contact pressure during the insertion of 25 mm, for different insertion speeds (0.25, 0.5, 1 and $2 \text{ mm s}^{-1}$ ). . . . .	120
4.6 Insertion force during the insertion of 25 mm, for different insertion speeds (0.25, 0.5, 1 and $2 \text{ mm s}^{-1}$ ). Experimental data reported from Nguyen et al. [36] and Avci et al. [37] included in order to validate the model. . . . .	121
4.7 Influence of the friction coefficient between the cochlear implant and the scala tympani walls on the maximum von Mises stress ( $S_{vM}$ ) present on the cochlear implant, for different insertion depths. . . . .	123
4.8 Mean electrode tip contact pressure during the insertion of 25 mm, for different friction coefficients (0, 0.05, 0.1, 0.2 and 0.3). . . . .	124
4.9 Insertion force during the insertion of 25 mm, for different friction coefficients (0, 0.05, 0.1, 0.2 and 0.3). . . . .	125
4.10 Mean electrode tip contact pressure during the electrode insertion, for different tip mechanical properties (Table 4.2). . . . .	126
4.11 Insertion force during the electrode insertion, for different tip mechanical properties (Table 4.2). . . . .	127
5.1 Bony labyrinth with the electrode array (left), Three different wires configurations, with the silicone partially removed (right). . . . .	144
5.2 Dimensions of the three different electrode arrays configurations. . . . .	146
5.3 Insertion force vs insertion depth among the different wires	

configurations. . . . .	147
5.4 Steps during an electrode array insertion for the helix p0.5 configuration: (a) 0mm, (b) 5mm, (c) 10mm, (d) 15mm, (e) 20mm, (f) 25mm. . . . .	148
5.5 Mean contact pressure at the electrode array tip during the cochlear implantation among the different wires configurations. . . . .	149
5.6 Mean contact pressure in the proximal and distal portion of the electrode array during the cochlear implantation among the different wires configurations. . . . .	150
5.7 Mean equivalent plastic strain (PEEK) in the implant wires during the cochlear implantation among the different wires configurations. . . . .	151
5.8 Incidence rate of the location of the maximum PEEK in the implant wires during the cochlear implantation among the different wires configurations. . . . .	151



## List of Tables

2.1	Isotropic and transversely isotropic mechanical properties of the basilar membrane . . . . .	53
2.2	Rayleigh damping property of the basilar membrane . . . . .	55
2.3	Mechanical properties of the bony structures and soft tissues . . . . .	56
2.4	Values of RMSE and MAE for three different frequency ranges: 20 Hz - 20 kHz, 20 Hz - 1 kHz and 1 kHz - 20 kHz . . . . .	59
3.1	Mechanical properties of the inner ear parts (Young's modulus, Poisson's ratio and density) . . . . .	85
4.1	Mechanical properties of the inner ear parts . . . . .	117
4.2	Mechanical properties used, for different tip lengths . . . . .	118
5.1	Cochlear implant's mechanical properties . . . . .	145
5.2	Mesh description of the electrode array . . . . .	146





# Chapter 1

## Thesis Report



## 1.1 Introduction

Hearing is a key function that supports the communication among individuals. It promotes the development of spoken language. The human ear consists in three main parts: the external ear, the middle ear, and the internal ear (see Figure 1.1). The external and middle ear structures are responsible for the sound conduction, whereas the internal ear is responsible for the sound interpretation and equilibrium [1].

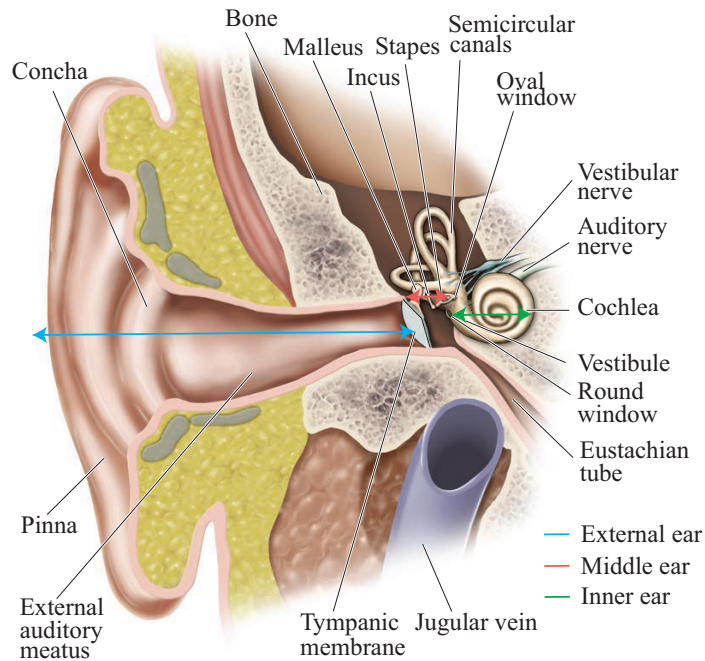


Figure 1.1: The three parts of the human ear, adapted from [2].

The sound waves are collected by the pinna and transmitted through the external acoustic meatus to the tympanic membrane. The tympanic membrane converts the sound waves into solid vibrations and transmits them to the stapes, through the malleus and incus. Finally, the inward and outward movement of the stapes footplate develops a pressure wave on the fluid inside the cochlea and consequently the vibration of the basilar membrane (BM).

The function of the middle ear is to convert the sound waves captured at the pinna into pressure waves in the fluid of the cochlea. Two small muscles, the tensor tympani and the stapedius, located within the middle ear have the function of protecting the ear from being activated in the presence of loud sounds, in the low frequency range [3].

The cochlea is the location where the acoustic energy (pressure waves) is transformed into neural signals. This structure acts as a mechanical frequency analyser (see Figure 1.2), decomposing a complex sound wave into simple elements or pure frequencies. The cochlea is a spiral-shaped structure, similar to a snail shell. It measures  $\approx 10$  mm wide. When uncoiled, it forms a tube with a length of approximately 35 mm [2].

Humans with normal hearing, are able to detect sounds with frequencies between 20 Hz (which induces a displacement of the BM  $\approx 1$  nm [4]) and 20 kHz. The upper limit tends to decrease with age (also known as presbycusis). Such decrease leads to high-frequency hearing loss, which frequently has a major adverse effect on communication, particularly in noisy and/or reverberant listening environments, as mentioned by Huang et al. [5].

As can be seen in Figure 1.3, the dynamic range of human hearing is approximately 130 dB SPL (Sound pressure level) at medium frequencies. A human is able to hear sounds up to  $20 \mu\text{Pa}$  or 0 dB SPL. This pressure deviation leads to an amplitude of motion at the tympanic membrane equal to approximately the diameter of a hydrogen atom [6].

### 1.1.1 The anatomy and physiology of the cochlea

The pressure wave developed at the cochlear cavity is known as the travelling wave. It propagates from the base toward the apex of the BM. It grows in amplitude and slows in velocity until a point of maximum displacement is reached. The maximum amplitude varies directly with the frequency of stimulation. The higher frequencies are caught at the base, whereas lower frequencies are perceived at the apex, as can be seen in Figure 1.2. This pressure wave is relieved by the round window, a membrane that separates the scala tympani from the middle ear cavity. This membrane presents a significant importance due to the incompressibility of the fluids inside the cochlea.

There are three fluid-filled chambers inside the cochlear structure, termed the

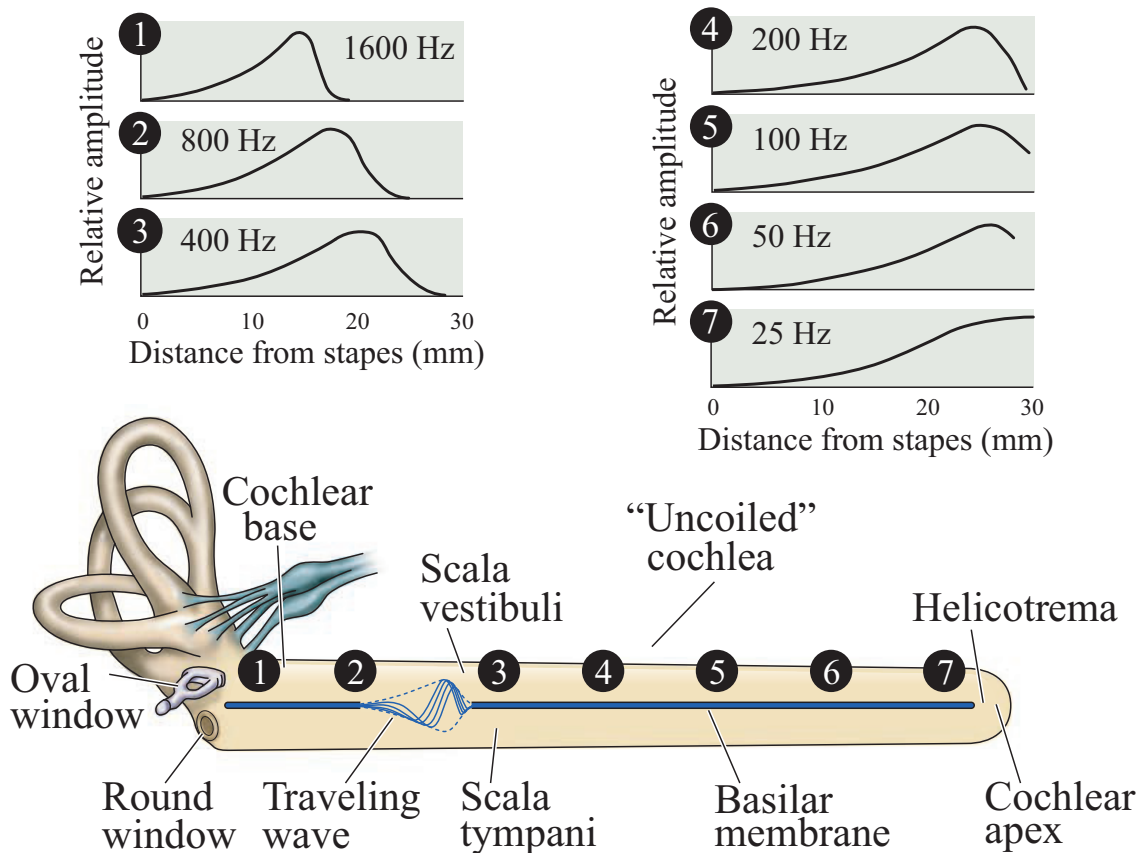


Figure 1.2: Traveling wave. Cochlea is represented as uncoiled. Adapted from [2].

scala vestibuli, the scala media and the scala tympani (see Figure 1.4). The scala media lies between the scala vestibuli and scala tympani, and contains endolymph. This fluid is rich in potassium and poor in sodium. This scala does not provide any direct connection with the other two scalae. On the other hand, a connection called the helicotrema positioned at the cochlear apex allows the flow of perilymph between the scala tympani and scala vestibuli [7]. Perilymph is a fluid with high sodium and low potassium concentrations resembling extracellular fluid.

An extremely thin membrane, called Reissner's membrane separates the scala vestibuli from the scala media. This membrane extends from the spiral lamina to the outer wall of the cochlea. It consists of two thin layers of cells. The layer seen on the scala media side is derived from otocyst and it is therefore ectodermal in origin.

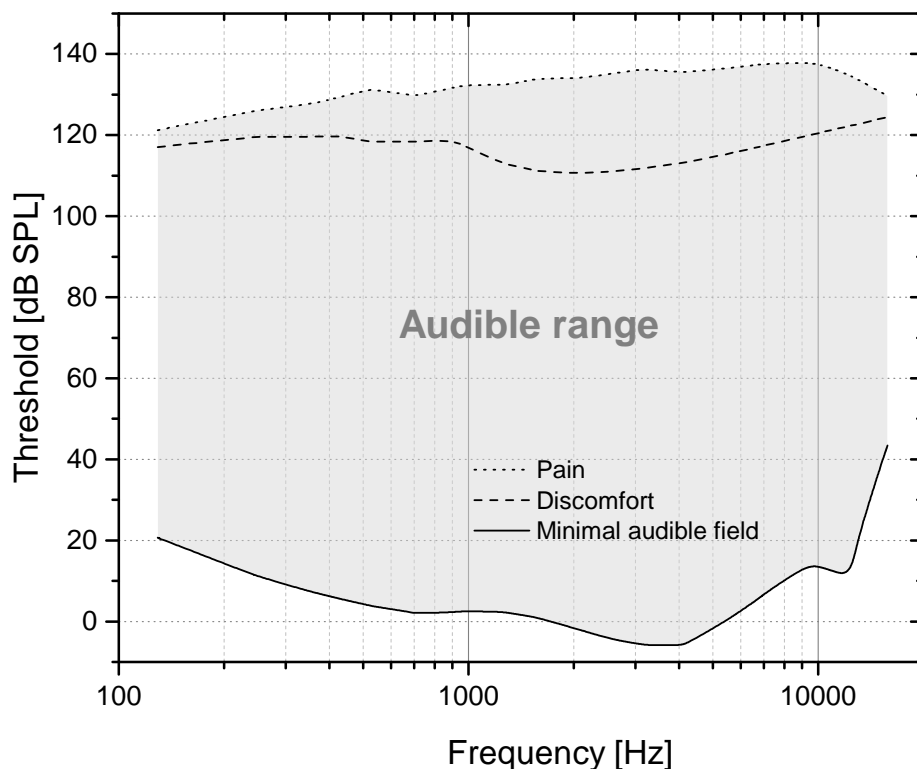


Figure 1.3: Thresholds of the human hearing in decibels. Thresholds are based on the Handbook of Psychology, Experimental Psychology [6].

The outer layer seen from the scala vestibuli side is mesodermal in origin, the cells are large, flat and elongated, as stated in Ear, Nose and Throat Histopathology [8]. The Reissner's membrane provides the electrical insulation required to sustain the endocochlear potential. However, its displacement does not ensure a physiological function [9].

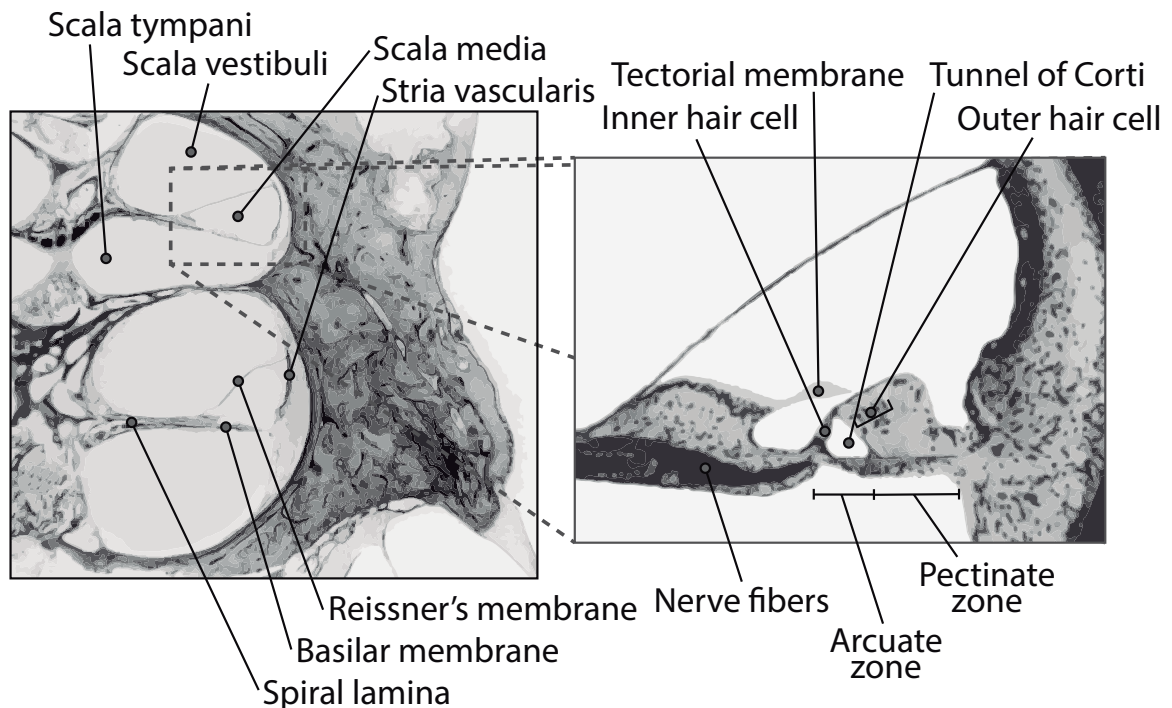


Figure 1.4: Inner ear scalae (left); Scala media and organ of Corti (right). Adapted from [8].

On the other hand, the BM separates the scala media from the scala tympani. The gradual variation of the mechanical properties leads to a rapid movement at higher frequencies near the base and slow movements at lower frequencies near the apex. The width of the BM varies along the cochlear duct, it is narrower at the base and larger at the apical end. The width at the base is approximately  $100\ \mu\text{m}$  and approaches  $500\ \mu\text{m}$  near the apex. Therefore, a higher stiffness is expected at the base, when compared with the apex, with the stiffness varying by approximately two

orders of magnitude, as stated in the book *Biomedical Engineering Fundamentals* [10]. The thickness of the BM varies along its length. This membrane shows a progressive increase from the base to the apex. Such increase is due to the increase in the population of mesothelial cells as stated in the book, *The cochlea* [11].

Since the mechanical properties of the BM change along the cochlea, every point of the BM exhibits a resonant frequency which decreases from base to apex, as mentioned by Reichenbach et al. [12]. The radial collagen fibers soaked in the BM are thick and short near the base, thus conferring a higher stiffness. Such fibers become progressively longer, thinner, and more compliant towards the apex [9]. In accordance with the work of Emadi et al. [13], the stiffness decays exponentially with the longitudinal distance from the base of the cochlea.

The radial direction of the BM is divided into two zones: the arcuate zone and the pectinate zone. The arcuate zone extends from the spiral lamina to the foot of the outer pillar cell, the remaining portion up to the basilar crest of the spiral ligament is known as pectinate zone. The inner zone of the spiral lamina is designated by osseous spiral lamina and consists of thin bone trabeculae [14].

The organ of Corti consists in supporting cells and mechanosensory hair cells (see Figure 1.5). Two mechanosensory hair cells lie at the organ of Corti, the inner and the outer hair cells. Both hair cells have elongated actin-based villi, called hair bundle, emerging from their apical surface [15]. Each hair bundle contains from 30 to a few hundred stereocilia.

Five different types of supporting cells are aligned in rows along the organ of Corti: Hensen's cells, Deiters' cells, pillar cells, inner phalangeal cells, and inner border cells (see Figure 1.5). Each supporting cell has a specific morphology. Hensen's cells



are cuboidal or slightly oblong. Inner phalangeal cells and inner border cells are columnar. The Deiters' and pillar cells are architecturally exquisite cells, with a strong cytoskeleton, elongated processes, and large structural demands [16].

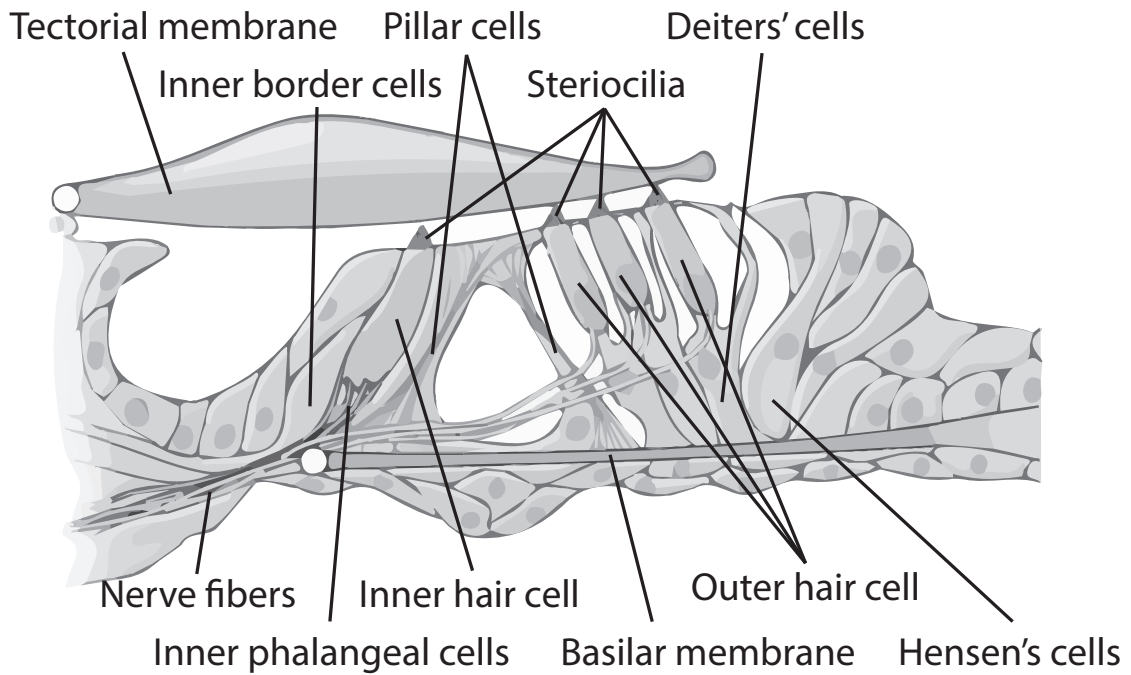


Figure 1.5: Schematic model of the organ of Corti. Adapted from [2].

### 1.1.2 Passive cochlea

The inner hair cells are aligned in a single row on the modiolar side of the organ of Corti, making a total between 3000 and 4000 in a human inner ear. The hair bundles of inner hair cells are arranged in a linear shape which maximize drag and their sensitivity to radial fluid velocity as mentioned by Ciganović et al. [17]. Inner hair cells present a flask-like shape and are around  $30\ \mu\text{m}$  of length [9]. The stereocilia of the inner hair cells are not in contact with the tectorial membrane, thus their response arise from the fluid velocity over their stereocilia rather than direct displacement [10]. They are known as the true hair cells, since they are responsible for the transduction of

acoustic signals into neural signals. Approximately 95 % of the fibers of the auditory nerve that project to the brain arise from the inner hair cells as stated in the book, Neuroscience [2].

### 1.1.3 Active cochlea

In contrast to the inner hair cells, approximately 5 % of all auditory nerve fibers innervate the outer hair cells. However, there are at least three times more outer hair cells than inner hair cells. Unlike inner hair cells, the outer hair cells have primarily efferent innervation [18]. These hair cells have a cylindrical shape with lengths ranging between 20  $\mu\text{m}$  at the cochlear base and 80  $\mu\text{m}$  at the apex [9]. The function of the efferent innervation in auditory system has been a matter of considerable debate. As mentioned by Smith et al. [19], the most frequent functions associated with the efferent innervation from the medial olivocochlear tracts are the protection of the cochlea from traumatic damage (e.g. loud sounds) and aiding in the detection of signals in noise. The medial olivocochlear system also plays a key role in auditory selective attention, suppressing the response to a neglected or discarded stimuli [19]. When the outer hair cells are damaged, even with the inner hair cells appearing unaffected, cochlear sensitivity is significantly reduced, with the frequency selectivity also being reduced. As a result, the input-output curves show a more linear characteristic in the region of the outer hair cell damage [7].

The outer hair cells play an essential role in the active mechanics of the cochlea. On the experimental work of Brownell et al. [20], an electrical stimulation of an isolated outer hair cell produced lengthening or shortening. The active process is a hallmark of the cochlea by its amplification, frequency tuning, compressive nonlinearity, and spontaneous otoacoustic emission, as mentioned by Tobias et al. [9]. Two mechanisms

characterize the active process of the cochlea: outer hair cell somatic motility and active hair bundle mechanics (see Figure 1.6).

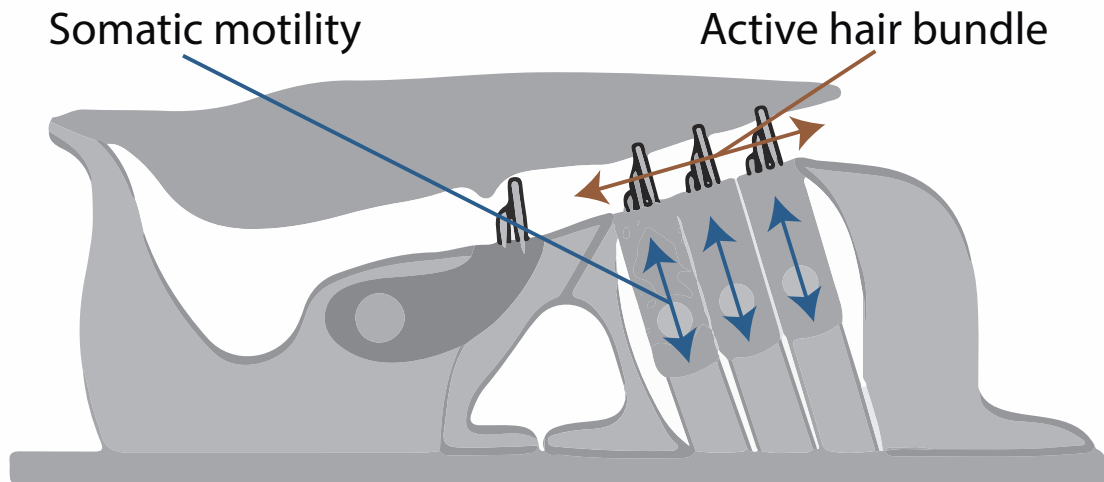


Figure 1.6: Two mechanisms of force production on the outer hair cells. Adapted from [21].

Outer hair cells elongate when depolarized, and shorten when hyperpolarized, in a nonlinear way [22, 9]. This mechanism is known as somatic motility. Prestin is a protein that is essential to sensitive hearing in mammals present in the outer hair cells. This protein shows voltage-dependent charge movement and motility [23]. As stated by Liberman et al. [24], in a mutant mice with absence of prestin, cochlear sensitivity is decreased in a frequency-dependent way. The reduction obtained by the authors was about 40 dB at 5.6 kHz to more than 60 dB at 22.6 kHz. In the mammalian auditory system there are three rows of outer hair cells located in the cochlea. Based on the work of Murakoshi et al. [25] the displacement of the BM is significantly affected even with a single row of outer hair cells damaged. The findings

of their study suggest that all three rows of outer hair cells are required for efficient cochlear amplification.

Another mechanism of force generation by outer hair cells is active hair bundle movement. Yi et al. [26] demonstrate that mammalian outer hair cells show a clear hair-bundle motion which dependent on outer hair cells somatic motility. As stated by the same author the hair-bundle motion may boost the motion of the inner hair cells stereocilia through the radial motion of the tectorial membrane.

#### 1.1.4 Hair-cell mechanotransduction

The stereocilia are organized at the top of each hair cell. They are simple and contains a core of parallel actin filaments in their structure. Each stereocilium tapers at their proximal end where they embed into the cuticular plate, forming a hinge about which each stereocilium pivots [2]. In mammalian cochlea, the tallest stereocilia in each outer hair cell are directly attached to the gelatinous tectorial membrane, so stimulation delivers force across the entire hair bundle.

The most important connections between the stereocilia are the tip links (see Figure 1.7), consists in fine protein filaments. Such links join each stereocilium to the longest adjacent process providing directional sensitivity. Each tip link contains four cadherin molecules. These molecules are members of a large family of proteins responsible for intercellular adhesion as stated by Tobias et al. [9]. Evoke hair bundle motions are on the order of  $\pm 30$  nm or less [9].

When the stereocilia are deflected positively or toward to highest stereocilium, the tension on the tip links increases, leading to a change on the conformation of mechano-electrical transducer channels with high open probability. The cations ( $K^+$  and  $Ca^{2+}$ ) flux into hair cells through the mechano-electrical transducer channels

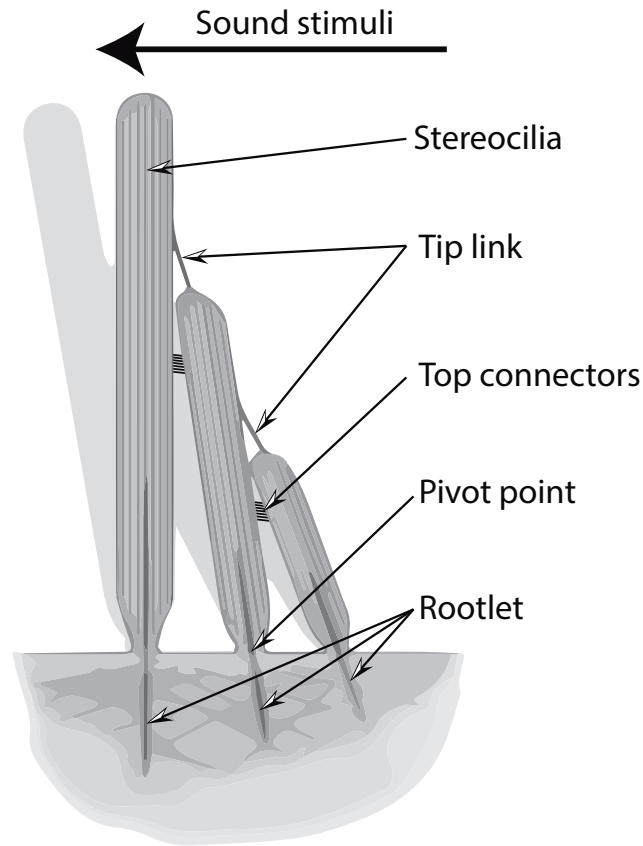


Figure 1.7: Schematic motion of the stereocilia.

causes a membrane depolarization. Such flux is driven by the potential difference and ion concentration difference. As mentioned by Fettiplace et al. [27], the probability of opening is influenced by hair bundle displacement over a maximal excursion of 100 and 200 nm. Such displacement is smaller than the diameter of a stereocilium.

The fluid inside the scala media, endolymph, contains  $\approx 150 \text{ mM K}^+$ ,  $2 \text{ mM Na}^+$ , and  $20 \mu\text{M Ca}^{2+}$ , exhibiting a positive potential of  $+80 \text{ mV}$  relatively to either blood plasma or perilymph. Such potential difference is essential for audition [28].

Figure 1.8 shows the potentials differences inside the cochlear partition at 15 mm from the stapes footplate. The experimental work was conducted by Békèsy [29] in 1952. An electrode was placed in the scala vestibuli and inserted up to the scala tympani. A potential difference of  $-20 \text{ mV}$  during the Reissner's membrane

perforation was achieved. When the electrode reached the endolymph at the scala media the potential difference jumped suddenly to a positive value of  $\approx +50$  mV.

This value remained constant within the whole endolymphatic place. During the penetration of the organ of Corti the potential difference was negative and  $\approx -40$  mV. The potential differences obtained drop slowly during oxygen deprivation or with death as mentioned by Békèsy [29].

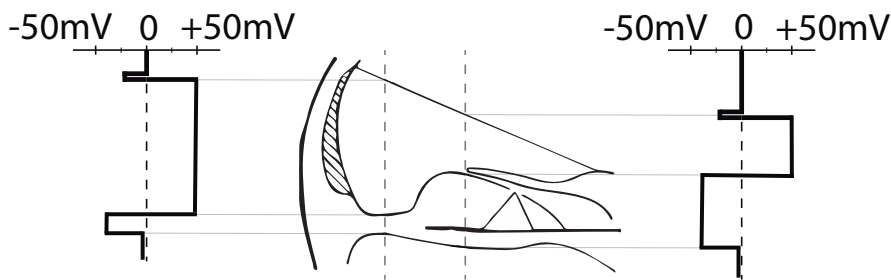


Figure 1.8: Potential differences inside the cochlear partition. Adapted from [29].

The potential difference between the endolymph relative to the perilymph of the tympanic scala near the round window was relatively higher in the order of  $+80$  mV. At this place, the cells presented a potential of  $-40$  mV with regard to the perilymph. The stria vascularis and the spiral ligament showed a negative potential and did not show any potential difference, respectively.

The depolarization triggers different function at the hair cells. In the inner hair cells, the depolarization results from the influx of calcium which consequently leads to the release of neurotransmitters at the base of the hair cell, thus resulting in the firing of neural impulses at the auditory nerve. On the other hand, depolarization and hyperpolarization in the outer hair cell leads to a change of the internal potential that results in the change of the cell length [30].

All sensory systems exhibit adaptation. This adaptation represents the decline in

sensory response to a steady or unchanging stimulus. There are currently two types of hair cell adaptation: fast and slow adaptation. The fast adaptation presents a time constant of a few milliseconds or less in mammals, whereas the slow has a time constant of a few tens of milliseconds.

The fast adaptation is associated by a rapid movement of the hair bundle in the opposite direction of the stimulus. It is believed that the direct re-closure of the mechano-electrical transducer channels is partially dependent on the action of  $\text{Ca}^{2+}$  ions. Slow adaptation also closes the mechano-electrical transduction channels, but on a different mechanism than fast adaptation.

Slow adaptation enforces the hair bundle to move in the direction of the stimulus, thus affecting the mechano-electrical transducer channels' open probability via tip-link tension. This tension is regulated by myosin motors which are attached to the upper end of the tip link, thus controlling the tension in the gating spring, as mentioned by Gianoli et al. [31] and Gillespie et al. [32].

The ion composition of the fluid inside the cochlea is maintained by epithelial ion transport. Impaired homeostatic leads to swelling or collapse of the Reissner's membrane. As example, fluctuation of potassium, K, in endolymph composition by a tear in Reissner's membrane, by drug action or by genetic causes lead to the degeneration of the hair cells with subsequent destruction of the synapsing afferent auditory nerve as stated by Vetter et al. [33]. K is maintained by the stria vascularis at the lateral wall of the cochlea. This ion enters in the hair cells through mechano-electrical transducer channels at the stereocilia and leaves the hair cell across their basolateral membranes via  $\text{K}^+$  selective ions channel. The concentration of K in the extracellular fluid come back to the spiral ligament by diffusion. This cycle is

then repeated, recycling and keeping the  $K$  constant at the scala media [34].

### 1.1.5 Otoacoustic emissions

As a result of the active process, the inner ear produces otoacoustic emissions. These signals can be measured with a sensitive microphone positioned in the external acoustic meatus. The cochlea is responsible for generating such sounds and in some way propagate them back to the middle ear and subsequently to the external acoustic meatus [9]. When the active process is impaired, vibrations of the BM at low and moderate sound intensities are affected and not interpreted. Thus, a higher stimulus is required to reach the threshold of excitation of the inner hair cells [35].

Some studies have demonstrated that evoked otoacoustic emissions are useful for determining the degree of sensorineural hearing loss. This measurement allows to evaluate the cochlear function in infants, toddlers, and other difficult-to-test patients. The outcome enables to monitor the healthiness of outer hair cells, evaluating the status of the cochlear efferent system and thus sections of the central auditory nervous system. More directly, identifying an apparent hearing loss in the absence of clinical or audiological evidence, also termed pseudohypacusis [35].

The normal human cochlea produces both spontaneously and evoked (in response to acoustic stimuli) otoacoustic emissions [36, 35]. The otoacoustic emissions are classified in two general types: spontaneous (SOAEs) and evoked otoacoustic emissions (EOAE). There are three subtypes of evoked otoacoustic emissions. The stimulus frequency otoacoustic emissions elicited by a single pure tone (SFOAEs), the transient evoked otoacoustic emissions (TEOAEs) using a click or toneburst stimulus, and the evoked using a pair of pure tones presented simultaneously and related in frequency, distortion product otoacoustic emissions (DPOAEs) [35].



Usually in humans, SOAEs appear without any source sound at a few frequencies in a healthy cochlea and seem to be a consequence of the cellular force generation by the outer hair cells, as mentioned in the book *Active Processes and Otoacoustic Emissions in Hearing* [37]. In SFOAE, a single-tone stimulus is applied. Separation of the SFOAE from the single-tone stimulus is obtained by scaled vector subtraction linked to stimulus-level manipulations or through the introduction of a second suppressor tone with different frequency. TEOAEs occur with a short duration stimulus (less than 3 ms) applied repetitively. The TEOAEs is dependent from the stimulus used. Due to recording restrictions, this method is limited to frequencies between 1000 and 4000 Hz [38]. Usually, the separation from the stimulus and the ear-canal-plus-middle-ear acoustic responses is achieved by time gating and/or waveform subtractions [35]. The DPOAEs, use two stimulus tones ( $f_1$  and  $f_2$ ) normally less than a half octave apart. The measurement is focused on the distortion product frequency ( $2f_1 - f_2$ ). This method measures the response during cochlear activation. Through the changing of the two primary tones (maintaining the ratio between  $f_2$  and  $f_1$  equal to 1.22), distortion products can be generated from different regions of the cochlea. As stated by Harris et al. [39] the DPOAE amplitude is systematically reduced when the ratio between  $f_2$  and  $f_1$  is increased or decreased. As with TEOAEs, the DPOAEs are also affected by the middle ear condition, thus conductive hearing loss should be negligible when DPOAEs are absent. If the TEOAEs or DPOAEs are present in a patient with moderate or profound sensorineural hearing loss, then the cause of the hearing impairment can arise from the neural portions of the auditory system [38].

### 1.1.6 Auditory Brainstem Response

The Auditory Brainstem Response (ABR) is a non invasive measurement. It consists of a sequence of up to seven vertex positive waves with negative valleys between them (see Figure 1.9). Each positive wave results from different section of the brainstem. As mentioned in the Handbook of clinical neurology [40], approximately 0.8 ms or one synaptic delay separates each peak from one another. This method not only measures the functioning of the cochlea but also the lower auditory pathways. The electric potentials are collected from subcutaneous or through surface electrodes located behind the ear and the vertex of the head.

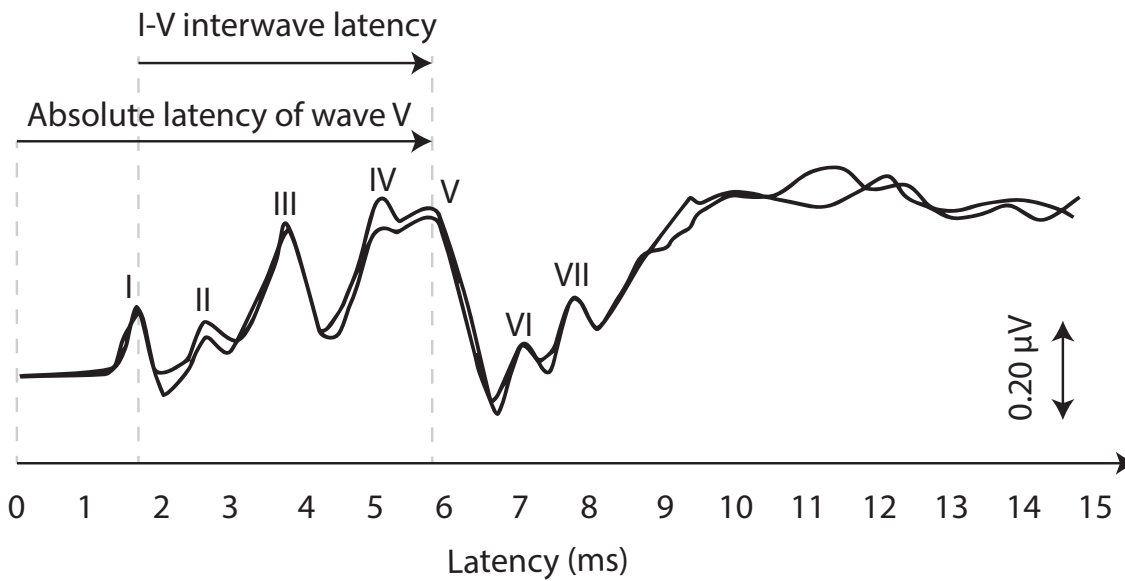


Figure 1.9: A normal ABR waveform using a click stimulus. The stimulus was applied at 0 ms. Adapted from Kramer and Brown [38].

A typical ABR requires approximately 2000 time-locked stimuli at a rate of approximately 11 to 41 s<sup>-1</sup>, and it is not affected by the level of attention, sleep-state, or drugs, and can be performed across all ages, including premature infants. The first positive wave, called wave I, has its origin in the cochlea and in the distal portion of the auditory portion of the 8th cranial nerve where the nervous impulse leaves the

cochlea. The wave II emerges at the proximal part of the 8th cranial nerve, the wave III in the cochlear nucleus, the wave IV in the superior olivary complex, and the wave V in the lateral lemniscus, and input to the inferior colliculus [38].

In an ABR, the wave V is the most relevant wave used for clinical assessment of ABR threshold. The latency of this wave increases as the sound intensity of the click stimulus decreases. Also, as the rate of stimulation increases, the latency of wave V increases, while the latency of wave I remains the same. The age is another factor that affects the ABR peak latency. In the work of Sharma et al. [41], infant's ABR mature at 3 years of age, after which the maturation of wave V becomes slower, reaching the adult value between 6 to 12 years of age. The maturation time is a crucial period in children with cochlear implants. The benefit of cochlear implantation depends on the ability of the brain to learn to classify neural activity derived by the electrode array. It is then important to perform the implantation as soon as possible, thus enabling the possible plastic reorganizations of synaptic transmission and wiring pattern in the brain [42]. As mentioned by McKay [43], the oral language performance and the speech understanding in individuals implanted after 7 years of age depends heavily on the use of hearing aids and by familiarity with oral language structure, such as lip reading and somatosensory information.

The assessment of auditory function after cochlear implantation should be different from the traditional method. In such cases, the ABR test can be performed by electrical stimulation through the cochlear implant, designated by electrically evoked auditory brainstem response (EABR) [44]. There are similarities between the EABR and ABR waveform pattern. Although, as stated by Starr and Brackmann [45], the EABR usually appears 1.5–2 ms earlier due to the direct stimulation of spiral

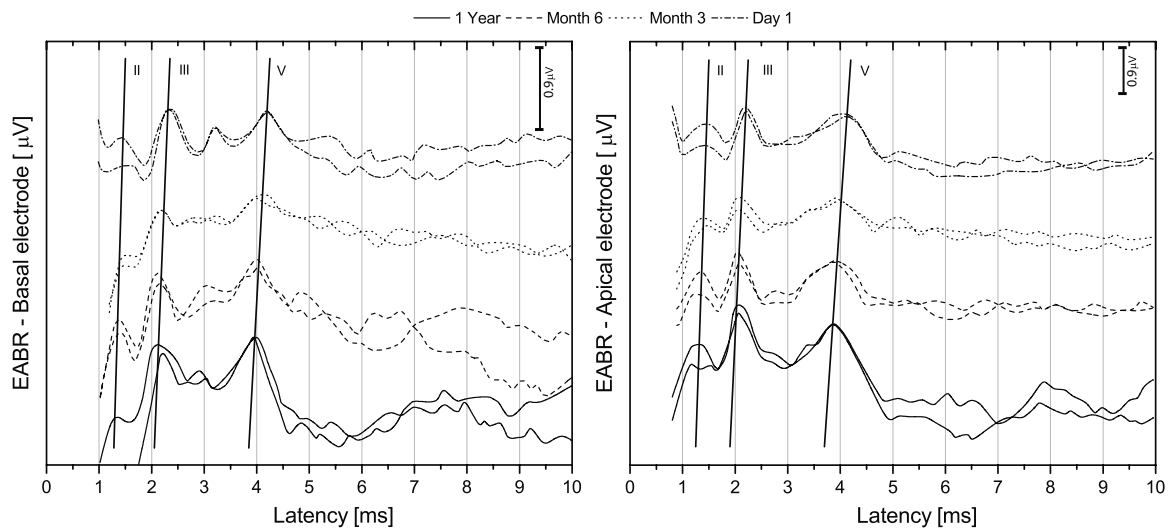


Figure 1.10: Electrically evoked auditory brainstem response reported from a child who was 3 years of age at the time of implant activation. EABR records were performed at 1 year, 6 months, 3 months and 1 day after implantation. Adapted from [47].

ganglion cells by the implant electrodes, which in the end masks the wave I. Starr and Brackmann [45] also did not find significant difference between the adult and children group on the EABR, regarding EABR wave latencies and thresholds. However, EABR wave latencies in children significantly decrease with the time of use of the cochlear implant, which should be related with the increased myelination and improved synaptic efficacy [46]. Figure 1.10 shows the EABR captured by apical and basal electrodes over the first year of implant use in a child with pre-lingual deafness. The age of the child at the time of insertion was 3 years old. Significant decreases of wave and interwave latencies over the first year of implant use was obtained by basal as well as by the apical electrode, thus showing an evident auditory brain stem and midbrain development provided by a consequent electrical stimulation.

### 1.1.7 Hearing disorders and pathologies

The inner ear can be affected by diseases from different origins. Such diseases can cause, for example, sensorineural hearing loss, tinnitus, and vertigo, among others. Hearing loss is the most common congenital disorder and the most frequent sensorineural disorder in developed countries [48]. The etiology of profound congenital hearing impairment is divided into environmental (50 %) and genetic causes (50 %). Environmental causes involve viral infections such as toxoplasmosis, rubella, cytomegalovirus and herpes simplex virus, whereas genetic causes are classified as syndromic (30 %) and non-syndromic (70 %).

The stereocilia located in the inner ear hair cells are microvilli-derived and unique cell structures with specific cochlear functions, including mechano-electrical transduction, cochlear amplification, adaptation, frequency selectivity, and tuning. Their function can be affected by several types of hereditary deafness, and syndromic hearing loss. Usher syndrome involves approximately 3-6 % of congenital profound deafness cases in children. It arises from defective stereocilial molecules and represents 50 % of all hereditary deaf-blindness cases.

The saccule and utricle of the membranous labyrinth exhibit a connection with a pouch located in the petrous bone and in a dura duplicate near the cerebellum, designated by endolymphatic sac [49]. Pressure regulation and fluid homeostasis are the key functions of endolymphatic sac. The enlargement of the vestibular aqueduct which forms this connection is the most common malformation of the inner ear, and is associated with hearing loss. This malformation is bilateral in 90 % of cases, as stated by Ciunan [48]. It is observed in the Pendred syndrome, branchiootorenal syndrome, distal renal tubular acidosis, and Waardenburg syndrome [48].

The stria vascularis, located at the lateral wall of the cochlear duct, and the vestibular dark cells are the main structures involved in the complex process of inner ear homeostasis. These structures are responsible for endolymph secretion, and have many similarities. Disorders lead to altered volume, ion concentrations, osmolarity and pressure in the inner ear and are associated with numerous diseases such as, for example the Alport syndrome. This disease results from mutations in genes encoding the collagen chains  $\alpha3$  (IV),  $\alpha4$  (IV) and  $\alpha5$  (IV). The thickening of the stria capillary basement membrane in the cochlea has suggested that the stria vascularis is the primary site of cochlear pathogenesis. It is also suggested that the reduction in the stria vascularis function has been implicated in the pathogenesis of presbycusis. In short, it is clear that without a regulation of inner ear fluid homeostasis, the function of the hair cells are compromised, leading to hearing loss [48, 50].

The efferent system of the inner ear has an important role in the human hearing, especially in noise protection, mediation of selective attention, and improvement of signal-to-noise ratio. This system can be affected by noise and ototoxic drugs. The reduced medial-olivocochlear efferents reflex strength has been associated with auditory processing disorders such as, for example dyslexia, ankylosing spondylitis, migraine and phonophobia in women, or poorer speech-in-noise recognition and language impairment in children. According to some authors, the efferent suppression of cochlear activity by the medial olivocochlear system, often caused by acoustic overexposure, appears to be enhanced in patients with tinnitus and/or hyperacusis [51, 52].

Ménière's disease is characterized by the following symptoms: aural fullness, tinnitus, and fluctuating hearing loss associated with episodes of vertigo. As the

disease progresses, permanent hearing loss develops instead of fluctuating hearing loss, resulting of the death of the hair cells. The incidence of Ménière's disease vary with the geographic location, with highest rates reported in Finland (513 cases per 100000 inhabitants) [53]. An endolymphatic hydrops (see Figure 1.11) is seen as pathophysiologically related with the Meniere's disease. The excess pressure affects the hydrostatic and osmotic pressure in the endolymphatic and perilymphatic space, leading to a distension of the Reissner's membrane. Schuknecht's theory [54] shows that several symptoms are caused by the Reissner membrane rupture, allowing for potassium rich endolymph to bathe the basal surface of hair cells as well as the eighth cranial nerve. It is believed that the contact with high potassium levels may be toxic to these structures. However, there are other theories, thus suggesting that Ménière's disease is multifactorial [48, 55, 53].

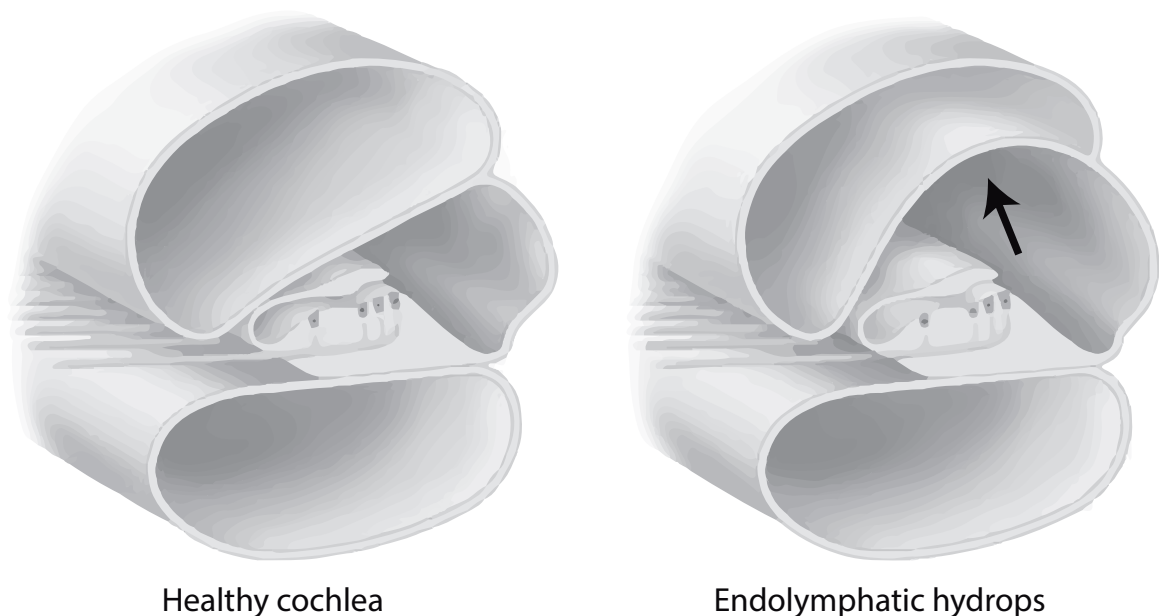


Figure 1.11: Development of endolymphatic hydrops.

Sudden sensorineural hearing loss (SSNHL) is frequently encountered in audiological and otolaryngologic practice. The incidence in Western countries is 5–20 per 100000

inhabitants [48]. SSNHL is often defined as sensorineural hearing loss of 30 dB or more, over at least three contiguous audiometric frequencies occurring within 3 days. Steroid therapy is the current treatment of idiopathic SSNHL. Infectious, autoimmune, traumatic, vascular, neoplastic, metabolic, and neurologic system are some categories with possible etiology for the SSNHL [48, 56].

Continuous exposure to sound levels over 80 dB can cause permanent hearing loss. The hearing loss emerge from the damage of hair cells and the ganglion cells with a higher vulnerability of outer hair cells than inner hair cells. Immediately after an acoustic trauma, it is noticed an increase of free  $\text{Ca}^{2+}$  in outer hair cells, a decrease of cochlear blood flow and a formation of reactive oxygen and reactive nitrogen species. The increase of free  $\text{Ca}^{2+}$  is influenced by the intra-cochlear Mg level. The Mg supplementation has protective effects in noise trauma and might arise from the reduction of calcium influx into the cell. Thus, magnesium deficiency increases the susceptibility to noise induced hearing loss [48]. The therapeutic effect of magnesium was suggested in the experimental work conducted in animals submitted to a series of sound impulses. The work shows that a systemic administration of magnesium significantly reduces hearing loss after 7 days [57]. The results also showed that the therapeutic effect decreased with the amount of time elapsed between the end of exposure and the beginning of treatment [58].

Ototoxic agents affect the function of several inner ear structures and impair the fine tuning of mechano-electrical transduction, resulting in inner ear symptoms. As example, aminoglycosides leads to deterioration of the glycocalyx, weakening the ciliary interconnection, called tip links. This change in stereociliary stiffness leads to an increase in the hair cell discharge rate and it is suggested to be linked with tinnitus



generation [59]. Besides aminoglycosides, medications with ototoxic adverse effects include loop diuretics, cytostatics, tuberculostatics, quinine, chloroquine, salicylic acid, and phenothiazines [58].

### 1.1.8 Therapy

Hearing aids are helpful tools for deaf patients. It is an electronic device able to amplify the sound and delivery it into the external acoustic meatus. Middle ear implants are used for sensorineural hearing loss of about 40–80 dB in middle frequencies. This type of implant is used when conventional hearing aids cannot be applied due to limitations associated with the external acoustic meatus. In severe to profound sensorineural hearing loss, cochlear implants are the most reliable tool [48]. This electronic device is able to restore the missing function of inner hair cells by converting the acoustic signal into electrical stimuli sent to the brain via afferent nerve fibers. Future developments focus on less traumatic electrodes, advanced signal processing, higher stimulation rates and greater numbers of channels. The straight cochlear implant electrodes assume a more lateral position, whereas perimodiolar electrodes are designed to lie adjacent to the modiolar wall. Special electrodes are available for ossified cochleas or cochleas with some type of malformation. The double electrode array has two electrode carriers that are inserted into the first and second turns via two cochleostomies [60] (see Figure 1.12).

Several pharmaceutical agents have been investigated for idiopathic sudden sensorineural hearing loss. Cortisone infusions together with a rheologic agent are a pharmaceutical therapy for acute inner ear symptoms. On the other hand, betahistine and arlevert are often used in the Meniere's disease for vertigo control and can reduce the number and intensity of vertigo episodes [48].

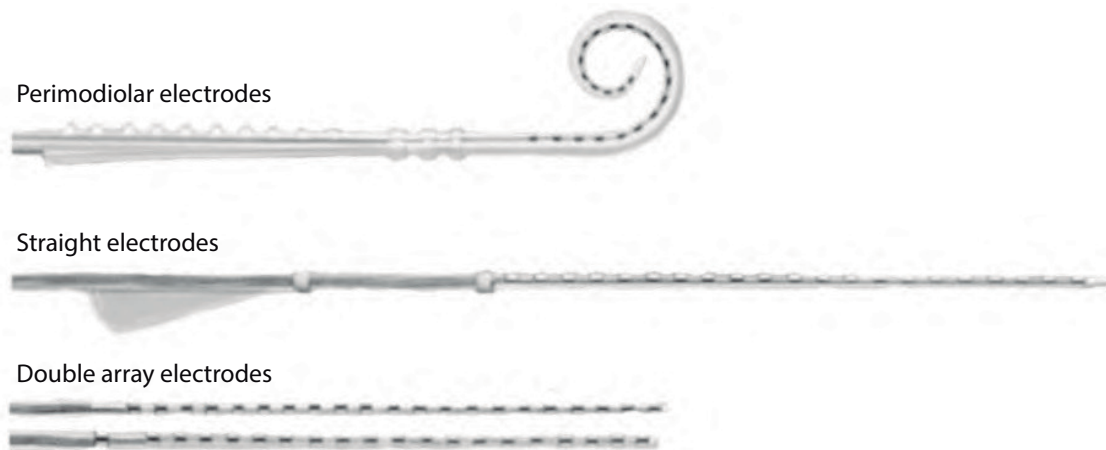


Figure 1.12: Electrode array types.

Acoustic therapies are an interesting approach for tinnitus treatment. They aim to reverse the neuroplastic changes involved with tinnitus by stimulating the auditory pathway. Several therapies are used in the tinnitus treatment, salient among them the tinnitus retraining therapy, the therapy for enriched acoustic environment, the auditory discrimination therapy, the therapy of amplitude modulated sounds, the neuro-modulation therapy and the binaural therapy. The therapy is selected according to the variable impact on the life quality of the patient being treated, resulting in a differentiated treatment for each patient [61].

Birds, fish, and other non-mammalian vertebrates have the ability to regenerate the inner hair cells. However, in an adult mammalian the regeneration of such structures does not exist. Thus, the loss of these cells, due to genetic or environmental factors, causes irreversible hearing loss. Current research focus on the use of exogenous stem cells in the search of novel approaches for inner ear therapy. Three different types of stem cells are mainly employed for cell regeneration: the embryonic stem cells, the adult stem cells and the induced pluripotent stem cells [62]. Nevertheless, certain questions need a detailed investigation and clarification: how the transplanted cells

will distribute along the cochlear duct, and the possibility that the endolymph can be toxic to the transplanted cells.

Gene therapy is a promising approach to prevent or slow the loss of hearing and/or balance. This therapy is not restricted to the addition of a healthy copy of the defective gene. It can also involve gene silencing or editing via nucleic acid-based strategies. The importance of connexin genes (family of membrane proteins that form the intercellular gap junction) in hearing has been demonstrated by genetic studies [63]. Mutations in connexin genes can result in hearing impairments [64, 48]. As an example, hearing in deaf connexin 30 null mice could be recovered by genetically overexpressing the connexin 26 gene [63].

## 1.2 Motivation and aim

Presbycusis or age-related hearing loss is the most common hearing loss, followed, by noise-induced hearing loss identified as the second most common form of sensorineural hearing deficit [65]. Exposure to loud noises results in excessive shearing forces on the stereocilia located at the organ of Corti. Such excessive deformation can cause the death of the hair cells, which consequently leads to a permanent hearing loss.

In 2018, the World Health Organization estimated around 466 million persons with disabling hearing loss in the world, which correspond to a global prevalence of 6.12% [66]. As mentioned in the World Health Organization [66], around half of 466 million are located in the South Asia and East Asia regions (Figure 1.13). Hearing loss is on the rise. The estimates show a possible rise until 630 million in 2030 and over 900 million in 2050. If predictions are correct, it will involve high costs for health

systems (Figure 1.14).

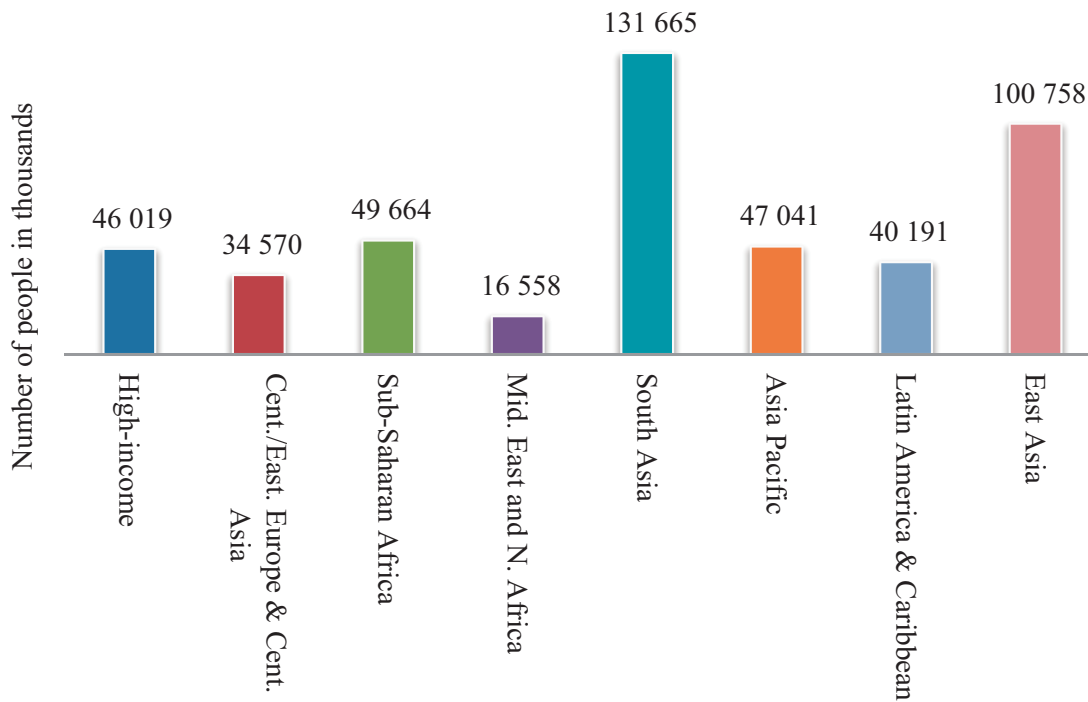


Figure 1.13: Prevalence of disabling hearing loss among regions, in 2018, adapted from the World Health Organization [66].

Moreover, as stated by Davis et al. [67] the adults often experience social isolation and stigmatization, abuse, psychiatric disturbance, depression, difficulties in relationships with partners as a consequence of the hearing impairment.

In children, hearing impairment can lead to a lower language performance. There is a relation of the severity of the disorder with the degree of hearing loss. The work of Oliveira et al. [68] shows a greater difficulty of speech perception and discrimination and language deficits, as the the degree of the hearing loss increases. As in children with bilateral hearing loss, school-age children with unilateral hearing loss also appear to have increased rates of grade failures, need for additional educational assistance, and behavioural problems in the classroom as stated by Lieu [69].

As mentioned by Sharma et al. [70], the age of implantation is a crucial factor

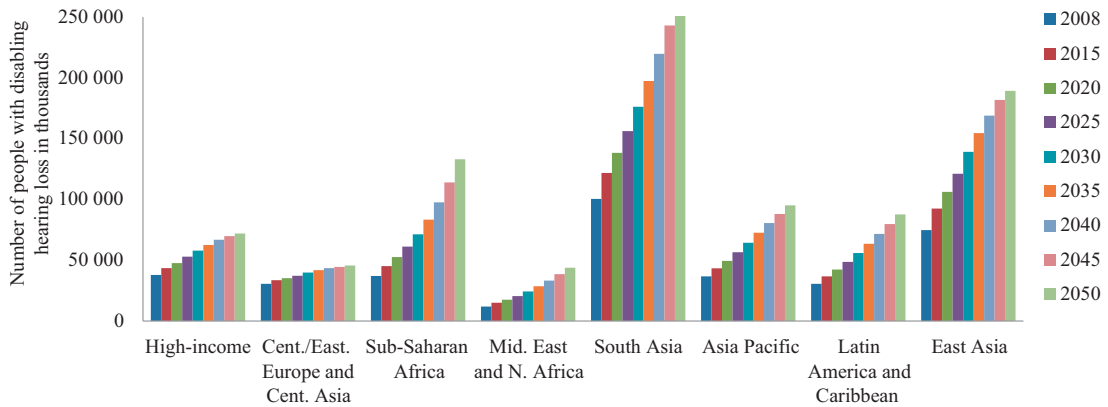


Figure 1.14: Projections of number of people with disabling hearing loss among regions, adapted from the World Health Organization [66].

that allow for good outcomes in children. Kral et al. [71] stated the optimal time for cochlear implantation within the first 3.5 and 4 years of life, this range is particularly important, because the central auditory pathways shows the maximum plasticity to sound stimulation. Nowadays, especially for pre-lingual deaf children, early cochlear implantation at around 12 months is recommended as hearing enables the development of language skills. It is known that if a child does not hear any sound stimulus until the age of 2, she will never learn to speak. The language learning at an early age is therefore essential.

To date, the usage of cochlear implants is the only way to restore the hearing when the cause is related with the death of the hair cells. Then, the role of the cochlear implant is to bypass the damaged parts of the cochlea and stimulate the auditory nerve directly. Therefore, the ear components between the pinna and the endings of the auditory nerve will give additional sound information, in the case of patients who have retained some residual hearing after implantation.

It is thus important to preserve the residual hearing during the cochlear implantation in order to obtain the best synergy between the cochlear implant and the

residual hearing. The material, design, and surgical techniques are some parameters that could be enhanced in order to reduce the negative impact caused by the cochlear implantation.

### 1.3 Thesis structure

This thesis is divided into six chapters. The first chapter, "Thesis report" provides a review of the literature related to the human cochlea. It brings the reader up to date on the most relevant aspects of this scientific area, including the anatomy and physiology of the human cochlea, the inner ear pathologies, and associated therapies. This chapter also includes the motivation aspects, the aim of the thesis, and the scientific contributions. The purpose of the chapter 2 is to describe the influence of the cochlea curvature and the mechanical properties of the BM on the cochlear mapping. The chapter 3 is devoted to the study of the effect of endolymphatic hydrops on the inner ear structures, more precisely on the BM. Using the finite element method (FEM), the work intends to increase the knowledge of the endolymphatic hydrops and consequently the Ménière's disease and its influence on the BM. Chapter 4 investigates new ways of reducing the intra-cochlear trauma, based on the study of several parameters related with the cochlear implant insertion, such as insertion speed, friction coefficient and implant stiffness. Chapter 5 seeks to increase the knowledge about the best wires configuration within the electrode array. Three types of configuration are studied, including the straight, zigzag and helix configuration. Last but not least, the "Thesis considerations" chapter highlights the contribution of all scientific research. It briefly summarize the main findings of all manuscripts written. It also discusses possible future research directions in the field.

## 1.4 Scientific contribution

The results of this PhD thesis have already been published. A list of publications is presented bellow:

### 1.4.1 Journal Articles and Book Chapters

- Areias, B., Parente, M. P. L., Gentil, F., Natal J., R., Insertion of a cochlear straight electrode array with different wires arrangements: a numerical study, submitted to an international journal.
- Areias, B., Parente, M. P. L., Gentil, F., Natal J., R. (2021), Cochlear implantation using a straight cochlear implant electrode - a numerical study, In J. Belinha, J. C. R. Campos, E. Fonseca, M. H. F. Silva, M. A. Marques, M. F. G. Costa & S. Oliveira (Eds), *Advances and Current Trends in Biomechanics: Proceedings of the 9th Portuguese Congress on Biomechanics* (1st ed.).
- Areias, B., Parente, M. P. L., Gentil, F., Caroça, C., Paço, J., Natal J., R., A finite element model to predict the consequences of endolymphatic hydrops in the basilar membrane, *International Journal for Numerical Methods in Biomedical Engineering*, DOI: 10.1002/cnm.3541.
- Areias, B., Parente, M. P. L., Gentil, F., Natal J., R., Finite element modelling of the surgical procedure for placement of a straight electrode array: Mechanical and clinical consequences, *Journal of Biomechanics*, DOI: 10.1016/j.jbiomech.2021.110812.
- Areias, B., Parente, M. P. L., Gentil, F., Natal J., R. (2021), Influence of the basilar membrane shape and mechanical properties in the cochlear response: a

numerical study, Part H: Journal of Engineering in Medicine, 235:7, 743-750,  
DOI: 10.1177/09544119211003443.

### **1.4.2 International Conference Presentations**

- Areias, B., Parente, M. P. L., Gentil, F., Almeida, E., Natal J., R., "Numerical modelling of the human cochlea and surgical techniques", 16th International Symposium on Computer Methods in Biomechanics and Biomedical Engineering, New York, 14-16 August 2019.
- Areias, B., Parente, M. P. L., Gentil, F., Almeida, E., Natal J., R., "Numerical study of the insertion of cochlear implants", Congress on Numerical Methods in Engineering (CMN 2019), Guimarães, 1-3 July 2019.
- Areias, B., Parente, M. P. L., Gentil, F., Almeida, E., Natal J., R., "Implementation of an elastomer dielectric behaviour using Abaqus", 2nd International Conference on Materials Design and Applications 2018 (MDA 2018), Porto, 5-6 July 2018.

### **1.4.3 National Conference Presentations**

- Areias, B., Parente, M. P. L., Gentil, F., Natal J., R., "Influence of the insertion speed during a straight electrode array implantation, a numerical study", 4th Doctoral Congress in Engineering, Porto, 28-29 June 2021, (video conference).
- Areias, B., Parente, M. P. L., Gentil, F., Natal J., R., "Cochlear implantation using a straight cochlear implant electrode, a numerical study", 9th Congresso Nacional de Biomecânica, Porto, 19-20 February 2021, (video conference).



- Areias, B., Parente, M. P. L., Gentil, F., Almeida, E., Natal J., R., "Numerical study of the human cochlea", 3rd Doctoral Congress in Engineering, Porto, 27-28 June 2019.
- Areias, B., Parente, M. P. L., Gentil, F., Almeida, E., Natal J., R., "Numerical modelling of human cochlea and associated pathologies", 8th Congresso Nacional de Biomecânica, Unhais da Serra, 15-16 February 2019.

## 1.5 References

- [1] Lawrence E. Wineski and Richard S. Snell. *Snell's clinical anatomy by regions*. Wolters Kluwer, Philadelphia, 10th edition. edition, 2019.
- [2] Dale Purves. *Neuroscience*. Oxford University Press, New York, sixth edition. edition, 2018.
- [3] B.M. Carlson. *The Human Body: Linking Structure and Function*. Elsevier Science, 2018.
- [4] Robert Fettiplace and Carole M. Hackney. The sensory and motor roles of auditory hair cells. *Nature Reviews Neuroscience*, 7:19–29, 2006.
- [5] Q. Huang and J. G. Tang. Age-related hearing loss or presbycusis. *European Archives of Oto-Rhino-Laryngology*, 267(8):1179–1191, 2010.
- [6] A.F. Healy, D.K. Freedheim, I.B. Weiner, J.A. Schinka, R.W. Proctor, and W.F. Velicer. *Handbook of Psychology, Experimental Psychology*. Wiley, 2003.
- [7] P.W. Flint, H.W. Francis, B.H. Haughey, M.M. Lesperance, V.J. Lund, K.T. Robbins, and J.R. Thomas. *Cummings Otolaryngology - Head and Neck Surgery*. Elsevier, 7th edition, 2020.
- [8] L. Michaels. *Ear, Nose and Throat Histopathology*. Springer London, 2012.
- [9] Tobias Reichenbach and A J Hudspeth. The physics of hearing: fluid mechanics and the active process of the inner ear. *Reports on Progress in Physics*, 77:076601, 2014.

- [10] Joseph D. Bronzino. *The biomedical engineering handbook*. The electrical engineering handbook series. CRC/Taylor & Francis, Boca Raton, 3rd edition, 2006.
- [11] Peter Dallos, Arthur N. Popper, and Richard R. Fay. *The cochlea*. Springer handbook of auditory research. Springer, New York, 1996.
- [12] T. Reichenbach, A. Stefanovic, F. Nin, and A. J. Hudspeth. Waves on reissner’s membrane: A mechanism for the propagation of otoacoustic emissions from the cochlea. *Cell Reports*, 1(4):374–384, 2012.
- [13] G. Emadi, C. P. Richter, and P. Dallos. Stiffness of the gerbil basilar membrane: Radial and longitudinal variations. *Journal of Neurophysiology*, 91(1):474–488, 2004.
- [14] H.L. Hawkins, T.A. McMullen, and R.R. Fay. *Auditory Computation*. Springer New York, 2012.
- [15] S. Jia, P. Dallos, and D. Z. He. Mechanoelectric transduction of adult inner hair cells. *J Neurosci*, 27(5):1006–14, 2007.
- [16] Guoqiang Wan, Gabriel Corfas, and Jennifer S Stone. Inner ear supporting cells: rethinking the silent majority. *Seminars in cell & developmental biology*, 24:448–59, 2013.
- [17] Nikola Ciganović, Amanuel Wolde-Kidan, and Tobias Reichenbach. Hair bundles of cochlear outer hair cells are shaped to minimize their fluid-dynamic resistance. *Scientific Reports*, 7(1):3609, 2017.
- [18] J.K. Mai and G. Paxinos. *The Human Nervous System*. Elsevier Science, 2011.

- [19] D. W. Smith and A. Keil. The biological role of the medial olivocochlear efferents in hearing: separating evolved function from exaptation. *Frontiers in Systems Neuroscience*, 9, 2015.
- [20] W. E. Brownell, C. R. Bader, D. Bertrand, and Y. de Ribaupierre. Evoked mechanical responses of isolated cochlear outer hair cells. *Science*, 227(4683):194–6, 1985.
- [21] A. W. Peng and A. J. Ricci. Somatic motility and hair bundle mechanics, are both necessary for cochlear amplification? *Hearing Research*, 273(1-2):109–122, 2011.
- [22] B. N. Evans, R. Hallworth, and P. Dallos. Outer hair cell electromotility - the sensitivity and vulnerability of the dc component. *Hearing Research*, 52(2):288–304, 1991.
- [23] J. Zheng, W. X. Shen, D. Z. Z. He, B. L. Kevin, L. D. Madison, and P. Dallos. Prestin is the motor protein of cochlear outer hair cells. *Nature*, 405(6783):149–155, 2000.
- [24] M. C. Liberman, J. G. Gao, D. Z. Z. He, X. D. Wu, S. P. Jia, and J. Zuo. Prestin is required for electromotility of the outer hair cell and for the cochlear amplifier. *Nature*, 419(6904):300–304, 2002.
- [25] M. Murakoshi, S. Suzuki, and H. Wada. All three rows of outer hair cells are required for cochlear amplification. *Biomed Research International*, 2015.
- [26] Li Yi and He David Z. The cochlear amplifier: Is it hair bundle motion of outer hair cells? *Journal of Otology*, 9(2):64–72, 2014.

- [27] R. Fettiplace and A. J. Ricci. Adaptation in auditory hair cells. *Current Opinion in Neurobiology*, 13(4):446–451, 2003.
- [28] F. Nin, H. Hibino, K. Doi, T. Suzuki, Y. Hisa, and Y. Kurachi. The endocochlear potential depends on two  $k^+$  diffusion potentials and an electrical barrier in the stria vascularis of the inner ear. *Proceedings of the National Academy of Sciences of the United States of America*, 105(5):1751–1756, 2008.
- [29] Georg Békésy. Dc resting potentials inside the cochlear partition. *Journal of the Acoustical Society of America*, 24(1):72–76, 1952.
- [30] Associação Brasileira De Otorrinolaringologia E Cirurgia Cervico Facial. *Tratado de Otorrinolaringologia e Cirurgia Cérvicofacial*. Elsevier Editora Ltda., 2017.
- [31] F. Gianoli, T. Risler, and A. S. Kozlov. The development of cooperative channels explains the maturation of hair cell’s mechanotransduction. *Biophysical Journal*, 117(8):1536–1548, 2019.
- [32] P. G. Gillespie and U. Muller. Mechanotransduction by hair cells: Models, molecules, and mechanisms. *Cell*, 139(1):33–44, 2009.
- [33] D. E. Vetter, J. R. Mann, P. Wangemann, J. Z. Liu, K. J. McLaughlin, F. Lesage, D. C. Marcus, M. Lazdunski, S. F. Heinemann, and J. Barhanin. Inner ear defects induced by null mutation of the *isk* gene. *Neuron*, 17(6):1251–1264, 1996.
- [34] N. Sperelakis. *Cell Physiology Source Book: Essentials of Membrane Biophysics*. Elsevier Science, 2011.
- [35] Brenda L. Lonsbury-Martin and Glen K. Martin. Chapter 6 - otoacoustic emissions. In Gastone G. Celesia, editor, *Disorders of Peripheral and Central*

- Auditory Processing*, volume 10 of *Handbook of Clinical Neurophysiology*, pages 115–135. Elsevier, 2013.
- [36] D. T. Kemp. Stimulated acoustic emissions from within the human auditory system. *The Journal of the Acoustical Society of America*, 64(5):1386–1391, 1978.
- [37] Geoffrey A. Manley, Richard R. Fay, and Arthur N. Popper. *Active processes and otoacoustic emissions in hearing*. Springer handbook of auditory research. Springer, New York, 2007.
- [38] S. Kramer and D.K. Brown. *Audiology: Science to Practice, Third Edition*. Plural Publishing, Incorporated, 2018.
- [39] F. P. Harris, B. L. Lonsburymartin, B. B. Stagner, A. C. Coats, and G. K. Martin. Acoustic distortion products in humans - systematic changes in amplitude as a function of f2/f1 ratio. *Journal of the Acoustical Society of America*, 85(1):220–229, 1989.
- [40] Jos J. Eggermont. Chapter 30 - auditory brainstem response. In Kerry H. Levin and Patrick Chauvel, editors, *Clinical Neurophysiology: Basis and Technical Aspects*, volume 160 of *Handbook of Clinical Neurology*, pages 451–464. Elsevier, 2019.
- [41] M. Sharma, S. S. Bist, and S. Kumar. Age-related maturation of wave v latency of auditory brainstem response in children. *Journal of Audiology and Otology*, 20(2):97–101, 2016.

- [42] A. Kral and J. Tillein. Brain plasticity under cochlear implant stimulation. *Adv Otorhinolaryngol*, 64:89–108, 2006.
- [43] C. M. McKay. Brain plasticity and rehabilitation with a cochlear implant. *Adv Otorhinolaryngol*, 81:57–65, 2018.
- [44] Nithreen Mohammed Said Abdelsalam and Pretty Omar Afifi. Electric auditory brainstem response (E-ABR) in cochlear implant children: Effect of age at implantation and duration of implant use. *Egyptian Journal of Ear, Nose, Throat and Allied Sciences*, 16(2):145–150, 2015.
- [45] A. Starr and D. E. Brackmann. Brain stem potentials evoked by electrical stimulation of the cochlea in human subjects. *Ann Otol Rhinol Laryngol*, 88(4 Pt 1):550–6, 1979.
- [46] J. J. Eggermont. On the rate of maturation of sensory evoked potentials. *Electroencephalogr Clin Neurophysiol*, 70(4):293–305, 1988.
- [47] K. A. Gordon, B. C. Papsin, and R. V. Harrison. Auditory brainstem activity and development evoked by apical versus basal cochlear implant electrode stimulation in children. *Clinical Neurophysiology*, 118(8):1671–1684, 2007.
- [48] R. R. Ciuman. Inner ear symptoms and disease: Pathophysiological understanding and therapeutic options. *Medical Science Monitor*, 19:1195–1210, 2013.
- [49] C. K. Nordstrom, N. Danckwardt-Lilliestrom, G. Laurell, W. Liu, and H. Rask-Andersen. The human endolymphatic sac and inner ear immunity:

- Macrophage interaction and molecular expression. *Frontiers in Immunology*, 9, 2019.
- [50] R. R. Ciuman. Stria vascularis and vestibular dark cells: characterisation of main structures responsible for inner-ear homeostasis, and their pathophysiological relations. *Journal of Laryngology and Otology*, 123(2):151–162, 2009.
- [51] E. A. Lopez-Poveda. Olivocochlear efferents in animals and humans: From anatomy to clinical relevance. *Front Neurol*, 9:197, 2018.
- [52] Joshua J. Sturm and Catherine J. C. Weisz. Hyperactivity in the medial olivocochlear efferent system is a common feature of tinnitus and hyperacusis in humans. *Journal of Neurophysiology*, 114(5):2551–2554, 2015.
- [53] Hetal H. Patel and Huseyin Isildak. Meniere’s disease an overview. *Operative Techniques in Otolaryngology-Head and Neck Surgery*, 27(4):184–187, 2016.
- [54] H. F. Schuknecht. Meniere’s disease: a correlation of symptomatology and pathology. *Laryngoscope*, 73:651–65, 1963.
- [55] B. S. Oberman, V. A. Patel, S. Cureoglu, and H. Isildak. The aetiopathologies of meniere’s disease: a contemporary review. *Acta Otorhinolaryngol Ital*, 37(4):250–263, 2017.
- [56] M. Kuhn, S. E. Heman-Ackah, J. A. Shaikh, and P. C. Roehm. Sudden sensorineural hearing loss: a review of diagnosis, treatment, and prognosis. *Trends Amplif*, 15(3):91–105, 2011.



- [57] L. Abaamrane, F. Raffin, M. Gal, P. Avan, and I. Sendowski. Long-term administration of magnesium after acoustic trauma caused by gunshot noise in guinea pigs. *Hearing Research*, 247(2):137–145, 2009.
- [58] F. Scheibe, H. Haupt, B. Mazurek, and O. Konig. Therapeutic effect of magnesium on noise-induced hearing loss. *Noise Health*, 3(11):79–84, 2001.
- [59] M. K. Schwaber. Medical evaluation of tinnitus. *Otolaryngologic Clinics of North America*, 36(2):287–292, 2003.
- [60] T. Lenarz. Cochlear implant - state of the art. *GMS Curr Top Otorhinolaryngol Head Neck Surg*, 16:Doc04, 2017.
- [61] D. Ibarra-Zarate and L. M. Alonso-Valerdi. Acoustic therapies for tinnitus: The basis and the electroencephalographic evaluation. *Biomedical Signal Processing and Control*, 59, 2020.
- [62] Luiz Gustavo Dufner-Almeida, Dayane Bernardino da Cruz, Regina Célia Mingroni Netto, Ana Carla Batisso, Jeanne Oiticica, and Rodrigo Salazar-Silva. Stem-cell therapy for hearing loss: are we there yet? *Brazilian Journal of Otorhinolaryngology*, 85:520–529, 2019.
- [63] S. Ahmad, W. X. Tang, Q. Chang, Y. Qu, J. Hibshman, Y. H. Li, G. Sohl, K. Willecke, P. Chen, and X. Lin. Restoration of connexin26 protein level in the cochlea completely rescues hearing in a mouse model of human connexin30-linked deafness. *Proceedings of the National Academy of Sciences of the United States of America*, 104(4):1337–1341, 2007.

- [64] S. Delmaghani and A. El-Amraoui. Inner ear gene therapies take off: Current promises and future challenges. *Journal of Clinical Medicine*, 9(7), 2020.
- [65] P. M. Rabinowitz. Noise-induced hearing loss. *Am Fam Physician*, 61(9):2749–56, 2759–60, 2000.
- [66] World Health Organization, 2018. World Health Organization. Available at <https://apps.who.int/iris/bitstream/handle/10665/260336/9789241550260-eng.pdf?sequence=1&ua=1>. Accessed 8th May 2021.
- [67] A. C. Davis and H. J. Hoffman. Hearing loss: rising prevalence and impact. *Bull World Health Organ*, 97(10):646–646A, 2019.
- [68] Patrícia Santos Oliveira, Letícia Macedo Penna, and Stela Maris Aguiar Lemos. Desenvolvimento da linguagem e deficiência auditiva: revisão de literatura. *Revista CEFAC*, 17:2044–2055, 2015.
- [69] J. E. Lieu. Speech-language and educational consequences of unilateral hearing loss in children. *Arch Otolaryngol Head Neck Surg*, 130(5):524–30, 2004.
- [70] S. D. Sharma, S. L. Cushing, B. C. Papsin, and K. A. Gordon. Hearing and speech benefits of cochlear implantation in children: A review of the literature. *Int J Pediatr Otorhinolaryngol*, 133:109984, 2020.
- [71] A. Kral and A. Sharma. Developmental neuroplasticity after cochlear implantation. *Trends Neurosci*, 35(2):111–22, 2012.

## Chapter 2

# Influence of the basilar membrane shape and mechanical properties in the cochlear response: a numerical study



**Article 1 - Influence of the basilar membrane shape and mechanical properties in the cochlear response: a numerical study**

B. Areias (1), M.P.L. Parente (1,2), F. Gentil (3), R.M. Natal Jorge (1,2)

1-INEGI, Institute of science and innovation in mechanical and industrial engineering, Porto, Portugal {bareias@fe.up.pt}

2-FEUP, Faculty of Engineering, University of Porto, Porto, Portugal {mparente@fe.up.pt, rnatal@fe.up.pt}

3-Escola Superior de Saúde - Politécnico do Porto; Clínica ORL – Dr. Eurico de Almeida; WIDEX {fernanda.fgnanda@gmail.com}

*Published in: Part H: Journal of Engineering in Medicine, 2021*

*doi: 10.1177/09544119211003443*

In this chapter, Article 1 presents a study to describe the influence of the cochlea curvature and the mechanical properties of the BM on the cochlear mapping.



## 2.1 Abstract

Hearing impairment is one of the most common health disorders, affecting individuals of all ages, reducing considerably their quality of life. At present, it is known that during an acoustic stimulation a travelling wave is developed inside the cochlea. Existing mathematical and numerical models available in the literature try to describe the shape of this travelling wave, the majority of them present a set of approaches based on some limitations either or both of the mechanical properties used and the geometrical description of the realistic representation. The present numerical study highlights the distinctions of using a spiral model of the cochlea, by comparing the obtained results with a straight, or simplified model. The influence of the implantation of transversely isotropic mechanical models was also studied, by comparing the basilar membrane with isotropic and transversely isotropic mechanical properties. Values of the root mean square error calculated for all models show a greater proximity of the cochlear mapping to the Greenwood function when the basilar membrane is assumed with transversely isotropic mechanical properties for both straight and spiral model. The root mean square errors calculated were: 2.05 mm, 1.70 mm, 2.72 mm, 2.08 mm, for the straight-isotropic, straight-transversely isotropic, spiral-isotropic and spiral-transversely isotropic model, respectively.

## 2.2 Keywords

basilar membrane, cochlea, finite element method, mechanical properties, travelling wave

## 2.3 Introduction

Approximately 466 million people worldwide suffer from some type of hearing loss, from which 93 % are adults, aged over 15 years of age [1]. Pathologies associated with the auditory system can be derived from vascular disorders, chronic inflammation, noise exposure, genetic susceptibility, tumors, Ménière disease, and ototoxic drugs [2, 3]. Physiological aging of the inner ear is often the reason for hearing losses, known as presbycusis, especially at older ages (over 50 years of age).

The sound pressure waves are directed through the external auditory meatus to the tympanic membrane, causing it to vibrate. This vibration is then transmitted to the middle ear ossicles and thereafter to the oval window, located at the base of the cochlea. The cyclic inward and outward motion of the stapes, the last ossicle in the ossicular chain, creates a hydraulic pressure gradient inside the cochlea, forcing the movement of the basilar membrane [4]. Such movement, stimulates the hair cells of the organ of Corti, which could result in the transmission of nerve impulses towards to the brain.

In 1961, Greenwood [5] developed a mathematical description for the cochlear frequency-position map. The cochlear-position map relates the location of maximum displacement of the basilar membrane as a function of frequency. Therefore, each location along the basilar membrane is associated with one frequency, designated by characteristic frequency. In contrast to outer hair cells which are displacement detectors, inner hair cells are sensitive to velocity (at least at low frequencies) because their hair bundles are not firmly embedded in the overlying tectorial membrane [6]. The characteristic frequency is thus related with this highly sensitive place of the basilar membrane. The travelling wave starts at the base of the cochlea and grows



in amplitude until the maximum is reached, and then sharply decreases. A sound composed by higher frequencies leads to a peak of the travelling wave near the base of the cochlea. On the other hand, a lower frequency sound moves the peak towards the apex of the cochlea.

The Greenwood function [5] (Equation 2.1) is composed by three constants,  $A$ , that adjusts the upper frequency limit, the slope,  $a$ , which scales or normalizes the length of the cochlea and  $k$ , which represents the constant of integration and adjusts the lower frequency limit.

$$f = A(10^{ax} - k) \quad (2.1)$$

The variable  $x$ , defines the fractional length along the cochlear spiral measured from the apex of the cochlea to the region of interest and can assume a value between 0 and 1, as stated by Greenwood [7]. In humans, the Greenwood function is given by the Equation 2.2.

$$f = 165.4(10^{2.1x} - 0.88) \quad (2.2)$$

Like in other animals, the human cochlea has the shape of a spiral tube, similar to a snail shell. In humans, the average length of the cochlea and the average length and width of the cochlear base is respectively 35.8 mm, 9.04 mm and 6.33 mm [8]. Non mammals like reptiles, birds, and mammals such as monotremes do not have a cochlear coiling. This peculiarity enables the cochlea to be longer, increasing the hearing frequency range, whereas uncoiled cochlea has been associated with relatively limited hearing ranges, due to its limited length, as stated by Manoussaki et al. [9]. The cochlear radii ratio is obtained as the ratio of the radius of curvature of the

midline basilar membrane at the base to that at the apex. Chadwick et al. [10] and Manoussaki et al. [9] showed that the radii ratio is an important factor that determines the lower limit frequency of hearing (greater radii ratios allow a lower frequency limit of hearing). Since different radii ratios are related to different energy density focusing at the apex. Although, one can find some controversy in the literature, the statistical results of Ritsche et al. [11] demonstrated that the radii ratio is not directly connected to low frequency hearing.

The study conducted by Manoussaki et al. [12] showed that the amplitude of movement in the basilar membrane is affected by the curvature of the cochlea. An increase in the amplitude of the outside wall and a decrease in the inside wall in the propagation direction was achieved using a mathematical model based on the energy conservation law [12]. The inside wall represents the side of the basilar membrane near the modiolus, whereas the outside wall denotes the side near the spiral ligament. Pierch et al. [13] found a significant correlation between the radii ratio and the angular length of the cochlea, indicating a dependence between the radii ratio with the number of turns of the cochlea. Another study conducted by Manoussaki and Chadwick [14] investigated the fluid mechanical effects induced by the coiled cochlea. The numerical results showed that the pressure on the basilar membrane decreases with increased curvature. Ren et al. [15] studied the coiling effects based on a three dimensional finite element hydrodynamic model. The authors assumed orthotropic properties for the basilar membrane for both models (straight and spiral) and no significant differences were found in terms of displacement and pressure distributions. Steele and Zais [16] reported a study relating the effects of the cochlear coiling on the displacement amplitude of the basilar membrane and on the pressure distribution in the scala

(vestibuli or tympani, since symmetry was assumed), as described in their symmetrical mathematical model. The results revealed that the basilar membrane amplitude at frequencies of 10 kHz, 4 kHz, 2 kHz and 1 kHz do not present significant differences between the straight and spiral model, showing thus no influence of the cochlear shape in these frequencies. On the other hand, the pressure in the scala decreased while increasing the coiling, showing consistency with the work of Manoussaki and Chadwick [14].

In addition to curvature influence, it is also accepted that mammalian cochleae are coiled in order to reduce the dimensions of the organ, which is positioned into a small space inside the skull, in the temporal bone, as mentioned by Békésy [17]. Other advantage is that the cochlear coil increases the efficiency of blood and vestibulocochlear synaptic transmission through the central shaft designated by modiolus. The present study is based on the finite element method, which is a tool that allows to simulate the travelling wave present in the human cochlea, in order to understand the effect of the cochlear shape on hearing and to study the influence of the cochlea curvature and the mechanical properties of the basilar membrane on the cochlear mapping.

## 2.4 Materials and Methods

In the present work a 3D finite element model of a straight and spiral human cochlea was developed. The basilar membrane was partitioned in 29 equi-length parts, where the part 1 and the part 29 lie at the base and the apex of the cochlea, respectively (Figure 2.1C and Figure 2.1D). The dimensions of the straight model were based on the literature [18], in contrast the geometry of the spiral model was

obtained through a set of MRI images of a male patient, 85 years-old, without cochlear pathologies. The dimensions of the basilar membrane were not recognized through the MRI, thus, the width, length and thickness were based on published studies [19, 20]. In this way, the basilar membrane was assumed to change linearly its width from  $100\ \mu\text{m}$  at the base to  $500\ \mu\text{m}$  at the apex, and its thickness from  $7.5\ \mu\text{m}$  to  $2.5\ \mu\text{m}$  along the longitudinal direction.

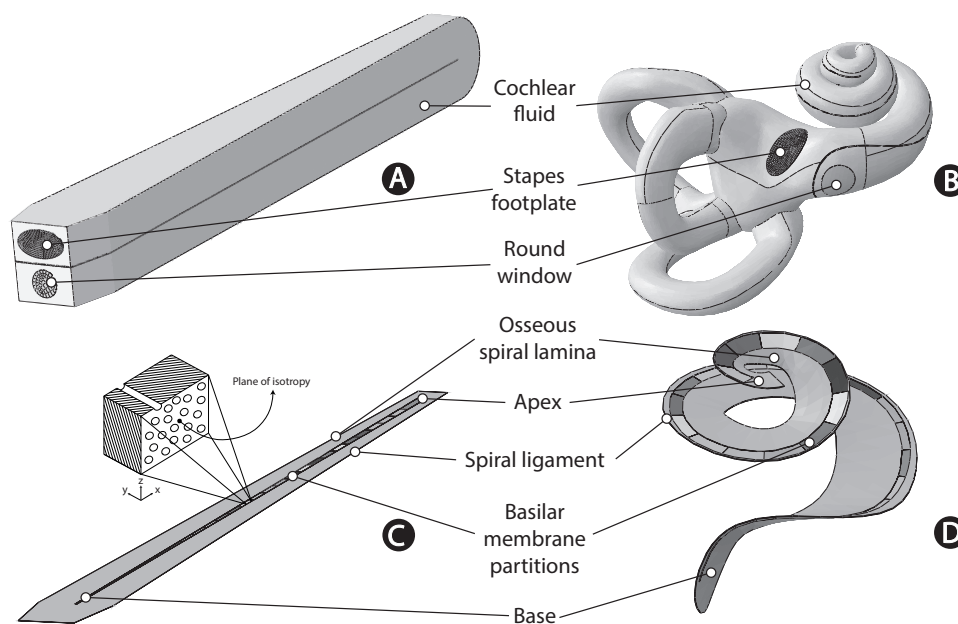


Figure 2.1: Representation of the straight model (A), the spiral model (B), the basilar membrane of the straight model (C) and the basilar membrane of the spiral model (D).

Both models were tested with isotropic or transversely isotropic mechanical properties in the basilar membrane. Initially, the straight-isotropic model was used to tuning iteratively the isotropic mechanical properties; posteriorly, those mechanical properties were applied in the spiral-isotropic model. In order to tune the straight-isotropic model, the results were compared with the function proposed by Greenwood in 1990 [7] and the experimental results published by Békésy in 1960 [17] and with other works in the literature [18, 21]. Inside each partition, in the

straight-isotropic model (see Table 2.1) the basilar membrane is assumed isotropic and homogeneous, with constant mechanical properties. The Young's modulus,  $E$ , and the Poisson's ratio,  $\nu$  used for the isotropic basilar membrane, for the different partitions is presented in Table 2.1. Additionally, there is a gradient of Young's modulus, shear modulus and damping along the basilar membrane, whereby, it is assumed that each partition has different mechanical properties. Therefore, there is a linear variation between partition 1 with  $E=30$  MPa to partition 24 with  $E=20$  MPa.

Table 2.1: Isotropic and transversely isotropic mechanical properties of the basilar membrane

Basilar Part	Isotropic Properties		Transversely isotropic properties								
	$E$ [MPa]	$\nu$ [-]	$E_x$ [MPa]	$E_y$ [MPa]	$E_z$ [MPa]	$\nu_{xy}$ [-]	$\nu_{yz}$ [-]	$\nu_{xz}$ [-]	$G_{xy}$ [MPa]	$G_{yz}$ [MPa]	$G_{xz}$ [MPa]
1 to 24	30-20	0.3	3-2	30-20	3-2	0.2	0.2	0.3	15-10	15-10	$\frac{E_x}{2(1+\nu_{xz})}$
24 to 29	20-3		2-0.3	20-3	2-0.3				10-1.5	10-1.5	

The Poisson's ratio was assumed  $\nu = 0.3$  based in other works [22, 23, 24], and constant along the basilar membrane. The work conducted by Liu et al. [25] showed that the Poisson's ratio has minor impact on the vertical displacement of the basilar membrane. Contrary to the Poisson's ratio, there is a gradient of Young's modulus, shear modulus and damping along the basilar membrane, whereby, it is assumed that each partition has different mechanical properties. The remaining models: straight-transversely isotropic, spiral-isotropic and spiral-transversely isotropic were modelled with the mechanical properties presented in the Table 2.1, which were derived from the straight-isotropic model, after being tuned. Thus, in order to set the transversely isotropic properties, the Young's modulus,  $E$ , in the isotropic analysis was considered similar to  $E_y$  in the transversely isotropic analysis (in the direction

of the radial fibers). The remaining transversely isotropic properties were calculated on the basis of the equations present on the study of Ren et al. [15]. A transversely isotropic material has 5 independent parameters, in this case the parameters are  $E_x$ ,  $E_y$ ,  $\nu_{xy}$ ,  $\nu_{xz}$ , and  $G_{xy}$ . The basilar membrane is mostly composed by radial fibers embedded in a soft matrix, thus, it can be assumed transversely isotropic and the following relations should be satisfied:  $E_z = E_x$ ;  $\nu_{xy} = \nu_{yz}$ ;  $G_{xy} = G_{yz}$  and  $G_{xz} = E_x/2(1 + \nu_{xz})$ . If  $E_y$  is the Young's modulus in the radial direction of the basilar membrane, it can be assumed to be related with the longitudinal direction,  $E_x$ , through the equation  $10E_x = E_y$ . The linear relation between  $E_x$  and  $E_y$  was based in other works already published in the literature [15]. However, in our model a value of 10 was assumed, since this value was determined in order to obtain a comparable magnitude of the displacement of the basilar membrane at 12 mm (see Figure 2.4 and 2.6).  $G_{xy}$  was assumed to be related with  $E_y$  by the following equation  $G_{xy} = E_y/2$  due the lack of data. The same assumption was made in the work of Ren et al. [15]. The Poisson's ratio was assumed as  $\nu_{xy} = \nu_{yz} = 0.2$  and  $\nu_{xz} = 0.3$  in order to comply with the transverse isotropy of the basilar membrane and the material stability requirement. The basilar membrane was considered homogeneous inside each part in all models.

The Rayleigh damping matrix,  $C$ , is expressed as a sum of two components, the stiffness-dependent part and the mass-dependent part. In terms of the Rayleigh damping, the mass-dependent part was considered null in this study, since the effects of rigid body motion were neglected. Thus, the damping matrix can be computed through the equation  $C = \beta K$ , with  $K$  being the stiffness matrix. The Rayleigh damping coefficient,  $\beta$ , applied in all models is listed in Table 2.2. The gradual

increase of the damping shows that a place near the apex of the cochlea, where the wave pressure in fluid has less energy due to a greater distance from the base of the cochlea, needs more “damping” in order to describe the lack of viscosity in the fluid. The density of the basilar membrane was assumed to be  $1200 \text{ kg m}^{-3}$  in all models. A linear variation of the mechanical properties was assumed between the parts along the basilar membrane length. The extension of the basilar membrane has a support function. This structure was simplified being considered with bone properties and anchored at two bony edges.

Table 2.2: Rayleigh damping property of the basilar membrane

Rayleigh damping property	$\beta$ [s]
Basilar Part	$1 \times 10^{-6} - 1 \times 10^{-5}$
	$1 \times 10^{-5} - 1 \times 10^{-3}$

The fluid inside the scala vestibuli and tympani were simulated using acoustic elements with water properties (the bulk modulus,  $\mathbf{K}$ , which describes how resistant the substance to compression is, was assumed equal to 2200 MPa [18, 26],  $\rho = 1000 \text{ kg m}^{-3}$  and inviscid [20, 27], the latter being a limitation of the model). The Young’s modulus,  $E$ , the Poisson’s ratio,  $\nu$ , and the density,  $\rho$ , of the bony structures that support the basilar membrane, the stapes and the round window are summarized in the Table 2.3. The walls of the two scalae were considered rigid. In total, the straight model (Figure 2.1A) was composed by 404131 nodes, whereas the spiral model (Figure 2.1B) was composed by 236379 nodes. Linear acoustic tetrahedral elements (AC3D4) were used to discretize the acoustic medium. In contrast, the bony structure, the basilar membrane, the stapes footplate and round window were modelled with the 3-node triangular (S3) and 4-node quadrilateral (S4) shell elements [28].

Table 2.3: Mechanical properties of the bony structures and soft tissues

		$E$ [MPa]	$\nu$ [-]	$\rho$ [kg m <sup>-3</sup> ]
Bony structures [29, 30, 31]		14100	0.3	2000
Stapes	Stapedial annular ligament [29, 32]	0.6		1200
	Stapes footplate [29, 30, 31]	14100		2500
Round window [18]		0.35		1200

As load, a pressure of 0.2 Pa (80 dB SPL) was applied at the stapes footplate. The frequency band in study was the human range commonly given between 20 Hz and 20 kHz. The numerical simulations were carried out using the commercial software Abaqus Standard [28]. A steady-state dynamic analysis was carried out. Such analysis provides the steady-state amplitude and phase of the response of the basilar membrane due to harmonic excitation at a given frequency. The amplitude and phase of the response in matrix form is then obtained through the Equation 2.3 and are directly available by Abaqus [28].

$$\begin{bmatrix} K^{NM} - \Omega^2 M^{NM} & -\Omega(C_m^{NM} + C_k^{NM}) \\ -\Omega(C_m^{NM} + C_k^{NM}) & -K^{NM} + \Omega^2 M^{NM} \end{bmatrix} \begin{Bmatrix} R(u^M) \\ I(u^M) \end{Bmatrix} = \begin{Bmatrix} R(P^N) \\ -I(P^N) \end{Bmatrix} \quad (2.3)$$

Where,  $\Omega$ , is the circular frequency,  $K$ , the stiffness matrix,  $M$ , the mass matrix,  $C_k$ , the stiffness proportional damping matrix,  $C_m$ , the mass proportional damping matrix,  $u$ , the complex displacement ( $R$  and  $I$  are the real and imaginary part, respectively) and,  $P$ , the complex force applied to the model.

The acoustic-structural coupling is described by Equation 2.4.

$$\frac{1}{\rho_f} \frac{\partial p}{\partial \mathbf{x}} \cdot \mathbf{n}^- + \ddot{\mathbf{u}} \cdot \mathbf{n}^- = 0 \quad (2.4)$$

Where,  $\rho_f$  is the fluid density,  $p$ , the acoustic pressure,  $\mathbf{n}^-$ , the normal vector



pointing into the fluid and  $\ddot{\mathbf{u}}$ , the structural acceleration.

## 2.5 Results

The relation between the characteristic frequency and the cochlear longitudinal location along the basilar membrane available in the literature provides information that allowed to tune the 3D finite element model. After the development of the numerical models, all models were compared with the function proposed by Greenwood [5] and the experimental results published by Békésy in 1960 [17]. The straight-isotropic model was considered in the tuning process. The mechanical properties of the remaining models were derived after this calibration. Figure 2.2 shows the comparison between the results of the present study and the experimental

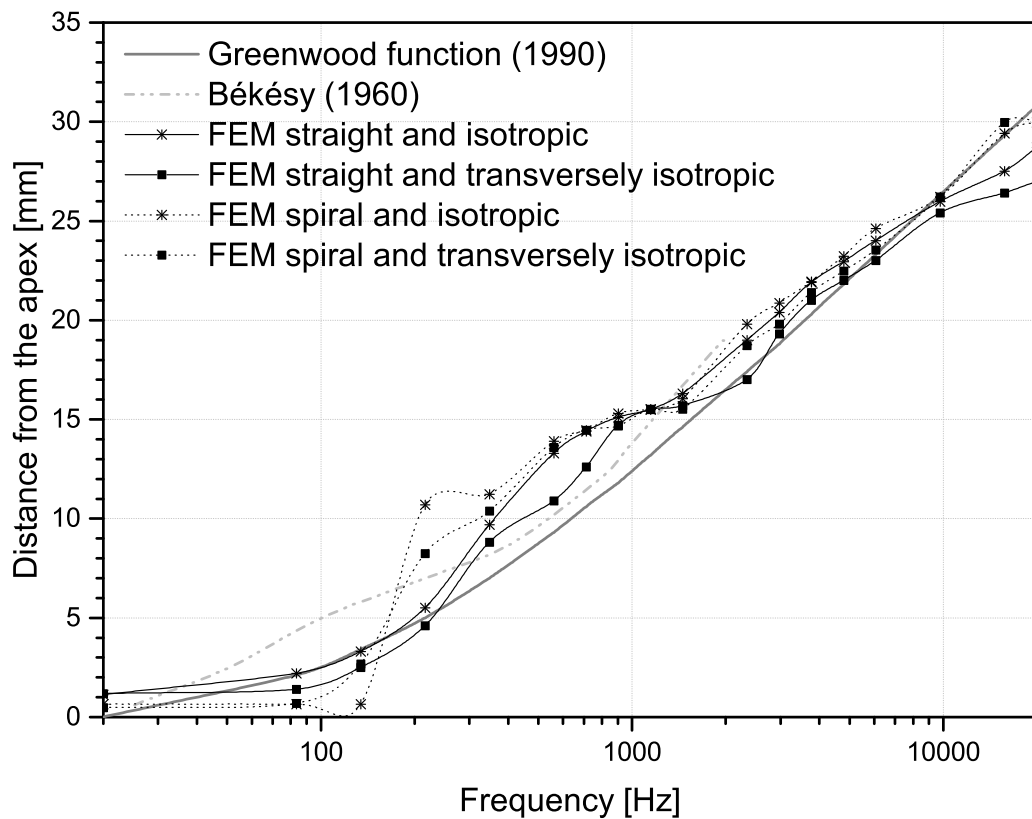


Figure 2.2: Place of the maximum response on the basilar membrane vs frequency.

data available in the literature.

The results show that when the spiral model is considered with isotropic properties in the basilar membrane, the cochlear-map diverges from the experimental data, mainly at frequencies below 1 kHz (Root-mean-square error - RMSE: 3.68 mm and 2.50 mm for spiral-isotropic and straight-isotropic model, respectively; see Table 2.4). This divergence is less pronounced when the basilar membrane was considered with transversely isotropic properties in both straight and spiral cochleae. Thus, using transversely isotropic mechanical properties, there is an approximation of the cochlear map to the Greenwood function in both straight and spiral models. Through a comparison between both cochlear shapes, the results suggest that the curvature of the cochlea has an influence in the location of maximum displacement, since the larger differences appear where the cochlea curvature is more pronounced (at the base and at the apex, however, less pronounced at the apex). In order to quantify this comparison, the RMSE was also calculated and the following values were obtained: 2.05 mm, 1.70 mm, 2.72 mm, 2.08 mm, for the straight-isotropic, straight-transversely isotropic, spiral-isotropic and spiral-transversely isotropic model, respectively (see Table 2.4). The lower value was obtained for the straight-transversely isotropic model, since it was the model (straight-isotropic) used initially to calibrate the mechanical properties. However, using the spiral model, a more accentuated drop of the RMSE was obtained, thus showing a faster approximation of the model to the Greenwood function. The Table 2.4 also shows the MAE (Mean absolute error), since the RMSE emphasizes greater errors than the small ones and is it more sensitive to the presence of false data, as mentioned by Kavuncuoglu et al. [33]. Through the Table 2.4, it is possible to check that the MAE values, which gives the same weight to all errors

Table 2.4: Values of RMSE and MAE for three different frequency ranges: 20 Hz - 20 kHz, 20 Hz - 1 kHz and 1 kHz - 20 kHz

		<i>straight-isotropic</i>	<i>straight-transversely isotropic</i>	<i>spiral-isotropic</i>	<i>spiral-transversely isotropic</i>
RMSE [mm]	20Hz - 20kHz	2.05	1.70	2.72	2.08
	20Hz - 1kHz	2.50	1.61	3.68	2.86
	1kHz - 20kHz	1.60	1.76	1.58	1.10
MAE [mm]	20Hz - 20kHz	1.69	1.36	2.24	1.63
	20Hz - 1kHz	1.94	1.43	3.33	2.52
	1kHz - 20kHz	1.49	1.30	1.37	0.92

shows the same trend as RMSE.

The obtained results are in good agreement with the study of Steele et al. [16] that did not find differences between the straight and spiral model between 1 kHz and 10 kHz. On frequencies higher than 1 kHz the values of RMSE were 1.60 mm, 1.76 mm, 1.58 mm and 1.10 mm, for the straight-isotropic, straight-transversely isotropic, spiral-isotropic and spiral-transversely isotropic model, respectively.

As shown in the Figure 2.3, it is perceptible that at low frequencies the maximum displacement appears near the apex and at higher frequencies, higher amplitudes of displacements are obtained close to the base of the cochlea. It is also possible to verify that the travelling wave becomes sharper and narrower when the frequency increases, as showed by Gan et al. [18]. Another characteristic of the travelling wave is the presence of variations in the wavelength along the cochlea. The travelling wave has a long wavelength near the stapes. As the distance to the stapes increases, the displacement amplitude of the basilar membrane increases until the maximum

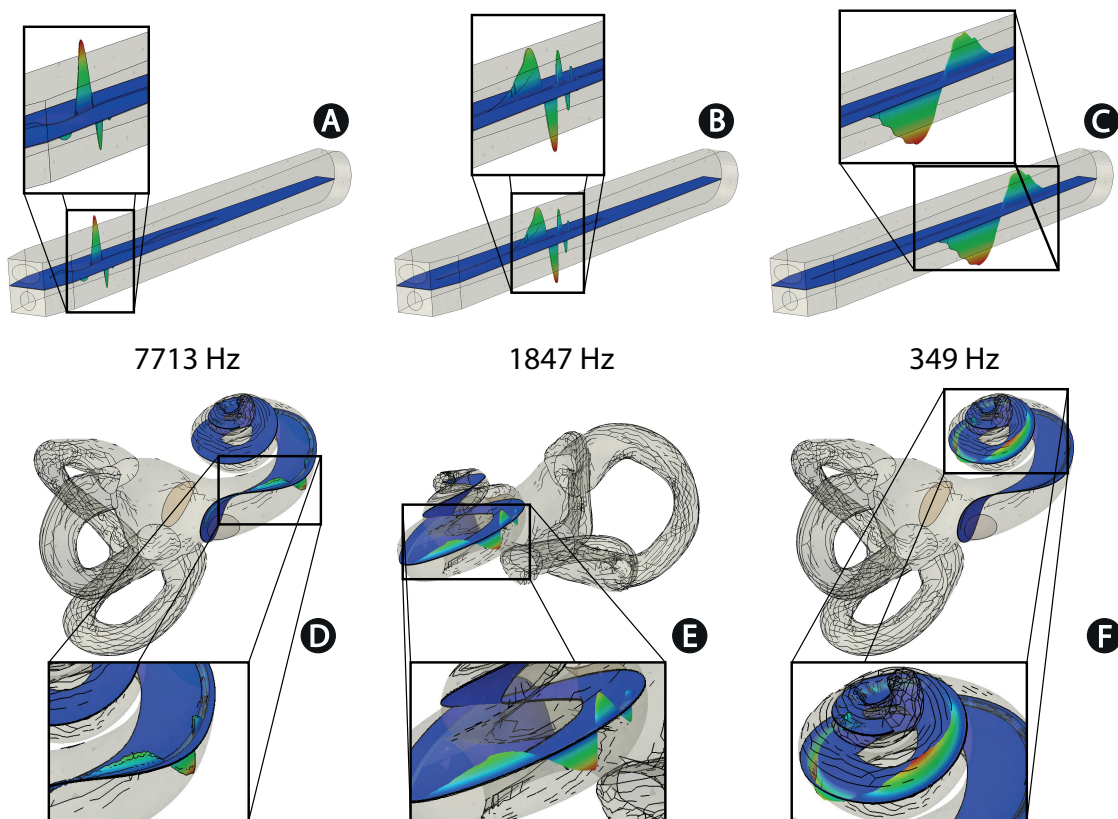


Figure 2.3: Basilar membrane displacement between the straight and isotropic model, and the spiral and transversely isotropic model for three frequencies (7713 Hz (A, D); 1847 Hz (B, E); 349 Hz (C, F)) and an 80 dB SPL.

is reached, at the same time the wavelength becomes shorter. The traveling wave disappears after the peak with a very short wavelength, as stated by Puria and Steele [34]. Such pattern demonstrates the standard wave behavior fundamental for the frequency sensitivity in the cochlea, first described by Békésy [17] and numerically studied by many researchers [18, 35, 26].

To further study the behavior of the basilar membrane, the displacement of the basilar membrane at 12 mm from the stapes, was normalized with respect to the stapes displacement and represented in terms of magnitude and phase angle in Figure 2.4 and Figure 2.5, respectively. The magnitude expressed in dB is calculated through the Equation 2.5.

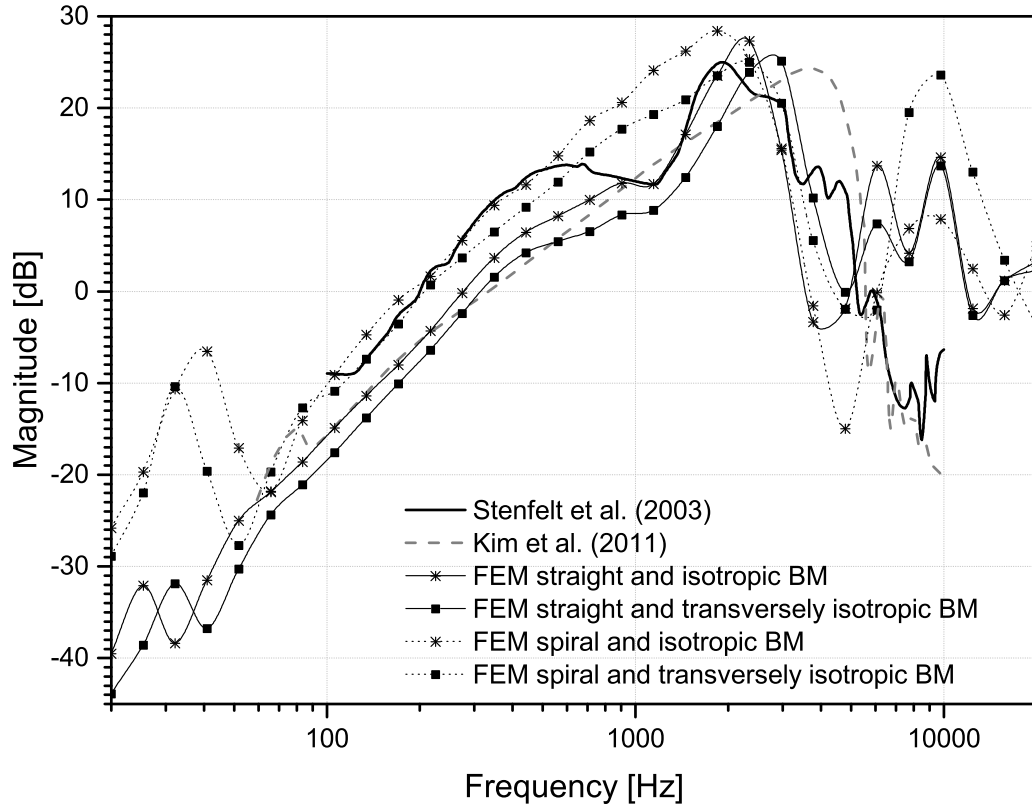


Figure 2.4: Magnitude of the displacement of the basilar membrane at 12 mm from the stapes normalized with respect to the stapes displacement.

$$\text{Magnitude [dB]} = 20 \log \frac{\text{Basilar membrane displacement}}{\text{Reference displacement}} \quad (2.5)$$

The results obtained from the straight and spiral model with isotropic and transversely isotropic properties were compared with experimental data, measured from seven temporal bones specimens and published by Stenfelt et al. [36], and also with the numerical model of Kim et al. [37] composed by the middle ear and a simplified straight cochlea (in both references the results were obtained at 12 mm from the stapes). The results obtained are in a good agreement with the literature mainly at middle frequencies. Some inconsistency is noticeable at the characteristic frequency magnitude peak. This difference can be attributed to imprecision in the basilar membrane definition, leading to small variations in the location of the characteristic

frequency. The results show a resonance near 2 kHz and thereafter a sharp drop, marking the ending of the travelling wave. The response of the basilar membrane in the straight model is similar between the models with isotropic and transversely isotropic mechanical properties. However, in the spiral model the differences are more pronounced and appear at lower frequencies ( $<100$  Hz) and at higher frequencies ( $>4$  kHz).

The phase angle of the basilar membrane at 12 mm (Figure 2.5) is almost constant and in phase with the stapes footplate until the characteristic frequency magnitude peak is reached. After the peak, the phase angle shows a fast decrease showing the presence of the travelling wave. All numerical models showed similar behavior.

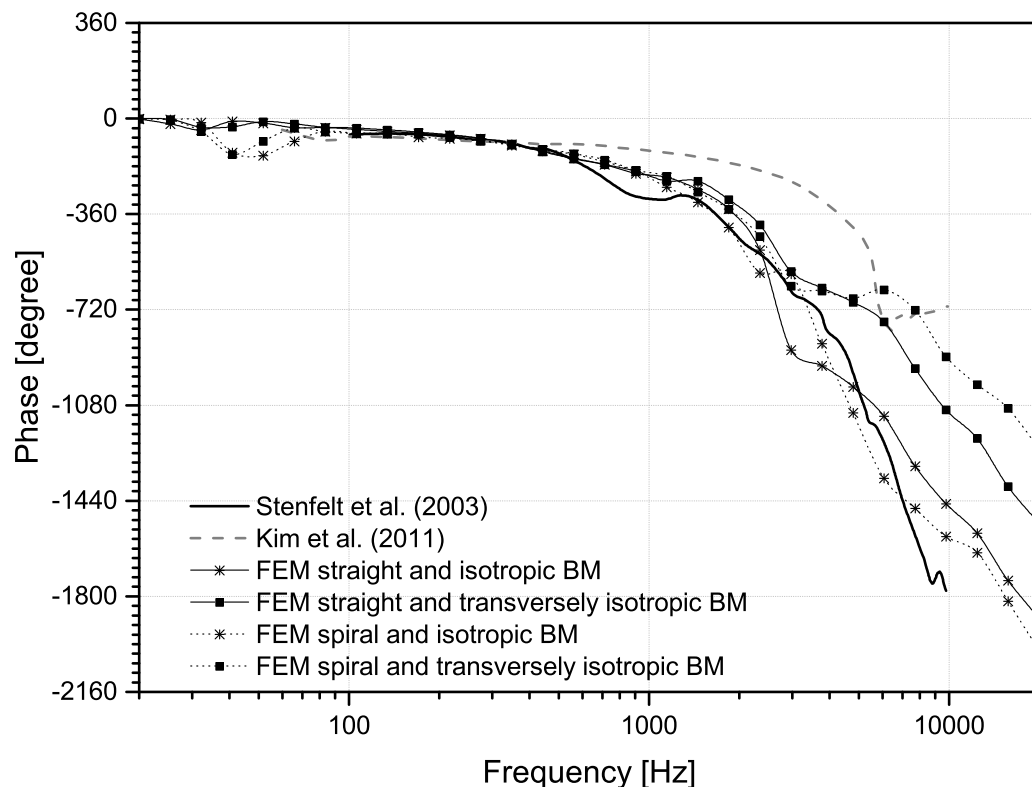


Figure 2.5: Phase of the displacement of the basilar membrane at 12 mm from the stapes normalized with respect to the stapes displacement.

Figure 2.6 shows the magnitude of the displacement of the basilar membrane

at 12 mm from the stapes using as reference 0.1 nm, rather the displacement of the stapes. The results were compared with the experimental data of Gundersen et al. [38] and the numerical data of Gan et al. [18]. As can be seen from Figure 2.6 the results obtained are in agreement with the literature, mainly at higher frequencies. However, it should be noted that in Figure 2.4 such particularity did not happen. This discrepancy can be attributed to the lack of the middle ear, thus the motion of the stapes may be affected and partially modified, forcing the stapes to vibrate in a different mode. The models developed in this work only consider the stapes footplate and the stapedial annular ligament, the acoustic pressure was applied on these structures.

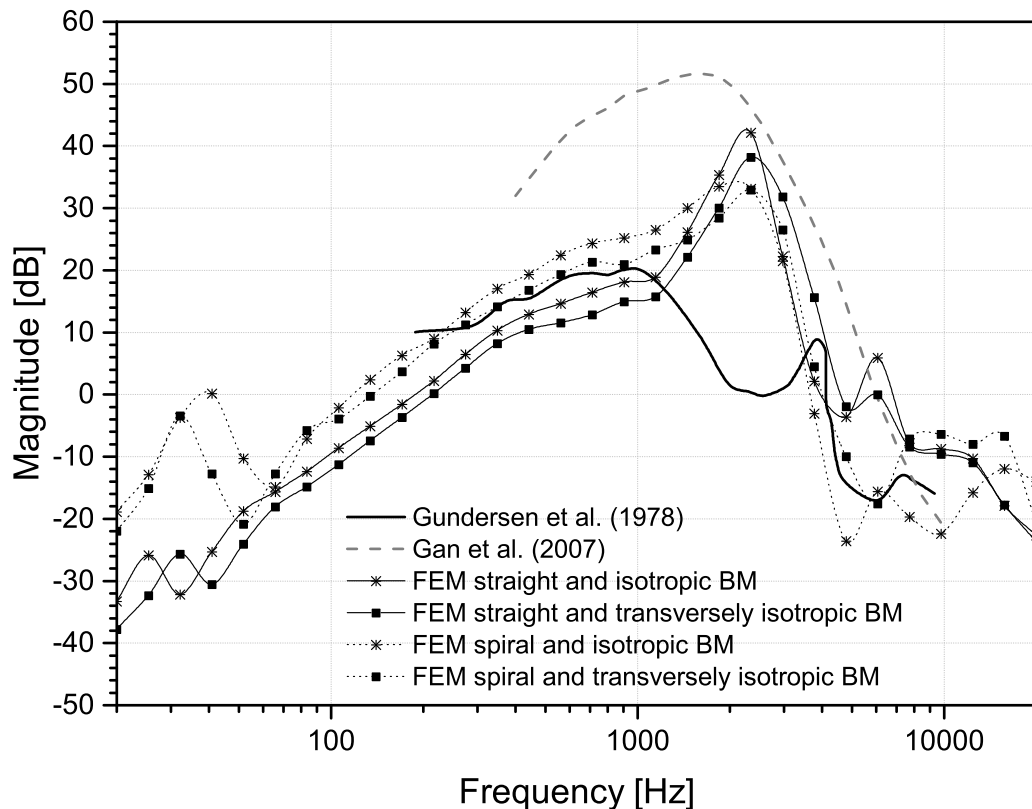


Figure 2.6: Magnitude of the displacement of the basilar membrane at 12 mm from the stapes using 0.1 nm as reference.

## 2.6 Conclusions

The 3D-finite element models allowed to evaluate the passive mechanical behavior of the human cochlea. The numerical results showed that both the straight and spiral model provides a good definition of the cochlear mapping when the basilar membrane was considered with transversely isotropic properties. When isotropic properties were applied in the basilar membrane of the spiral model, the maximum deviation was registered at lower frequencies, possible due to the high curvature of the scalae near the apex, since this did not happen in the straight model. It is known that the basilar membrane presents in its composition compact bundles of small collagenous filaments aligned mainly in radial orientation, it is then important to consider such characteristic using transversely isotropic properties. All models reproduced the magnitude and phase of the basilar membrane at 12 mm from the stapes. However the 3D model has some limitations. The dimensions of the basilar membrane were based in a numeric study, although, an experimental study could be used instead [39]. Besides the previously mentioned, other simplifications, such as, the use of an inviscid fluid, the non consideration of the scala media and the Reissner's membrane were considered in our numeric study. The group intends now to develop a novel sensitivity study in order to conclude the influence of each parameter in the basilar membrane response.

## 2.7 Conflict of interest statement

The authors declare that there is no financial, professional or other personal interest of any nature or kind in any product, service and/or company that could be constructed as influencing the position.



## 2.8 Acknowledgements

The authors truly acknowledge the funding provided by Ministério da Ciência, Tecnologia e Ensino Superior - Fundação para a Ciência e a Tecnologia (Portugal), under grant: SFRH/BD/129397/2017. This research was also supported by the Portuguese Foundation of Science and Technology under the research project UIDB/50022/2020.

## 2.9 References

- [1] WHO. *Global estimates on prevalence of hearing loss*, 2018 (accessed January 5, 2021). <http://www.who.int/deafness/Global-estimates-on-prevalence-of-hearing-loss-Jul2018.pptx>.
- [2] J. Lohler, L. E. Walther, F. Hansen, P. Kapp, J. Meerpohl, B. Wollenberg, R. Schonweiler, and C. Schmucker. The prevalence of hearing loss and use of hearing aids among adults in germany: a systematic review. *European Archives of Oto-Rhino-Laryngology*, 276(4):945–956, 2019.
- [3] Aage R. Møller. *Hearing : anatomy, physiology, and disorders of the auditory system*. Academic Press, Amsterdam ; Boston, 2nd edition, 2006.
- [4] L. Robles and M. A. Ruggero. Mechanics of the mammalian cochlea. *Physiological reviews*, 81:1305–52, 2001.
- [5] Donald D. Greenwood. Critical bandwidth and the frequency coordinates of the basilar membrane. *The Journal of the Acoustical Society of America*, 33(10):1344–1356, 1961.
- [6] J. J. Guinan, A. Salt, and M. A. Cheatham. Progress in cochlear physiology after bekesy. *Hearing Research*, 293(1-2):12–20, 2012.
- [7] D. D. Greenwood. A cochlear frequency-position function for several species - 29 years later. *Journal of the Acoustical Society of America*, 87(6):2592–2605, 1990.
- [8] J. Meng, S. Li, F. Zhang, Q. Li, and Z. Qin. Cochlear size and shape variability and implications in cochlear implantation surgery. *Otol Neurotol*, 37(9):1307–13, 2016.

- [9] D. Manoussaki, R. S. Chadwick, D. R. Ketten, J. Arruda, E. K. Dimitriadis, and J. T. O'Malley. The influence of cochlear shape on low-frequency hearing. *Proceedings of the National Academy of Sciences of the United States of America*, 105(16):6162–6166, 2008.
- [10] Richard Chadwick, Daphne Manoussaki, Emiliios Dimitriadis, B. Shoelson, Darlene Ketten, J. Arruda, and Malley. Cochlear coiling and low-frequency hearing. In *Auditory Mechanisms: Processes and Models*, 2006.
- [11] I. S. Ritsche, J. M. Fahlke, F. Wieder, A. Hilger, I. Manke, and O. Hampe. Relationships of cochlear coiling shape and hearing frequencies in cetaceans, and the occurrence of infrasonic hearing in miocene mysticeti. *Foss. Rec.*, 21(1):33–45, 2018.
- [12] D. Manoussaki, E. K. Dimitriadis, and R. S. Chadwick. Cochlea's graded curvature effect on low frequency waves. *Physical Review Letters*, 96(8), 2006.
- [13] M. Pietsch, L. A. Davila, P. Erfurt, E. Avci, T. Lenarz, and A. Kral. Spiral form of the human cochlea results from spatial constraints. *Scientific Reports*, 7, 2017.
- [14] D. Manoussaki and R. S. Chadwick. Effects of geometry on fluid loading in a coiled cochlea. *Siam Journal on Applied Mathematics*, 61(2):369–386, 2000.
- [15] Liu-Jie Ren, Cheng Hua, Guang-Hong Ding, Lin Yang, Pei-Dong Dai, and Tian-Yu Zhang. Three-dimensional finite element hydrodynamical modeling of straight and spiral cochlea. *AIP Conference Proceedings*, 1965(1):030003, 2018.
- [16] C. R. Steele and J. G. Zais. Effect of coiling in a cochlear model. *Journal of the Acoustical Society of America*, 77(5):1849–1852, 1985.

- [17] Georg Von Békésy. *Experiments in hearing*. McGraw-Hill series in psychology. McGraw-Hill, New York,, 1960.
- [18] Rong Z. Gan, Brian P. Reeves, and Xuelin Wang. Modeling of sound transmission from ear canal to cochlea. *Annals of Biomedical Engineering*, 35:2180–2195, 2007.
- [19] Lifu Xu, Xinsheng Huang, Na Ta, Zhushi Rao, and Jiabin Tian. Finite element modeling of the human cochlea using fluid-structure interaction method. *Journal of Mechanics in Medicine and Biology*, 15:1550039, 2015.
- [20] Frank Böhnke and Arnold Wolfgang. 3d-finite element model of the human cochlea including fluid-structure couplings. *ORL*, 61:305–310, 1999.
- [21] Wenjuan Yao, Yiqiang Chen, Jianwei Ma, Chaosun Gan, and Dejiang Wang. Numerical simulation on the dynamic behavior of the basilar membrane in the spiral cochlea. *Biomedical Research*, 27:977–984, 2016.
- [22] Annalisa De Paolis, Marom Bikson, Jeremy T. Nelson, J. Alexander de Ru, Mark Packer, and Luis Cardoso. Analytical and numerical modeling of the hearing system: Advances towards the assessment of hearing damage. *Hearing Research*, 349:111–128, 2017.
- [23] Yao Wen-juan, Ma Jian-wei, and Hu Bao-lin. Numerical model on sound-solid coupling in human ear and study on sound pressure of tympanic membrane. *Mathematical Problems in Engineering*, 2011:282696, 2011.
- [24] Konrad Kamieniecki, Janusz Piechna, and Pawel Borkowski. Basilar membrane vibration in time domain predicted by fluid–structure interaction model in pre- and post-stapedotomy state. *Procedia IUTAM*, 24:48–63, 2017.

- [25] S. Liu and R. D. White. Orthotropic material properties of the gerbil basilar membrane. *J Acoust Soc Am*, 123(4):2160–71, 2008.
- [26] Monika Kwacz, Piotr Marek, Paweł Borkowski, and Wiktor Gambin. Effect of different stapes prostheses on the passive vibration of the basilar membrane. *Hearing Research*, 310:13–26, 2014.
- [27] Jong-Hoon Nam, Yanju Liu, and Sheryle M. Gracewski. A computational study on traveling waves in the gerbil cochlea generated by electrical impulse. *AIP Conference Proceedings*, 1703(1):070004, 2015.
- [28] Dassault Systemes. *ABAQUS analysis user's guide*. 2016.
- [29] Bruno Areias, Carla Santos, Renato M Natal Jorge, Fernanda Gentil, and Marco Pl Parente. Finite element modelling of sound transmission from outer to inner ear. *Proceedings of the Institution of Mechanical Engineers. Part H, Journal of engineering in medicine*, 230:999–1007, 2016.
- [30] Q. Sun, R. Z. Gan, K.-H. Chang, and K. J. Dormer. Computer-integrated finite element modeling of human middle ear. *Biomechanics and modeling in mechanobiology*, 1:109–22, 2002.
- [31] F. Gentil, M. Parente, P. Martins, C. Garbe, R. N. Jorge, A. Ferreira, and João Manuel R. S. Tavares. The influence of the mechanical behaviour of the middle ear ligaments: a finite element analysis. *Proceedings of the Institution of Mechanical Engineers. Part H, Journal of engineering in medicine*, 225:68–76, 2011.

- [32] R. Z. Gan, F. Yang, X. Zhang, and D. Nakmali. Mechanical properties of stapedial annular ligament. *Med Eng Phys*, 33(3):330–9, 2011.
- [33] H. Kavuncuoglu, E. Kavuncuoglu, S. M. Karatas, B. Benli, O. Sagdic, and H. Yalcin. Prediction of the antimicrobial activity of walnut (*juglans regia* L.) kernel aqueous extracts using artificial neural network and multiple linear regression. *J Microbiol Methods*, 148:78–86, 2018.
- [34] Sunil Puria and Charles Steele. Mechano-acoustical transformations. In *The Senses: A Comprehensive Reference*, 2008.
- [35] C. R. Steele. Toward three-dimensional analysis of cochlear structure. *Orl-Journal for Oto-Rhino-Laryngology and Its Related Specialties*, 61(5):238–251, 1999.
- [36] S. Stenfelt, S. Puria, N. Hato, and R. L. Goode. Basilar membrane and osseous spiral lamina motion in human cadavers with air and bone conduction stimuli. *Hearing Research*, 181(1-2):131–143, 2003.
- [37] N. Kim, K. Homma, and S. Puria. Inertial bone conduction: Symmetric and anti-symmetric components. *Jaro-Journal of the Association for Research in Otolaryngology*, 12(3):261–279, 2011.
- [38] T. Gundersen, O. Skarstein, and T. Sikkeland. A study of the vibration of the basilar membrane in human temporal bone preparations by the use of the mossbauer effect. *Acta Otolaryngol*, 86(3-4):225–32, 1978.

- [39] K. A. Bhatt, M. C. Liberman, and Jr. Nadol, J. B. Morphometric analysis of age-related changes in the human basilar membrane. *Ann Otol Rhinol Laryngol*, 110(12):1147–53, 2001.





## Chapter 3

# A finite element model to predict the consequences of endolymphatic hydrops in the basilar membrane



**Article 2 - A finite element model to predict the  
consequences of endolymphatic hydrops in the basilar  
membrane**

B. Areias (1), M.P.L. Parente (1,2), F. Gentil (3), C. Carocha (4), J. Paço (4),  
R.M. Natal Jorge (1,2)

1-INEGI, Institute of science and innovation in mechanical and industrial  
engineering, Porto, Portugal {bareias@fe.up.pt}

2-FEUP, Faculty of Engineering, University of Porto, Porto, Portugal  
{mparente@fe.up.pt, rnatal@fe.up.pt}

3-Escola Superior de Saúde - Politécnico do Porto; Clínica ORL – Dr. Eurico de  
Almeida; WIDEX {fernanda.fgnanda@gmail.com}

4-Núcleo académico-clínico de otorrinolaringologia e cirurgia cervico-facial do  
Hospital CUF Tejo/ NOVA Medical School, Universidade Nova de Lisboa, Lisboa,  
Portugal {cristinacaroca@icloud.com, joao.paco@nms.unl.pt}

*Published in: International Journal for Numerical Methods in Biomedical*

*Engineering, 2021*

*doi: 10.1002/cnm.3541*

This chapter is devoted to the study of the effect of endolymphatic hydrops on the inner ear structures, more precisely on the BM. Using the finite element method, the work intends to increase the knowledge of the endolymphatic hydrops and consequently the Ménière's disease and its influence on the BM.



### **3.1 Abstract**

Ménière's disease is an inner ear disorder, associated with episodes of vertigo, fluctuant hearing loss, tinnitus, and aural fullness. Ménière's disease is synonymous with idiopathic endolymphatic hydrops. Clinical evidences show that this disease is often incapacitating, negatively affecting the patients' everyday life. The pathogenesis of Ménière's disease is still not fully understood and remains unclear.

Previous numerical studies available in the literature related with endolymphatic hydrops, are very scarce. The present work applies the finite element method to investigate the consequences of endolymphatic hydrops in the normal hearing, caused by the Ménière's disease.

The obtained results for the steady state dynamics analysis are in accordance with clinical evidences. The results show that the basilar membrane is not affected in the same intensity along its length and that the lower frequencies are more affected by the endolymphatic hydrops. From a clinical point of view, this work shows the relationship between the increasing of the endolymphatic pressure and the development of hearing loss.

### **3.2 Keywords**

cochlea, Ménière's disease, basilar membrane, hearing, endolymphatic hydrops

### 3.3 Introduction

In 1861, the French physician Prosper Ménière described, for the first time, a series of symptoms present in patients, caused by the inner ear, which became known as the Ménière's disease [1, 2]. The diagnostic criteria of the Ménière's disease includes spontaneous episodes of vertigo, tinnitus, and fluctuating hearing loss. The presence of hearing loss during an episode of vertigo has been a key factor for the accurate diagnosis, as stated by Baloh [3].

The inner ear is situated in the petrous part of the temporal bone. It consists of the bony and membranous labyrinth filled with perilymph and endolymph, respectively. The bony labyrinth is lined by endosteum and contains in its interior the suspended membranous labyrinth [5]. There are three longitudinal channels within the cochlea, the scala vestibuli, the scala tympani and a distinct channel, the scala media (Figure 3.1). The scala vestibuli and tympani communicate with each other at the helicotrema. The scala media is positioned between the other two, it is closed and ends at the apex. Two elastic membranes form the upper and lower boundary of the

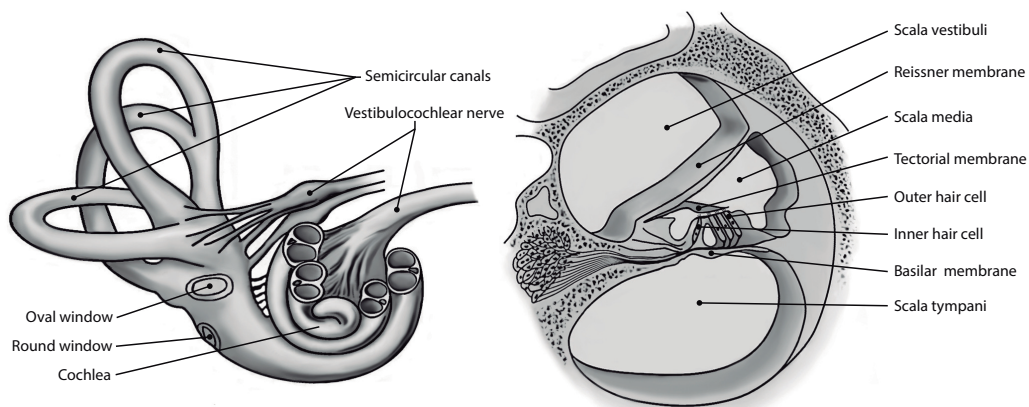


Figure 3.1: Anatomy of the human inner ear, adapted from Neuroscience by Purves [4].

scala media, and separate it from the other scalae. The Reissner's membrane is a thin membrane that separates the scala media from the scala vestibuli. On the other side, the basilar membrane forms the partition between the scala media and the scala tympani, having more relevance to the auditory system [6, 7]. In a healthy person, the endolymphatic and the perilymphatic pressure is equal and subjected to the same fluctuations [8, 9]. Therefore, if the differential pressure between the endolymph and perilymph is different from zero, a deformation of the flexible structures, including the basilar membrane is expected. This deformation tends to decrease the compliance of the basilar membrane, leading to a change in the natural frequency of its components and, in turn, the response of the auditory system [10]. In some cases, the differential pressure results in the rupture of the membrane. The presence of herniations and scarring due to prior ruptures as mentioned by Schuknecht and Gulya [11]. Rupture of the membrane may contribute to episodic vertigo symptoms and other functional changes in the inner ear [12]. Endolymphatic hydrops is a disorder of the inner ear and consists of an excessive build-up of endolymph fluid volume and pressure. Ménière's disease is synonymous with a spontaneous development of endolymphatic hydrops, without a known cause [12, 13].

In 1938, Hallpike and Cairns [10] reported a study of two cases that are currently considered key points of the Ménière's disease. In his study, the dilatation of the endolymphatic system that affects the scala media and the saccule, and the degeneration of the Corti's organ was observed. According to Olivetto et al. [14], Ménière's disease often affects only one ear, but the cases of bilateral disease are not rare. There are no differences with respect to gender, as mentioned by Vassiliou et al. [15]. In Finland, the prevalence of the disease is at least 43 per 100 000 population

[16]. Another study held in southern Finland showed a peak prevalence of 1709 per 100 000 in elderly people, aged between 61 - 70 years [17]. Many authors state that the Ménière's disease prevalence seems to increase with age and the onset of symptoms appears around the third and fourth decade of life [15, 17, 18, 19].

The study of Havia et al. [17] showed a decrease in the prevalence of the Ménière's disease in the older age groups, justifying such occurrence by the fact that some individuals with Ménière's disease have been excluded from the study by their numerous other diseases and symptoms, such as brain ischemia.

A large number of factors have been suggested as the cause for the development of endolymphatic hydrops. Paparella [20] and Merchant et al. [21] refer to causes such as the decreased endolymph absorption by the endolymphatic sac, the excessive endolymph production, genetic abnormalities, ionic imbalance (especially of sodium chloride), viral infections, autoimmune reactions, vascular irregularities, allergic responses, hypocellularity of the mastoid and penaqueductal air cells among others. For the majority of the patients, the current treatment of this disease includes drug therapies and lifestyle modifications. For rare cases, surgical treatments are applied. As stated by Haijin et al. [22], drugs therapies are based in hydrochlorothiazide, potassium chloride sustained-release and betahistine. Restrictions on consumption of salt, nicotine and alcohol intake are part of lifestyle modifications.

According Classification Committee of the Barany Society in cooperation with several national and international organizations and AAO-HNS Equilibrium Committee, Ménière disease was recently classified in definitive diagnosis and probable diagnosis depending on clinical appearance. The clinical course usually is progressive and fluctuates unpredictably, where treatment is a challenge. The diagnostic criteria



for definitive Ménière disease are based on two or more spontaneous attacks of vertigo, each lasting 20 minutes to 12 hours; audiometrically documented fluctuating low- to mid-frequency sensorineural hearing loss in the affected ear on at least 1 occasion before, during, or after 1 of the episodes of vertigo; fluctuating aural symptoms (hearing loss, tinnitus, or fullness) in the affected ear. Probable Ménière disease may be diagnosed based an occurrence of at least 2 episodes of vertigo or dizziness lasting 20 minutes to 24 hours; fluctuating aural symptoms (hearing loss, tinnitus, or fullness) in the affected ear; other causes excluded by other tests [23].

Therefore, in order to improve current treatments, it is important to understand the effects of the endolymphatic hydrops in the inner ear, more precisely in the basilar membrane.

Using the finite element method, the present work intends to increase the knowledge of the endolymphatic hydrops and consequently the Ménière's disease and its influence on the basilar membrane. With the finite element method, it is possible to obtain a quantitative response on how the basilar membrane is affected along its length and what are the audible frequencies more affected by the endolymphatic hydrops. Unlike already published works in literature, the present study applies an exponential approach to the mechanical properties of the basilar membrane and employs a cochlear spiral shape based on magnetic resonance images.

### **3.4 Materials and Methods**

The human cochlea has an intricate spiral shape (Figure 3.2). This anatomical geometry was considered on our work and was obtained from a set of MRI images of a male patient, without cochlear pathologies. The width and thickness of the basilar

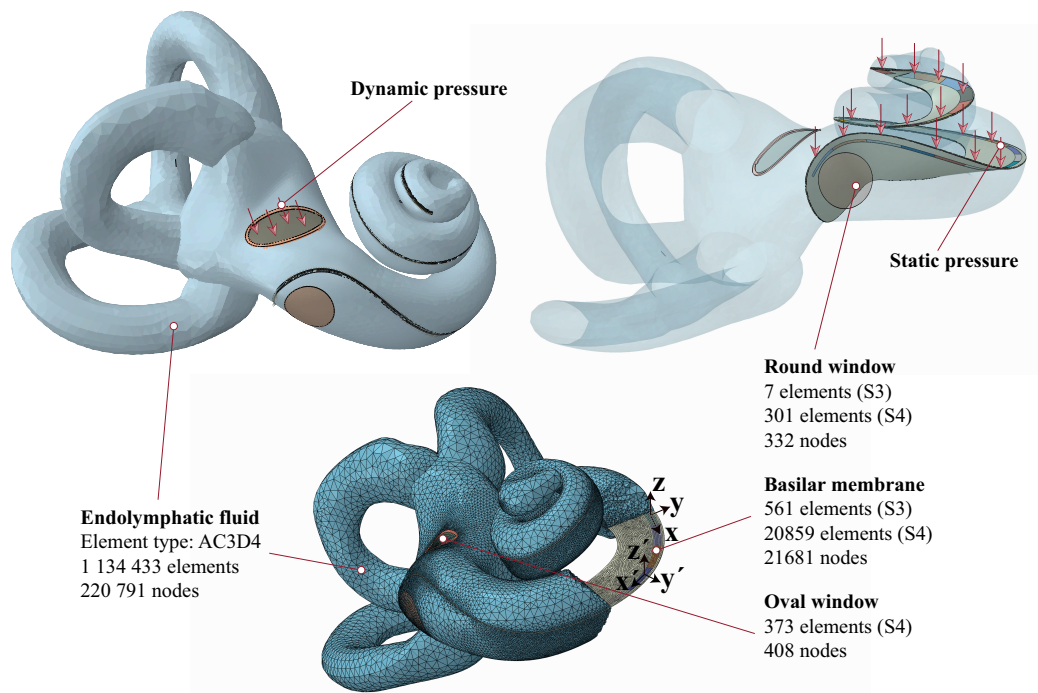


Figure 3.2: 3D finite model of the inner ear. Red arrows show the location and direction of the static and dynamic pressure. Finite element mesh characterization of all parts.

membrane were acquired in the literature and assumed to change linearly from  $100\ \mu\text{m}$  at the base to  $500\ \mu\text{m}$  at the apex, and from  $7.5\ \mu\text{m}$  to  $2.5\ \mu\text{m}$  along the longitudinal direction, respectively [24, 25]. The basilar membrane was considered with 31mm in length. The review work of Koch et al. [26] is based on a set of 15 published works (1884 - 2016) which addresses the various techniques used to calculate the cochlear duct length. The length of the basilar membrane considered in our work is in concordance with all methods studied by the cited study, direct (28.0 – 40.1), indirect (24.0 – 36.4), 3d reconstruction (29.7 – 38.9) and spiral coefficients (29.07 – 37.45).

The basilar membrane was divided along its length into equal parts. The length of each part was considered approximately 1 mm (see Figure 3.3). The shell elements (S4) used in the basilar membrane mesh have a characteristic length of 0.05mm

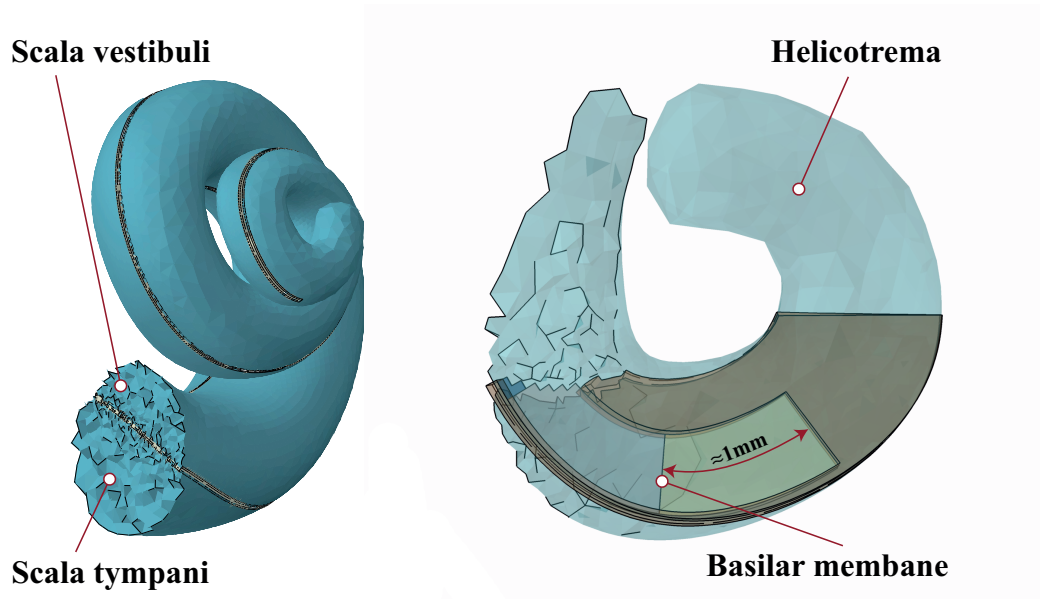


Figure 3.3: 3D finite model of the inner ear. Detail of the scala vestibuli, the scala tympani, and the helicotrema.

which provides a good accuracy. The division in parts enabled to impose the gradient of stiffness along the basilar membrane length, which is responsible for the frequency-place map of the cochlea, known as cochlear map. The scala media and the Reissner's membrane were not considered in our work. The helicotrema allows the communication between the scala vestibuli and tympani, see Figure 3.3. As the cochlear map follows an exponential evolution [27], it was then assumed, based on the work of Emadi et al. [28] that the mechanical properties should also vary in an exponential way. Thus, two exponential equations (Equation 3.1 and 3.2) were formulated in order to describe the evolution of the Young's modulus,  $E_y$ , and the Rayleigh damping coefficient,  $\beta$ , along the basilar membrane. Both equations were determined through a calibration process, using with a sequence of numerical simulations in order to approximate the cochlear map obtained to the function proposed by Greenwood [27].

$$\beta \text{ [s]} = 2 \times 10^{-6} e^{0.14x} \quad 0 < x < 31\text{mm} \quad (3.1)$$

$$E_y \text{ [MPa]} = -2.3e^{\frac{x}{12.2}} + 32 \quad 0 < x < 31\text{mm} \quad (3.2)$$

In contrast to the Equation 3.1 and 3.2, the Equation 3.3 and 3.4 use the distance,  $x_p$ , expressed as a proportion of the basilar membrane length from the round window, ranging between 0 and 1.

$$\beta \text{ [s]} = 2 \times 10^{-6} e^{4.34x_p} \quad 0 < x_p < 1 \quad (3.3)$$

$$E_y \text{ [MPa]} = -2.3e^{2.54x_p} + 32 \quad 0 < x_p < 1 \quad (3.4)$$

The basilar membrane was modelled under plane stress conditions with shell elements. The Young's modulus in the transverse direction of the basilar membrane (direction of the radial fibers [29, 30]) was defined by Equation 3.2. The distance,  $x$ , represents the distance from the base of the cochlea to the point of interest on the basilar membrane, expressed in mm. The longitudinal Young's modulus,  $E_x$ , expressed in MPa is then obtained through the equation  $10E_x = E_y$ . The basilar membrane was modelled with orthotropic properties, for which the following relations can be established,

$$G_{xy} = G_{yz} \quad (3.5)$$

$$G_{xz} = \frac{E_x}{2(1 + \nu_{xz})} \quad (3.6)$$

The shear modulus,  $G_{xy}$ , is related with  $E_y$  using Equation 3.7 [31, 32].

$$G_{xy} = \frac{E_y}{2} \quad (3.7)$$

The Poisson's ratio was assumed after a series of iterations as  $\nu_{xy} = \nu_{yz} = 0.2$  and  $\nu_{xz} = 0.3$  in order to comply with the material stability requirements and also to achieve a cochlear map comparable to the Greenwood function. The density of the basilar membrane was considered to be  $1200 \text{ kg m}^{-3}$  and to be constant along its length. The perilymph was simulated considering water properties ( $K=2200 \text{ MPa}$ ,  $\rho = 1000 \text{ kg m}^{-3}$  and inviscid). The Young's modulus, the Poisson's ratio and the density of the oval window and round window are summarized in the Table 3.1. As boundary conditions, the free edges of the oval window, the round window and the basilar membrane were considered fixed in all degree of freedom. The surfaces of the acoustic elements which contact the endosteum were considered as stationary rigid walls. The constructed 3D model was simplified, with only the passive mechanism being considered.

The 3D finite element model is composed by 243 212 nodes and 1 156 534 elements. Acoustic elements were used to model the perilymph. A dynamic load of  $0.2 \text{ Pa}$  (80 dB SPL) was applied to the stapes footplate in all numerical simulations (see Figure 3.2). The frequency band between 100 Hz and 10 kHz was considered in this study. The static pressure (see Figure 3.2) which allows to simulate the endolymphatic hydrops

Table 3.1: Mechanical properties of the inner ear parts (Young's modulus, Poisson's ratio and density)

Inner ear parts		$E$ [MPa]	$\nu$ [-]	$\rho$ [kg m <sup>-3</sup> ]
Oval window	Stapes footplate [33, 34, 35]	14100	0.3	2500
	Stapedial annular ligament [33, 36]	0.6		1200
	Round window [24]	0.35		1200

at two different stages was set at 67 Pa and 130 Pa. This pressure differential between both scalae were replaced by a mechanic pressure applied at the basilar membrane on the scala vestibuli side. A nonlinear static analysis was carried out at the first step to apply the static pressure. This step is followed by a steady state dynamic analysis that provides the steady state amplitude and phase of the response due to harmonic excitation at a given frequency. Both analysis were carried out using the commercial software Abaqus Standard [37].

In a linear elastic material behaviour, the total stress,  $\boldsymbol{\sigma}$ , is related to the total elastic strain,  $\boldsymbol{\varepsilon}^{el}$ , through the elasticity tensor,  $\mathbf{D}^{el}$ , as follows.

$$\boldsymbol{\sigma} = \mathbf{D}^{el} \boldsymbol{\varepsilon}^{el} \quad (3.8)$$

In order to define an orthotropic material subdivided with shell elements under plane stress conditions, only the values  $E_x$ ,  $E_y$ ,  $\nu_{xy}$ ,  $G_{xy}$ ,  $G_{xz}$  and  $G_{yz}$  are needed. The shear moduli  $G_{xz}$  and  $G_{yz}$  are listed because may be required for modeling the transverse shear deformation in a shell. Thus the elasticity tensor can be defined by the Equation 3.9.

$$\mathbf{D}^{el} = \begin{bmatrix} \frac{1}{E_x} & -\frac{\nu_{xy}}{E_x} & 0 \\ -\frac{\nu_{xy}}{E_x} & \frac{1}{E_y} & 0 \\ 0 & 0 & \frac{1}{G_{xy}} \end{bmatrix} \quad (3.9)$$

In an acoustic medium, the constitutive behaviour of the fluid is assumed to be inviscid and compressible, so that, the dynamic pressure,  $p$ , relates to the volumetric strain,  $\varepsilon_v$ , through the bulk modulus,  $\mathbf{K}_f$ , as expressed by the Equation 3.10.

$$p = -\mathbf{K}_f \varepsilon_v \quad (3.10)$$

### 3.5 Results

Figure 3.4 shows the magnitude and phase of the basilar membrane velocity relative to stapes footplate velocity at 12 mm from the round window. The numerical results obtained were compared with experimental data reported in the literature in order to validate the model. The experimental results reported by Stenfelt et al. [38] which were acquired from a human cadaver temporal bone at 12 mm from the round window are represented in Figure 3.4. The data of Gundersen et al. [39] extracted using the Mössbauer technique and recalculated later by Stenfelt et al [38] was also included. The resonance peak is very similar between the compared data. The response of Stenfelt et al. [38] and Gundersen et al. [39] resonate at approximately 2 kHz and 3.6 kHz, respectively. Our findings showed a resonance peak near 2.5 kHz that is in accordance with the experimental data. The phase angle has the same tendency of the experimental results. The sharp decrease of the phase angle above 3 kHz suggests the presence of the travelling wave inside the cochlea. An increase in the basilar membrane velocity relative to stapes footplate is observed between 7 kHz

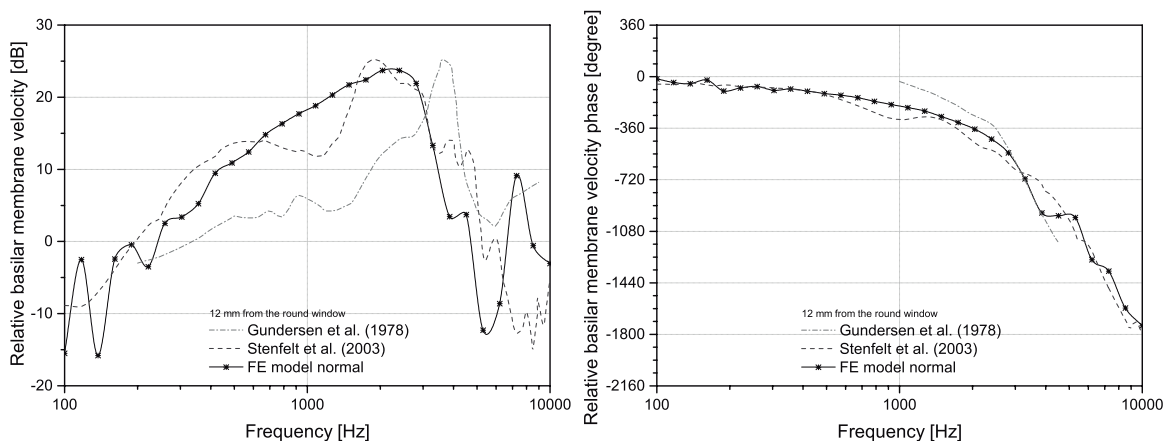


Figure 3.4: Comparison and validation of the magnitude and phase of basilar membrane velocity relative to stapes footplate velocity with experimental results at 12 mm from the round window.

and 9 kHz. Most of the works in the literature, by contrast, simplify the geometry of the cochlea, considering it as a tapered box. Since our work is based in MRI, such irregular geometry can lead to the presence of peaks as observed between 7 kHz and 9 kHz. However, the peak observed is smaller than half of the maximum registered, which result in a lesser importance.

Figure 3.5 shows the cochlear map obtained using the finite element model of the passive normal cochlea and the respective comparison with the function proposed by Greenwood [27] and the experimental results published by Békésy in 1960 [40]. In this work the active mechanism present in the outer hair cell, which provides a local positive feedback along the cochlear partition, as mentioned by Ren and Gillespie [41], was not considered. The cochlear map correlates the location of maximum vibration

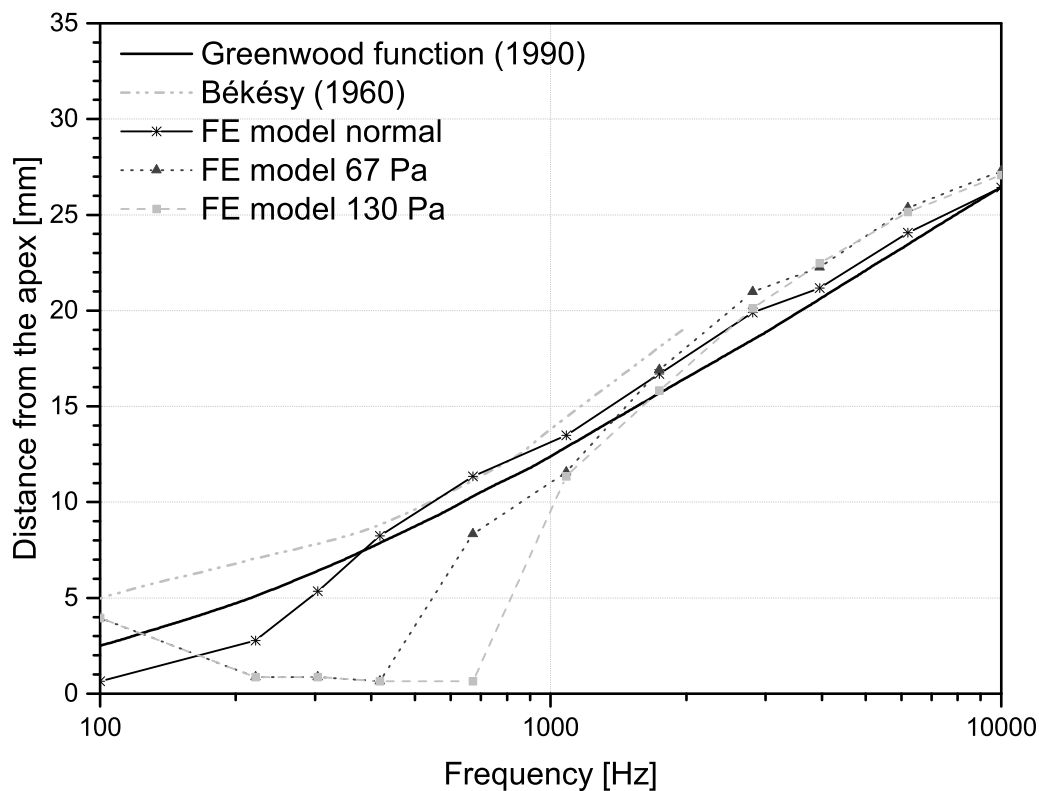


Figure 3.5: Cochlear map validation and comparison with different endolymphatic hydrops stages.



of the basilar membrane as a function of frequency along the basilar membrane, this frequency is termed characteristic frequency. The results obtained are close to the data obtained in the literature, which allowed to validate the model. In Figure 3.5 the cochlear map for different pressures applied on the basilar membrane is also shown, thus simulating the endolymphatic hydrops at different stages. The early stage of chronic hydrops occurs with minimal change in pressure ( $<67$  Pa) between endolymph and perilymph. The pressure value was based in the experimental work of Böhmer which used guinea pigs in his study. The use of experimental models, mainly guinea pigs and rats have the advantage of being easy to handle, and their ears are very similar to those of humans, as mentioned by Albuquerque et al. [42]. At this stage, the negligible increase of the pressure is mainly due to the high flexibility of the endolymphatic boundaries which allows the endolymph volume to grow without a high increase in the pressure [12, 43]. It is known that high differences of pressure between the endolymph and the perilymph affects the resonant characteristics of the basilar membrane. In the study of Böhmer [44], a pressure gradient of approximately 125 Pa, corresponding to a pressure gradient 100 times higher than the one caused by the sound pressure of loud tones, was able to strongly affect the normal behaviour of the basilar membrane. In order to study a severe endolymphatic hydrops a pressure differential of 130 Pa was considered on the present work [45]. The curve "FE model normal" shows the response of the basilar membrane in normal condition or when it is not under any static pressure. For lower frequencies, which are captured at locations near the apex of the cochlea, major changes were found, as the static pressure increased. Such differences are also shown in the Figure 3.6 in terms of magnitude of the basilar membrane displacement. No notorious differences at higher

frequencies were registered, as can be seen in Figure 3.5 and Figure 3.6. The basilar membrane changed the mode of vibration mainly at lower frequencies. There was no notorious peak of displacement near the apex when the static pressure differential was applied, as expected for a normal traveling wave developed inside the cochlea (see Figure 3.6). The peak of displacement was also less pronounced and extended to lower frequencies as the static pressure increased. In summary, the increase in static pressure reduced the frequency selectivity present in a normal cochlea.

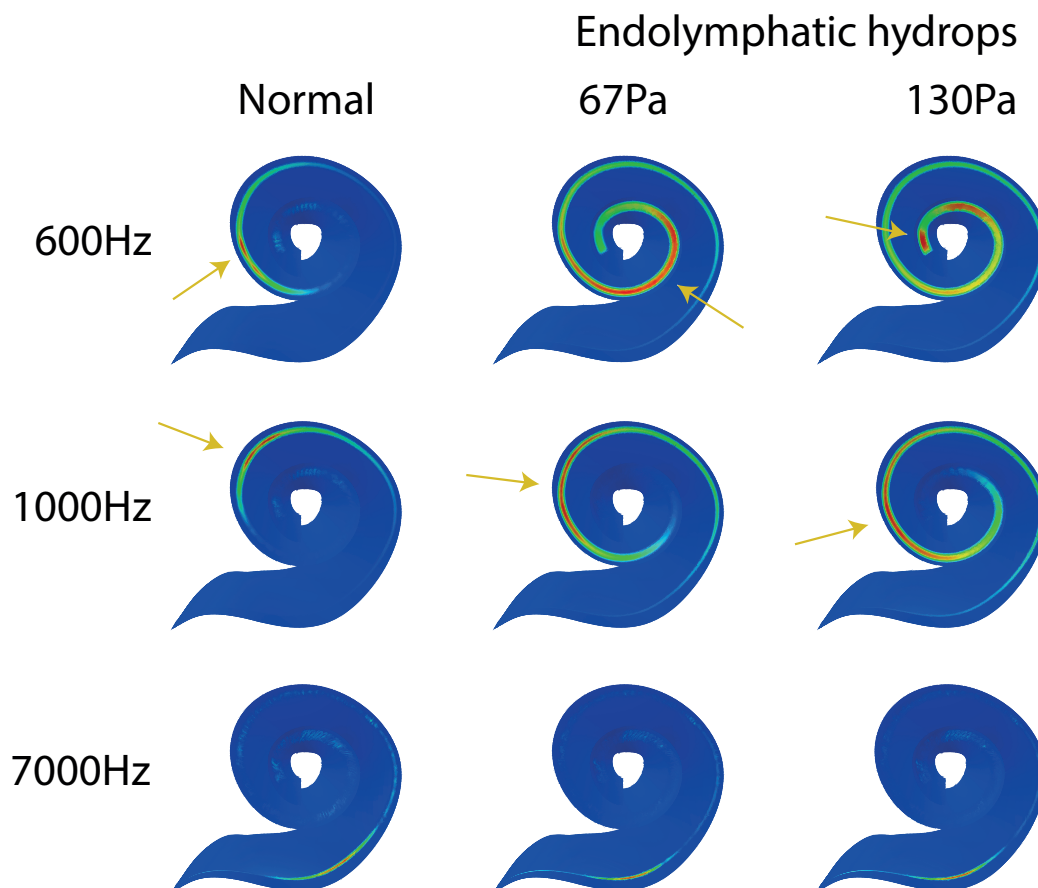


Figure 3.6: Magnitude of the basilar membrane displacement at 600Hz, 1000Hz and 7000Hz for normal condition and two endolymphatic hydrops stages.

The three frequency points intend to show the influence of the endolymphatic hydrops at the low, medium, and high frequencies, which are the three frequency bands frequently used in clinical environment.

Figure 3.7 shows the magnitude and the phase of the displacement in the basilar membrane was extracted at 19 mm from the apex of the cochlea. The maximum value of the displacement did not change when the static pressure differential was applied, neither did the frequency nor the amplitude. The phase of the displacement shows a sharp decrease at the same frequency, for which the maximum displacement was observed, thus showing the presence of the traveling wave. In short, the application of a static pressure differential had reduced effects in the response of the basilar membrane at positions near the base of the cochlea, where the higher frequencies are captured.

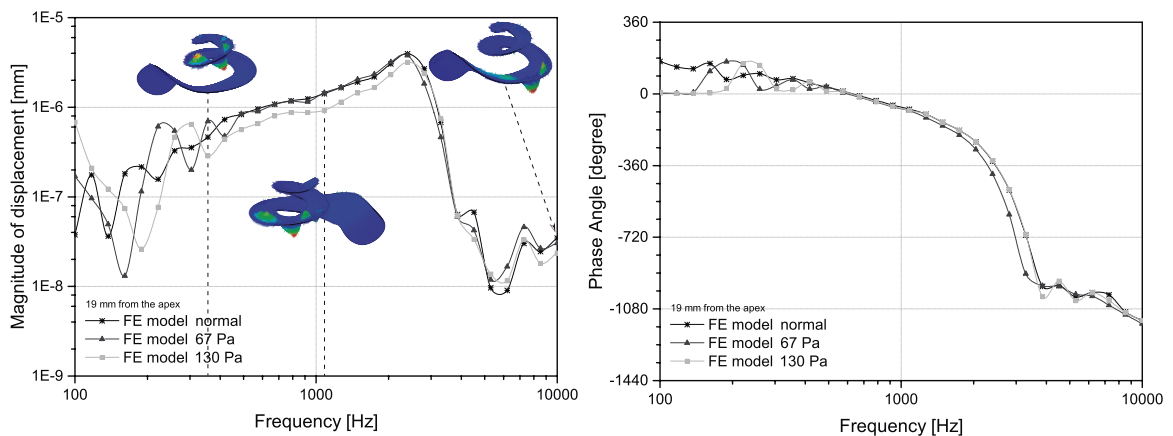


Figure 3.7: Magnitude and phase of the basilar membrane displacement at 19 mm from the apex of the cochlea. Basilar membrane illustrations correspond to the FE model normal, the displacement was amplified.

Figure 3.8 shows the magnitude and phase of the basilar membrane near the middle of the basilar membrane, more precisely, at 15 mm from the apex of the cochlea. At this location, the basilar membrane shows to be highly affected by the static pressure. There is a decrease in the magnitude and an increase in the frequency at which the maximum displacement was obtained, as the static pressure increased. A decrease of 6 dB and 9 dB in the magnitude of the displacement was recorded due

to a static pressure of 67 Pa and 130 Pa, respectively. The phase of the displacement indicated to be affected by static pressure. As expected, the sharp decrease of the phase was registered at a higher frequency, as the static pressure increased. Such changes in the dynamic behaviour of the basilar membrane can be explained by the increase of the basilar membrane stiffness owing to the static pressure applied [46].

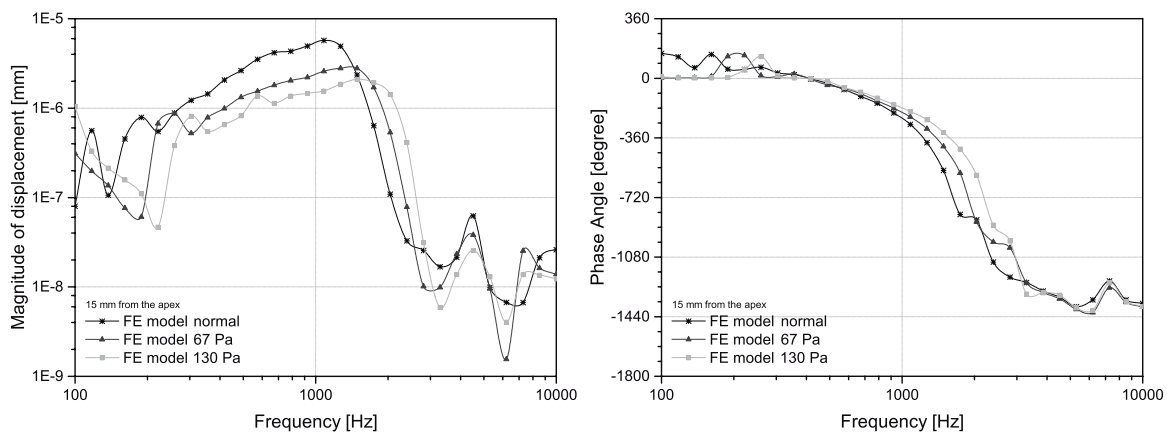


Figure 3.8: Magnitude and phase of the basilar membrane displacement at 15 mm from the apex of the cochlea.

Figure 3.9 shows the response of the basilar membrane at 7 mm from the apex of the cochlea. At this location, the obtained results showed that the basilar membrane is highly affected. The tendency is the same as the previous position, near the middle of the cochlea, but more pronounced. A decrease in the magnitude of 12 dB and 16 dB was recorded for 67 Pa and 130 Pa pressure differentials, respectively. There was also a considerable change in the phase, increasing the frequency at which the sharp decrease was observed. The endolymphatic hydrops can result in an increase of the basilar membrane displacement at some frequencies as shown in Figure 3.7, Figure 3.8 and Figure 3.9. However, the position where is identified the maximum amplitude of displacement (near the characteristic frequency) tends to decrease its amplitude which will result in deficient stimulation of the vestibulocochlear nerve

and consequently a reduction of hearing. Accordingly, it is important to study the location around the maximum amplitude where the vibration will be translated into hearing. The results obtained on this study, using the finite element method are in agreement with the experimental results available in the literature, which describes the lower frequencies as the first frequency band to be affected, due to the influence of the endolymphatic hydrops on the basilar membrane response [47, 48, 49]. Tinnitus, a perception of noise or ringing sounds is common in people with the Ménière's disease. In almost all the cases of tinnitus, the perceived tones are confined to low tones or low pitch tones [19, 50]. The symptoms appear to be linked with the apex of the cochlea and to be a consequence of the static pressure present inside the scala media.

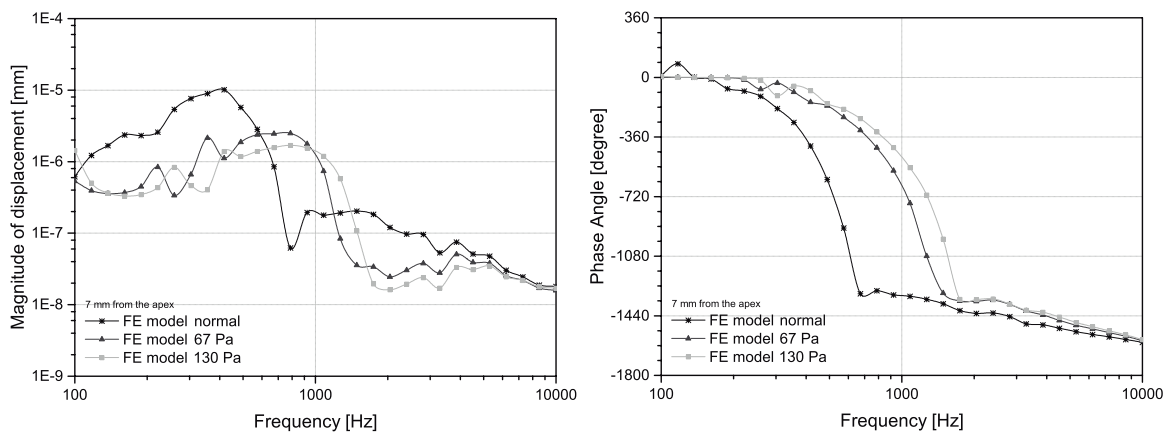


Figure 3.9: Magnitude and phase of the basilar membrane displacement at 7 mm from the apex of the cochlea.

Diplacusis, a pathology where patients, for a given pure single-frequency stimulus, perceive two different frequency sounds (one frequency from each ear) may also be a consequence of the endolymphatic hydrops. The basilar membrane frequency shift can explain this pathology because a single frequency sound can be perceived as a slightly lower frequency.

In order to study the influence of the static pressure on the maximum displacement

of the basilar membrane, a static pressure between 0 Pa to 130 Pa was applied. Figure 3.10 shows the evolution of the maximum displacement in the basilar membrane for different static pressures inside the mentioned range. The maximum displacement is always located at the apex of the cochlea (where the basilar membrane stiffness is lower; see illustration in Figure 3.10) and follows approximately a logarithmic evolution. Therefore, a logarithmic fit was also included in Figure 3.10. The static pressure of 130Pa is not enough to deform the basilar membrane and touch the bottom of the scala tympani.

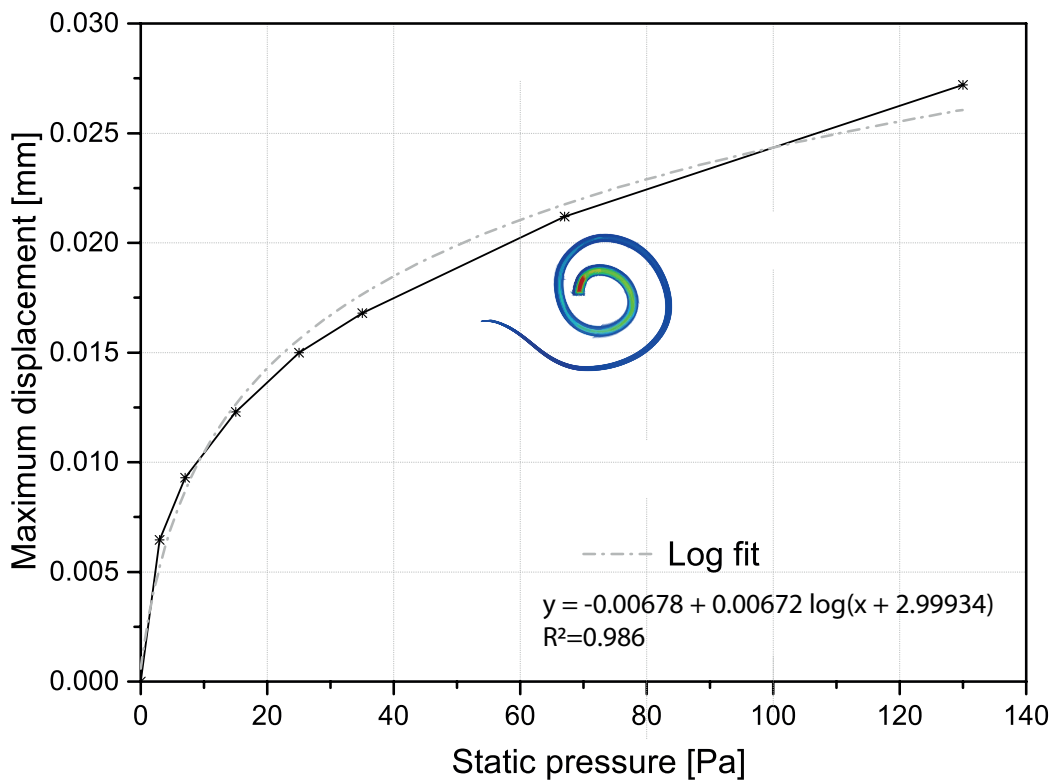


Figure 3.10: Maximum displacement of the basilar membrane imposed by the static pressure.

### 3.6 Conclusions

Ménière’s disease is a disorder of the inner ear that is characterized by a set of unpleasant and painful symptoms. The cause of Ménière’s disease is still unclear

but likely involves both genetic and environmental factors. This disease affects the dynamic behaviour of the basilar membrane, but not equally along its length, thus representing a higher hearing loss at specific audible frequencies. Using the finite element method, it is possible to investigate the consequences and the changes that the endolymphatic hydrops causes in the inner ear and hearing. This work shows the relationship between the increasing of the endolymphatic pressure and the development of hearing loss. Therefore, a steady state dynamic analysis was conducted in the audible frequency range, between 100 Hz and 10 kHz. Two static pressures, 67 Pa and 130 Pa differentials were applied to the basilar membrane, thus simulating the endolymphatic hydrops. Our finite element model shows that the endolymphatic hydrops affects mainly the lower frequencies. As expected, the static pressure leads to greater deformations near the apex of the cochlea, where the stiffness is lower. Such deformation follows approximately a logarithmic evolution, and, in this context a logarithmic fit was formulated. Thus, from a biomedical point of view it is then expected that the hearing loss should be more accentuated on the lower frequencies. For these frequencies, a high pitched sound becomes heard as low pitched (see Figure 3.6), if the basilar membrane amplitude is able to trigger the mechanotransduction process, since the peak of the travelling wave changes its frequency to a location nearest to the apex. Based on the numerical analysis, patients with endolymphatic hydrops are not expected to develop complications on higher frequencies. From our numerical study, we can see that with the increasing static pressure, the basilar membrane is increasingly affected towards the round window. Since the portion of the basilar membrane closer to the round window presents a higher stiffness, it will be less affected by a small change in the static pressure, when

compared to the region closer to the apex of the cochlea, where the stiffness is lower. In addition, the static pressure can theoretically affect the motion of the hair cells, mainly decoupling them from the tectorial membrane. In such cases, if the disease is left untreated, it is known that the hearing loss will reach the remaining frequencies, and may even result in a permanent hearing loss. Accordingly, diplacusis may be a consequence of the endolymphatic hydrops. The basilar membrane frequency shift can explain the diplacusis because a single frequency sound can be perceived as a slightly lower frequency so patients with endolymphatic hydrops can perceive two different frequency sounds corresponding to a given single-frequency sound. Tinnitus, a symptom of the Ménière's disease, arises mainly at low-pitch sounds, probably indicating deafness on these frequencies. Other diseases, such as otosclerosis, occurs with hearing loss at low frequencies. Nonetheless, endolymphatic hydrops presents other symptoms, e.g. vertigo or balance problems that otosclerosis does not. Such differences will help to distinguish different pathologies with hearing loss at low frequencies.

In the present work, a more realistic distribution of the pressure and propagation of the travelling wave was obtained due to the usage of a non-linear function to describe the basilar membrane properties and an improved geometrical description of the cochlear shape.

The outcomes obtained in this work, intend to support the medical community to ensure a swift detection of the disease, based on the symptoms described by the patients, such as a poor hearing at low frequencies, thus resulting in a rapid and efficient treatment, avoiding its spread to values that may result in permanent hearing loss.



### **3.7 Conflict of interest statement**

The authors declare that there is no financial, professional or other personal interest of any nature or kind in any product, service and/or company that could be constructed as influencing the position.

### **3.8 Acknowledgements**

The authors truly acknowledge the funding provided by Ministério da Ciência, Tecnologia e Ensino Superior - Fundação para a Ciência e a Tecnologia (Portugal), under grant: SFRH/BD/129397/2017. This research was also supported by the Portuguese Foundation of Science and Technology under the research project UIDB/50022/2020.

### 3.9 References

- [1] Prosper Ménière. Mémoire sur des lésions de l'oreille interne donnant lieu à des symptômes de congestion cérébrale apoplectiforme. *Gazette médicale de Paris*, 16:597–601, 1861.
- [2] Prosper Ménière. Sur une forme de surdité grave dépendant d'une lésion de l'oreille interne. *Gazette médicale de Paris*, 16:29, 1861.
- [3] R. W. Baloh. Prosper meniere and his disease. *Arch Neurol*, 58(7):1151–6, 2001.
- [4] Dale Purves. *Neuroscience*. Oxford University Press, New York, 6th edition. edition, 2018.
- [5] Lawrence E. Wineski and Richard S. Snell. *Snell's clinical anatomy by regions*. Wolters Kluwer, Philadelphia, 10th edition. edition, 2019.
- [6] Susan Standring. *Gray's anatomy : the anatomical basis of clinical practice*. Elsevier Limited, New York, 41st edition. edition, 2016.
- [7] D.H. McFarland. *Netter's Atlas of Anatomy for Speech, Swallowing, and Hearing*. Elsevier Health Sciences, 2nd edition. edition, 2014.
- [8] Yasuya Nomura. *Morphological aspects of inner ear disease*. Springer Japan, New York, 1st edition. edition, 2014.
- [9] S. Takeuchi, T. Takeda, and H. Saito. Pressure relationship between perilymph and endolymph associated with endolymphatic infusion. *Annals of Otology Rhinology and Laryngology*, 100(3):244–248, 1991.

- [10] C. S. Hallpike and H. Cairns. Observations on the pathology of meniere's syndrome. *Proc R Soc Med*, 31(11):1317–36, 1938.
- [11] H. F. Schuknecht and A. J. Gulya. Endolymphatic hydrops - an overview and classification. *Annals of Otology Rhinology and Laryngology*, 92(5):1–20, 1983.
- [12] A. N. Salt and S. K. Plontke. Endolymphatic hydrops: pathophysiology and experimental models. *Otolaryngologic Clinics of North America*, 43(5):971–83, 2010.
- [13] A. Mucha, S. Fedor, and D. DeMarco. Vestibular dysfunction and concussion. *Handb Clin Neurol*, 158:135–144, 2018.
- [14] Elena Olivetto, Edi Simoni, Valeria Guaran, Laura Astolfi, and Alessandro Martini. Morphological and functional structure of the inner ear: Its relation to ménière's disease. *Audiological Medicine*, 10(4):160–166, 2012.
- [15] A. Vassiliou, P. V. Vlastarakos, P. Maragoudakis, D. Candiloros, and T. P. Nikolopoulos. Meniere's disease: Still a mystery disease with difficult differential diagnosis. *Ann Indian Acad Neurol*, 14(1):12–18, 2011.
- [16] J. Kotimaki, M. Sorri, E. Aantaa, and J. Nuutinen. Prevalence of meniere disease in finland. *Laryngoscope*, 109(5):748–753, 1999.
- [17] M. Havia, E. Kentala, and I. Pyykko. Prevalence of meniere's disease in general population of southern finland. *Otolaryngology-Head and Neck Surgery*, 133(5):762–768, 2005.
- [18] D. Celestino and G. Ralli. Incidence of meniere's disease in italy. *Am J Otol*, 12(2):135–8, 1991.

- [19] R. J. Caparosa. Medical treatment for meniere's disease. *Laryngoscope*, 73:666–72, 1963.
- [20] M. M. Paparella. Pathogenesis of meniere's disease and meniere's syndrome. *Acta Otolaryngol Suppl*, 406:10–25, 1984.
- [21] S. N. Merchant, J. C. Adams, and J. B. Jr. Nadol. Pathophysiology of meniere's syndrome: are symptoms caused by endolymphatic hydrops? *Otol Neurotol*, 26(1):74–81, 2005.
- [22] Yi Haijin, Guo Hong, Wang Chunhong, and Xia Yin. Management of meneere's disease - the beijing tiantan hospital experience. *Journal of Otology*, 9(2):106 – 109, 2014.
- [23] G. J. Basura, M. E. Adams, A. Monfared, S. R. Schwartz, P. J. Antonelli, R. Burkard, M. L. Bush, J. Bykowski, M. Colandrea, J. Derebery, E. A. Kelly, K. A. Kerber, C. F. Koopman, A. A. Kuch, E. Marcolini, B. J. McKinnon, M. J. Ruckenstein, C. V. Valenzuela, A. Vosooney, S. A. Walsh, L. C. Nnacheta, N. Dhepyasuwan, and E. M. Buchanan. Clinical practice guideline: Meniere's disease executive summary. *Otolaryngology-Head and Neck Surgery*, 162(4):415–434, 2020.
- [24] Rong Z. Gan, Brian P. Reeves, and Xuelin Wang. Modeling of sound transmission from ear canal to cochlea. *Annals of Biomedical Engineering*, 35(12):2180–2195, 2007.
- [25] W. Liu, F. Atturo, R. Aldaya, P. Santi, S. Cureoglu, S. Obwegeser, R. Glueckert, K. Pfaller, A. Schrott-Fischer, and H. Rask-Andersen. Macromolecular

- organization and fine structure of the human basilar membrane - relevance for cochlear implantation. *Cell Tissue Res*, 360(2):245–62, 2015.
- [26] R. W. Koch, H. M. Ladak, M. Elfarnawany, and S. K. Agrawal. Measuring cochlear duct length - a historical analysis of methods and results. *Journal of Otolaryngology-Head & Neck Surgery*, 46, 2017.
- [27] D. D. Greenwood. A cochlear frequency-position function for several species - 29 years later. *Journal of the Acoustical Society of America*, 87(6):2592–2605, 1990.
- [28] G. Emadi, C. P. Richter, and P. Dallos. Stiffness of the gerbil basilar membrane: radial and longitudinal variations. *J Neurophysiol*, 91(1):474–88, 2004.
- [29] Salvatore Iurato. Functional implications of the nature and submicroscopic structure of the tectorial and basilar membranes. *The Journal of the Acoustical Society of America*, 34:1386–1395, 1962.
- [30] I. U. Teudt and C. P. Richter. Basilar membrane and tectorial membrane stiffness in the CBA/CaJ mouse. *J Assoc Res Otolaryngol*, 15(5):675–94, 2014.
- [31] Y. Kim, J. S. Kim, and G. W. Kim. A novel frequency selectivity approach based on travelling wave propagation in mechanoluminescence basilar membrane for artificial cochlea. *Sci Rep*, 8:12023, 2018.
- [32] Liujie Ren, Hua Cheng, Guang-Hong Ding, Lin Yang, Pei-Dong Dai, and Tian-Yu. Zhang. Three-dimensional finite element hydrodynamical modeling of straight and spiral cochlea. *AIP Conference Proceedings*, 1965(1):030003, 2018.
- [33] Bruno Areias, Carla Santos, R N Jorge, Fernanda Gentil, and Marco Pl Parente. Finite element modelling of sound transmission from outer to inner

- ear. *Proceedings of the Institution of Mechanical Engineers. Part H, Journal of engineering in medicine*, 230(11):999–1007, 2016.
- [34] Q Sun, R Z Gan, K-H Chang, and K J Dormer. Computer-integrated finite element modeling of human middle ear. *Biomechanics and modeling in mechanobiology*, 1(2):109–22, 2002.
- [35] F Gentil, M.P. Parente, P Martins, C Garbe, R N Jorge, A Ferreira, and João Manuel R S Tavares. The influence of the mechanical behaviour of the middle ear ligaments: a finite element analysis. *Proceedings of the Institution of Mechanical Engineers. Part H, Journal of engineering in medicine*, 225(1):68–76, 2011.
- [36] R. Z. Gan, F. Yang, X. Zhang, and D. Nakmali. Mechanical properties of stapedial annular ligament. *Med Eng Phys*, 33(3):330–9, 2011.
- [37] Dassault Systemes. *ABAQUS analysis user’s guide*. 2016.
- [38] S. Stenfelt, S. Puria, N. Hato, and R. L. Goode. Basilar membrane and osseous spiral lamina motion in human cadavers with air and bone conduction stimuli. *Hearing Research*, 181(1-2):131–143, 2003.
- [39] T. Gundersen, O. Skarstein, and T. Sikkeland. A study of the vibration of the basilar membrane in human temporal bone preparations by the use of the mossbauer effect. *Acta Otolaryngol*, 86(3-4):225–32, 1978.
- [40] Georg Von Békésy. *Experiments in hearing*. McGraw-Hill, New York, 1960.
- [41] T. Ren and P. G. Gillespie. A mechanism for active hearing. *Current Opinion in Neurobiology*, 17(4):498–503, 2007.

- [42] Agnes Afrodite Sumarelli Albuquerque, Maria Rossato, José Antonio Aparecido de Oliveira, and Miguel Angelo Hyppolito. Understanding the anatomy of ears from guinea pigs and rats and its use in basic otologic research. *Brazilian Journal of Otorhinolaryngology*, 75(1):43–49, 2009.
- [43] C. H. Long and T. Morizono. Hydrostatic pressure measurements of endolymph and perilymph in a guinea pig model of endolymphatic hydrops. *Otolaryngol Head Neck Surg*, 96(1):83–95, 1987.
- [44] A. Böhmer. Hydrostatic pressure in the inner ear fluid compartments and its effects on inner ear function. *Acta Otolaryngol Suppl*, 507:3–24, 1993.
- [45] A. Böhmer. Experimental endolymphatic hydrops and inner ear pressure. In Arne Ernst, Robert Marchbanks, and Madjid Samii, editors, *Intracranial and Intralabyrinthine Fluids*, pages 81–84. Springer, Berlin, Heidelberg, 1996.
- [46] Sinyoung Lee and Takuji Koike. Simulation of the basilar membrane vibration of endolymphatic hydrops. *Procedia IUTAM*, 24:64–71, 2017.
- [47] C. R. Ding, X. D. Xu, X. W. Wang, X. H. Jia, X. Cheng, X. Liu, L. Yang, B. S. Tong, F. L. Chi, and D. D. Ren. Effect of endolymphatic hydrops on sound transmission in live guinea pigs measured with a laser doppler vibrometer. *Neural Plast*, 2016:8648297, 2016.
- [48] C. S. Brown, S. D. Emmett, S. K. Robler, and D. L. Tucci. Global hearing loss prevention. *Otolaryngologic Clinics of North America*, 51(3):575–592, 2018.
- [49] J. Magnan, O. N. Ozgirgin, F. Trabalzini, M. Lacour, A. L. Escamez, M. Magnusson, E. A. Guneri, J. P. Guyot, D. Nuti, and M. Mandala. European

position statement on diagnosis, and treatment of meniere's disease. *J Int Adv Otol*, 14(2):317–321, 2018.

- [50] E. Douek and J. Reid. The diagnostic value of tinnitus pitch. *J Laryngol Otol*, 82(11):1039–42, 1968.



## Chapter 4

# Finite element modelling of the surgical procedure for placement of a straight electrode array: mechanical and clinical consequences



**Article 3 - Finite element modelling of the surgical  
procedure for placement of a straight electrode array:  
mechanical and clinical consequences**

B. Areias (1), M.P.L. Parente (1,2), F. Gentil (3), R.M. Natal Jorge (1,2)

1-INEGI, Institute of science and innovation in mechanical and industrial  
engineering, Porto, Portugal {bareias@fe.up.pt}

2-FEUP, Faculty of Engineering, University of Porto, Porto, Portugal  
{mparente@fe.up.pt, rnatal@fe.up.pt}

3-Escola Superior de Saúde - Politécnico do Porto; Clínica ORL – Dr. Eurico de  
Almeida; WIDEX {fernanda.fgnanda@gmail.com}

*Published in: Journal of Biomechanics, 2021*

*doi: 10.1016/j.jbiomech.2021.110812*

This chapter investigates new ways of reducing the intra-cochlear trauma during a cochlear implant insertion. Different parameters, related with the cochlear implant insertion, such as insertion speed, friction coefficient and implant stiffness are studied.



## 4.1 Abstract

A cochlear implant is an electronic device implanted into the cochlea to directly stimulate the auditory nerve. Such device is used in patients with severe-to-profound hearing loss. The cochlear implant surgery is safe, but involves some risks, such as infections, device malfunction or damage of the facial nerve and it can result on a poor hearing outcome, due to the destruction of any present residual hearing. Future improvements in cochlear implant surgery will necessarily involve the decrease of the intra-cochlear damage. Several implant related variables, such as materials, geometrical design, processor and surgical techniques can be optimized in order for the patients to recover their normal hearing capacities. The straight electrode is a type of cochlear implant that many authors indicate as being the less traumatic.

In this work, the influence of the insertion speed, the friction coefficient between the cochlear wall and the electrode array, and several configurations of the cochlear implant tip were studied. The numerical simulations of the implantation showed the same pattern of the insertion force against insertion depth, thus indicating the different phases of the insertion. Results demonstrated that lower insertion speeds, friction coefficients and tip stiffness, led to a reduction on the contact pressures and insertion force. It is expected that these improved configurations will allow to increase the residual hearing while reducing surgical complications.

## 4.2 Keywords

cochlea, cochlear implant, intra-cochlear damage, straight electrode, finite element method

## 4.3 Introduction

Hearing and balance are the crucial functions of the inner ear which allow the perception and discrimination of sounds and accelerations. The cochlea and the semicircular canals, which form the inner ear, are located within the petrous part of the temporal bone, being positioned according to Figure 4.1. There are many environmental factors that can damage the hair cells within the inner ear, thus causing hearing loss. Loud noise exposure and presbycusis are the most common causes for hearing loss in adults, both resulting in an initial high frequency sensorineural hearing loss as refereed in the Encyclopedia of Otolaryngology, Head and Neck Surgery [1]. Such hearing impairments are frequently derived from the damage or destruction of the sensory hair cells inside the cochlea, as mentioned by Eshraghi et al. [2]. On the other hand, in children, the congenital hearing loss is one of the most prevalent chronic conditions, that can result from environmental factors and genetic abnormalities, with

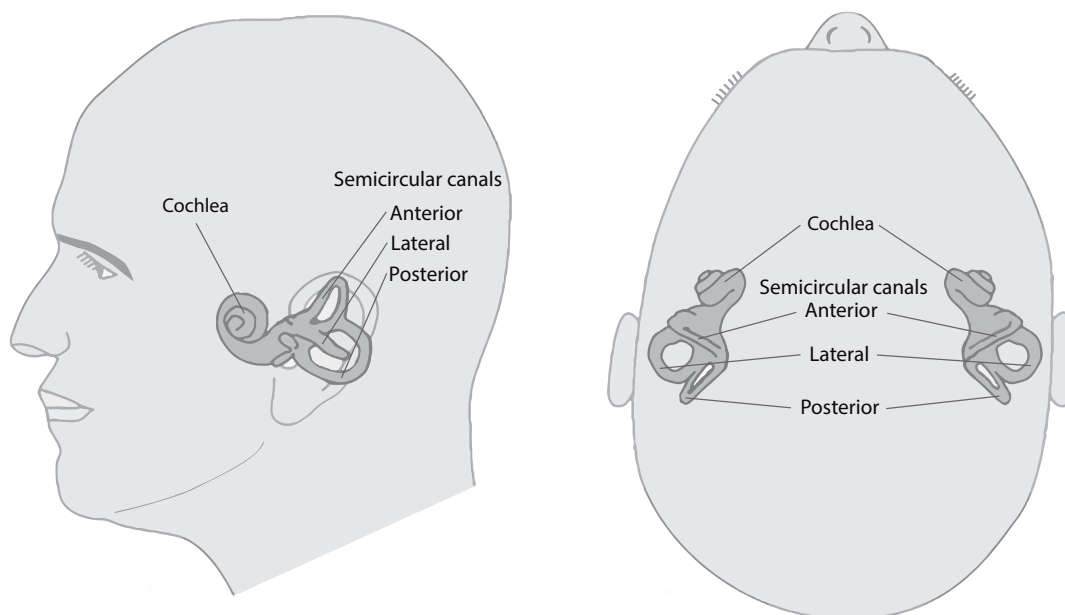


Figure 4.1: Position and orientation of the inner ear.

the same incidence rate, as stated by Korver et al. [3]. This disability affects between 1 to 3 per 1000 live births, according to Allen and Goldman [4].

Cochlear implant surgery is an effective treatment indicated for deafness and severe hearing loss. A cochlear implant (Figure 4.2) consists in an external part and an internal part. The external part is composed by the signal processor with a microphone and a transmitter coil. The internal part contains a receiver-stimulator and an electrode array to be inserted into the scala tympani. As refereed by Kha and Chen [5] and Stover and Lenarz [6], the electrode array is usually made with platinum wires, allowing for a good resistance to corrosion, embedded in a silicon elastomer, which provide a good malleability during the insertion process.

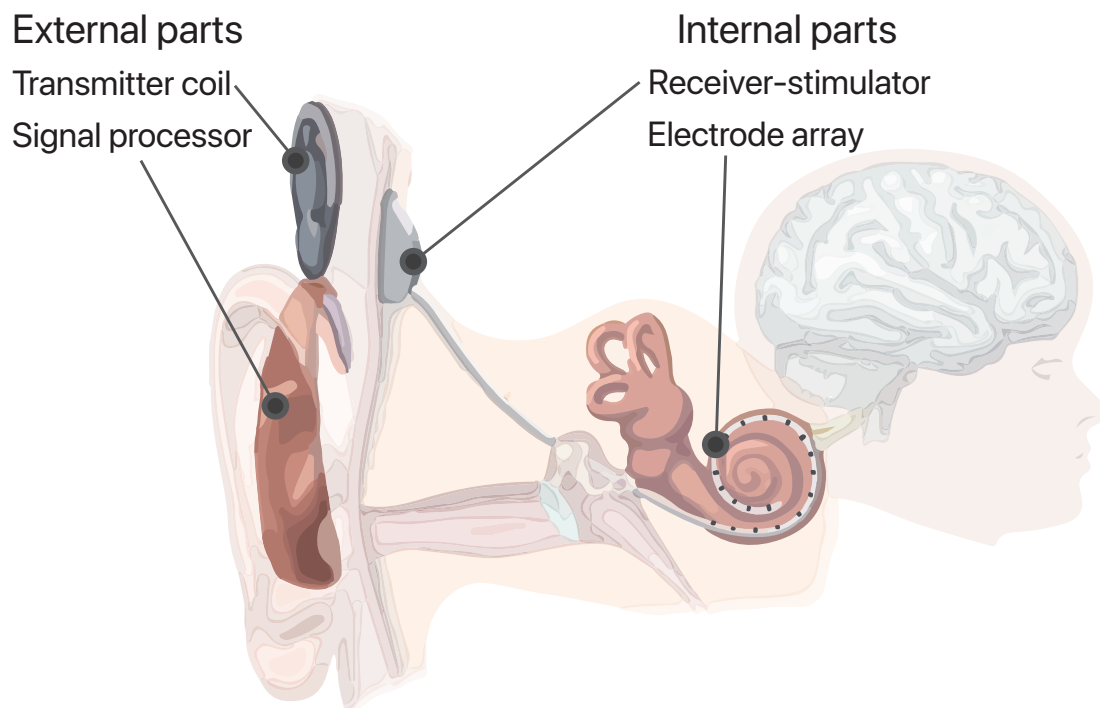


Figure 4.2: Illustration of the cochlear implant position with external and internal part, adapted from Kral [7].

The interest in electrical stimulation of the human ear began in 1800 with Volta [8]. Volta connected each pole of a battery to a probe and then each probe was

inserted in each ear canal. The flow of the current between the poles was described as a “jolt in the head” followed by a kind of “crackling, jerking, or bubbling” sound. One hundred and sixty years later, in 1957, Djourno and Eyries [9] performed the first direct electrical stimulation. The patient received an electrode designed by the otolaryngologist Djourno and the operation was conducted by the otolaryngologist Eyries. The postoperative outcomes showed a good intensity discrimination, but the differentiation of different frequencies was very poor and was not detectable for frequencies above 1 kHz. Few weeks later the device failed, leading Eyries to refuse new implantations, as described by Eshraghi et al. [2].

The cochlear implant reimplantation, due for instance to device failure, has a reduced intra-cochlear damage, according to Kim et al. [10]. However, the insertion of cochlear implants carries certain risks and possible complications that are classified from minor to major complications. The major complications are related with the surgical technique and include flap necrosis, wrong electrode placement, device failure, severe cutaneous infections, meningitis, cholesteatoma and rare facial nerve injury, as mentioned by Cohen and Hoffman [11] and Loundon et al. [12]. Minor complications comprise dizziness, vertigo at early stages and middle ear abnormalities and persistent otitis media observed in more advanced stages as specified by Loundon et al. [12]. Major complications can lead to further surgeries, with explantation or reimplantation of the cochlear implant. On the other hand, minor complications only require medical treatment in most of cases, as said by Terry et al. [13].

The study conducted by Dettman et al. [14], showed that children with less than one year of age who underwent cochlear implant surgery, were able to achieve similar rates of language acquisition in comparison to their normally hearing peers.



The results from the same author, for a group of children aged between one and two years of age also showed significantly greater rates of language acquisition in younger children, which suggests that the implantation should be made as soon as possible. Nevertheless, the drawback of implantation is related to the risk of cardiac arrest, which increases as the age decreases, due to the use of general anaesthesia, as mentioned by Cohen et al. [15].

Regarding the incidence rate of complications in the postoperative period, a rate of 20% in a group of 403 patients was reported in a study conducted by Farinetti et al. [16], of which 15% were minor complications and 5% major complications. Another research published in 2018 by Sefein [17], showed approximately the same incidence rate, of around 19%. The same study also observed different distribution of complication rates between the pediatric and adult groups. Magnet displacement and postoperative otitis media tended to be higher in the pediatric group as mentioned by Sefein [17].

Cochlear implants are divided in perimodiolar, straight and double array electrode. Each cochlear implant has its advantages and disadvantages, and each of them is better suitable for a certain type of pathology and condition of the cochlea. As mentioned by Gibson and Boyd [18], the slim straight electrode implant demonstrates useful preservation of residual hearing. On the other hand, in the work of Eshraghi et al. [19], the straight electrodes may present an equal or even a greater risk of damage when compared with the perimodiolar implant. Indeed, there seems to be an inconsistency between the works published in the damage induced by the surgery process. Such discrepancies can be explained by the experience of the surgeon and by the surgical techniques utilized. Overall, damage is expected in the lateral wall due

to the insertion of the straight electrode [20].

Current research is focused on new strategies relating to the electrode design, in order to improve the neuronal health (by developing less traumatic electrodes) and the spatial selectivity.

The insertion of a cochlear implant is performed through the scala tympani, and currently there are three surgical approaches in use: the cochleostomy technique, the round window technique and the enlarged round window technique [21]. In the cochleostomy approach, the electrode is inserted through a hole drilled into the scala tympani, separated from the round window and may be the method of choice in comparison to the round window enlargement because it involves less drilling, as mentioned by Richard et al. [22]. In contrast, the insertion through the round window can be made with or without drilling. The enlargement of the round window should be performed when the patient does not present residual hearing and the anatomy is less favourable, thus allowing a good visualization of the scala tympani. The study conducted by Jiam and Limb [23] showed significant differences of electrode dislocation incidence between the round window group and the cochleostomy group in the order of 240%. In sum, the round window approach should be the preferred method, because it seems to be the less traumatic, as stated by Richard et al. [22], Sikka et al. [24] and Jiam and Limb [23].

The finite element method is known as a tool which can help the medical community in the search of new surgical techniques and consequently to improve old procedures. The present study uses the finite element method, in order to evaluate and obtain new ways of reducing the intra-cochlear trauma, based on the study of several parameters related with the cochlear implant insertion, such as insertion speed,

friction coefficient and implant stiffness.

## 4.4 Materials and Methods

The anatomical geometry of the human cochlea was obtained from a magnetic resonance imaging scan, of a male patient, without cochlear pathologies. A straight electrode (Figure 4.3) was considered in order to simulate the insertion of the cochlear implant. The straight electrode has a length of 25 mm and a diameter ranging between 0.55 mm at proximal end and 0.3 mm at distal end. The distal side ends with a hemispherical tip. Dimensions and shape of the electrode array were based on the standard commercially available CI622 cochlear implant manufactured by the Cochlear medical device company [25].

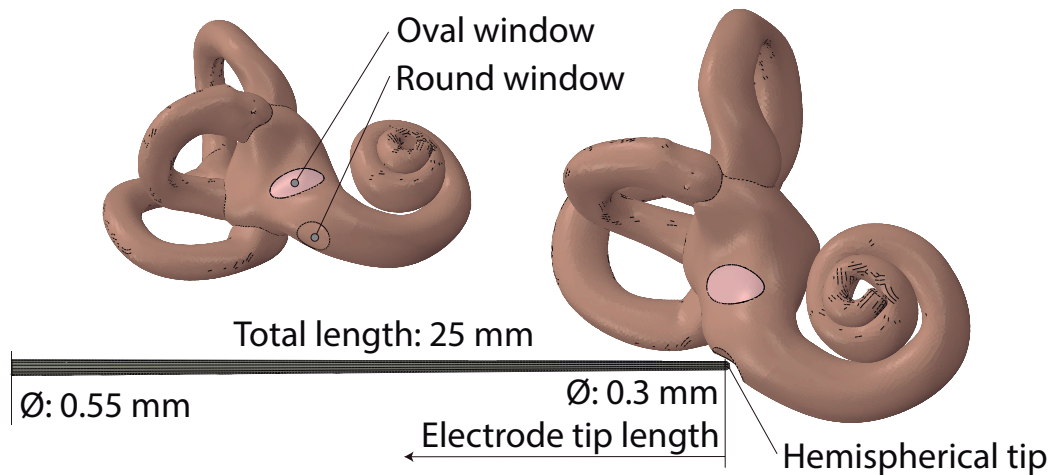


Figure 4.3: Finite element model of the CI622 cochlear implant and the cochlear wall. Demonstration of the electrode tip length.

In order to conduct the numerical analysis, the cochlear implant was meshed with linear hexahedral elements, with reduction integration (C3D8R). The cochlear wall was modelled with 4-node shell elements (S4). In total, the finite element mesh for the cochlear implant was composed by 9036 nodes. The cochlear wall was discretized with 28137 nodes.

The numerical analyses were carried out using the finite element Abaqus/Explicit software package [26]. An explicit dynamics procedure using an explicit central-difference time integration rule was applied. The accelerations at the beginning of an increment are computed using Equation 4.1.

$$\ddot{u}_{(i)}^N = (M^{NJ})^{-1} (P_{(i)}^J - I_{(i)}^J) \quad (4.1)$$

Where  $\ddot{u}_{(i)}^N$  is the acceleration at the increment  $i$ ,  $M^{NJ}$  is the mass matrix,  $P_{(i)}^J$  is the applied load vector, and  $I_{(i)}^J$  is the internal force vector.

The central-difference integration operator is explicit, thus the kinematic states  $(\dot{u}_{(i+\frac{1}{2})}^N$  and  $u_{(i+1)}^N)$  are calculated using the known values from the previous increment  $(\dot{u}_{(i-\frac{1}{2})}^N$  and  $\ddot{u}_{(i)}^N)$ , according to the Equation 4.2 and 4.3.

$$\dot{u}_{(i+\frac{1}{2})}^N = \dot{u}_{(i-\frac{1}{2})}^N + \frac{\Delta t_{(i+1)} + \Delta t_{(i)}}{2} \ddot{u}_{(i)}^N \quad (4.2)$$

$$u_{(i+1)}^N = u_{(i)}^N + \Delta t_{(i+1)} \dot{u}_{(i+\frac{1}{2})}^N \quad (4.3)$$

The explicit procedure requires no iterations and no tangent stiffness matrix, the scheme is not unconditionally stable and thus smaller time steps are required. In Abaqus, the size of the stable time increment can be computed using Equation 4.4.

$$\Delta t \approx \frac{L_{min}}{c_d} \quad (4.4)$$

Where  $L_{min}$  is the smallest element dimension in the entire model and  $c_d$  is the dilatational wave speed.

In order to establish the friction between two surfaces in contact, Abaqus uses the Coulomb friction model. These surfaces can carry shear stresses up to a certain

magnitude across their interface before starting to slide. The critical shear stress is defined in the Coulomb friction model as  $\tau_{crit}$ , and depends of the normal contact pressure,  $p$  according to the following Equation:  $\tau_{crit} = \mu p$ .

In the present study different implant insertion speeds ( $v_{insertion}$ : 0.25, 0.5, 1 and  $2 \text{ mm s}^{-1}$ ) and different friction coefficients ( $\mu$ : 0, 0.05, 0.1, 0.2, 0.3) between the cochlear lateral wall and the cochlear implant were simulated. The insertion speed values used on this work are in accordance with other studies available on the literature, which refer to speeds ranging between  $0.25 \text{ mm s}^{-1}$  [27, 28] to  $1.6 \text{ mm s}^{-1}$  [29]. The mechanical properties considered for the biological structures are detailed in Table 4.1. As result, the mean contact pressure at the cochlear implant tip and the insertion force was obtained. The mean contact pressure at the tip is given by the average of the contact pressure between the cochlear implant tip and the cochlear wall. For this average, only the pressure values from the superficial nodes at the hemispherical tip were considered.

In order to study the influence of the tip length and stiffness, different tip lengths (Figure 4.3) and Young's modulus were considered. The values used are summarized in Table 4.2.

In all numerical simulations, the petrous part of the temporal bone was fixed in all degree of freedom and an imposed displacement of 25 mm was applied at the proximal surface of the cochlear implant, thus leading to a complete insertion of the electrode

Table 4.1: Mechanical properties of the inner ear parts

	$E$ [MPa]	$\nu$ [-]	$\rho$ [kg m <sup>-3</sup> ]
Cochlear wall [30, 31, 32]	14100	0.3	2000
Cochlear implant [33, 5]	1000		1000

Table 4.2: Mechanical properties used, for different tip lengths

Tip length [mm]	$E$ [MPa]	$\nu$ [-]	$\rho$ [kg m <sup>-3</sup> ]
2.5	250 (25 %)	0.3	1000
	500 (50 %)		
	750 (75 %)		
5	250 (25 %)		
	500 (50 %)		
	750 (75 %)		

array.

## 4.5 Results

In order to understand how the angular position of the implant tip evolves during the insertion procedure, a first study was conducted, using an insertion speed of  $1 \text{ mm s}^{-1}$  and considering no friction. Figure 4.4 shows the relation between the insertion depth in millimetres and the angular position of the implant tip, during the insertion. Since this is mainly a geometrical constrained problem, no other velocities were considered for this first study. A linear regression was also carried out, which allows to observe that the curve follows approximately a linear regression except between the 10 mm and 18 mm deep, where a certain deviation was verified. The initial contact was reached at about 8 mm deep. After that, an adaptation of the electrode array to the cochlear wall was verified.

Franz and Clark [34] indicated the range between the 8 mm and 10 mm of insertion

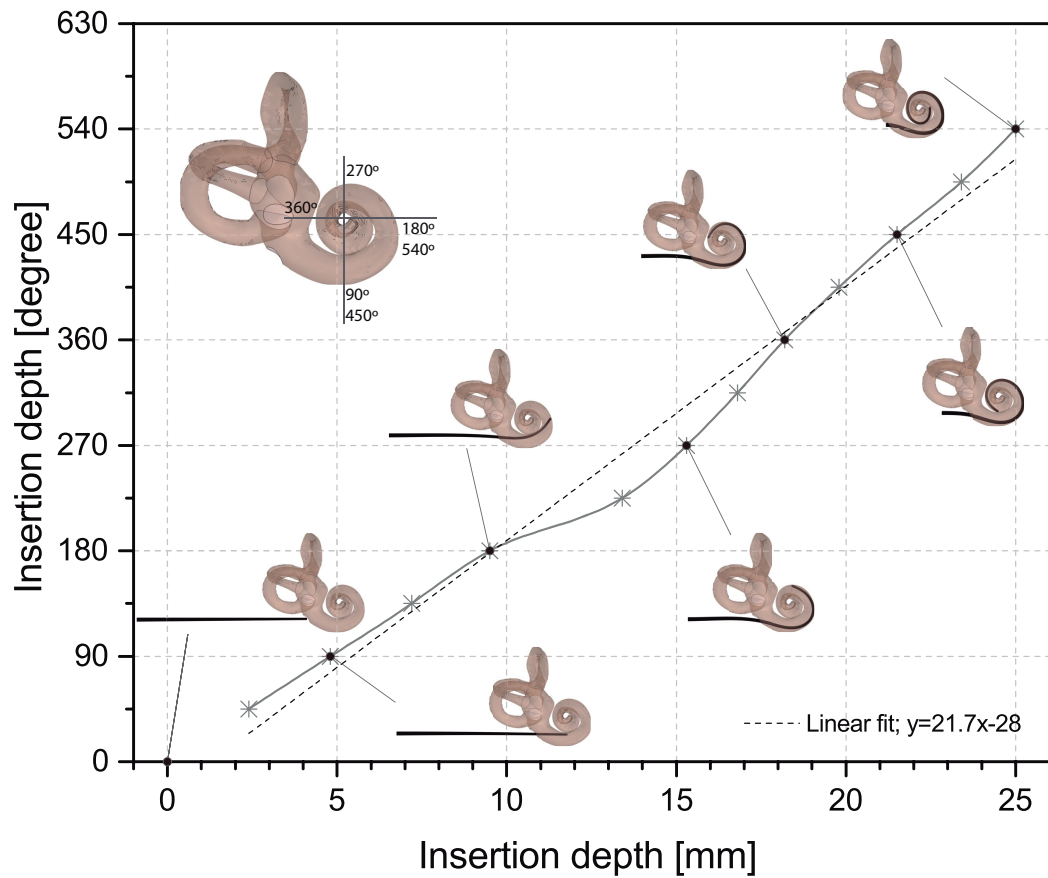


Figure 4.4: Relation between the insertion depth in millimetres vs in degrees ( $v_{\text{insertion}}=1 \text{ mm s}^{-1}$ , without friction).

as the most critical range of the insertion process. Similarly, De Seta et al. [35] mentioned the critical range between  $150^\circ$  and  $180^\circ$ . There appears to be a connection between the achieved deviation, due to the electrode adaptation, and the damage induced by the cochlear implant.

Since the insertion speed is a variable of the insertion procedure, different insertion speeds were simulated and its influence on the contact pressures computed. Figure 4.5 shows the evolution between the mean contact pressure at the cochlear implant tip and the insertion depth, for different insertion speeds. No differences in contact pressures were found for insertions with speeds lower than  $1 \text{ mm s}^{-1}$ . For  $2 \text{ mm s}^{-1}$  insertion speed, an increase in the contact pressure was verified, after an insertion

length of 15 mm. This difference amounted to approximately 50 %, for an insertion length of 25 mm.

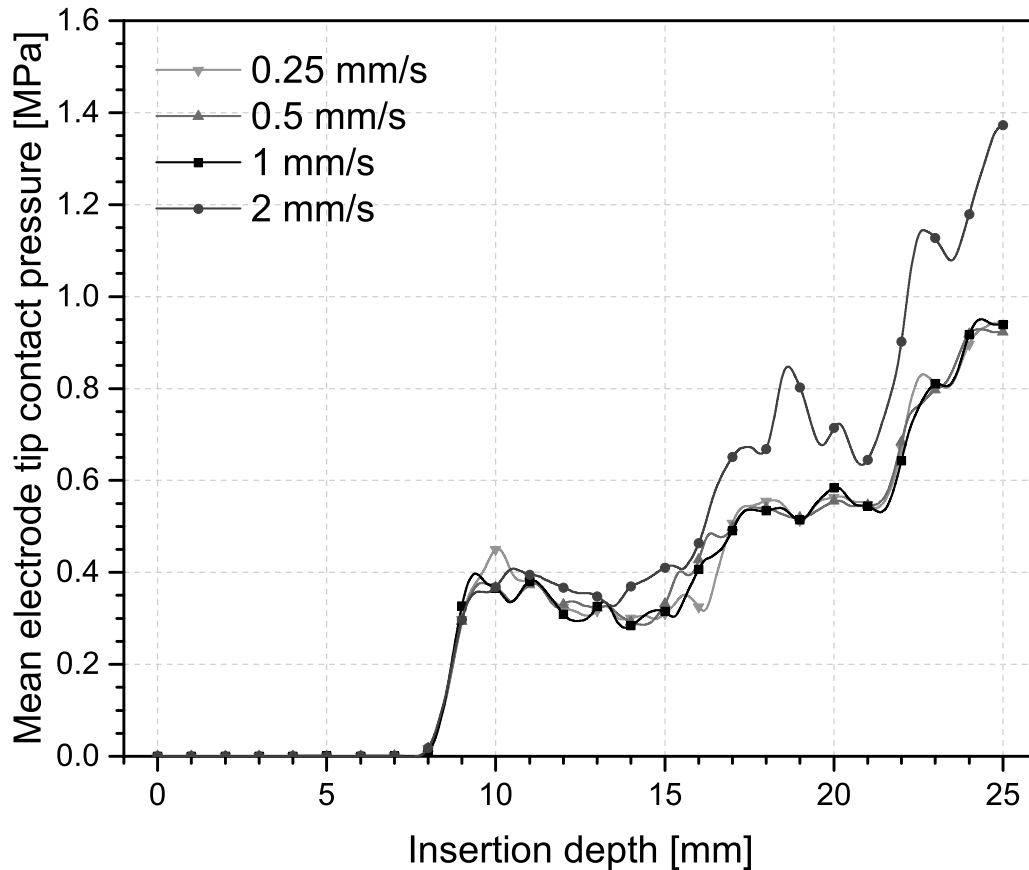


Figure 4.5: Mean electrode tip contact pressure during the insertion of 25 mm, for different insertion speeds (0.25, 0.5, 1 and 2 mm s<sup>-1</sup>).

Figure 4.6 shows that the relation between the insertion force and the insertion depth follows the same trend, among the different insertion speeds. The initial contact occurs for an insertion depth of 8 mm. After the initial contact, a sharp increase in the insertion force was identified, thus showing the adaptation of the electrode array to the cochlear wall. A second sharp increase in the insertion force was found, for all insertion speeds, after a insertion length of 20 mm. In order to fully insert the implants, the insertion force increases approximately 250 % in relation to the 20 mm insertion length.



In order to validate the model, two experimental data reported in the literature were also included in the Figure 4.6. The study conducted by Nguyen et al. [36] comprise the insertion of eight electrode arrays with an in-house made motorized insertion tool using an actuator speed controlled via a laboratory set at  $0.8 \text{ mm s}^{-1}$ . Another experimental study carried out by Avci et al. [37] at a speed of  $0.5 \text{ mm s}^{-1}$  was also represented. The grey area indicates  $\pm 1$  SD of the same work.

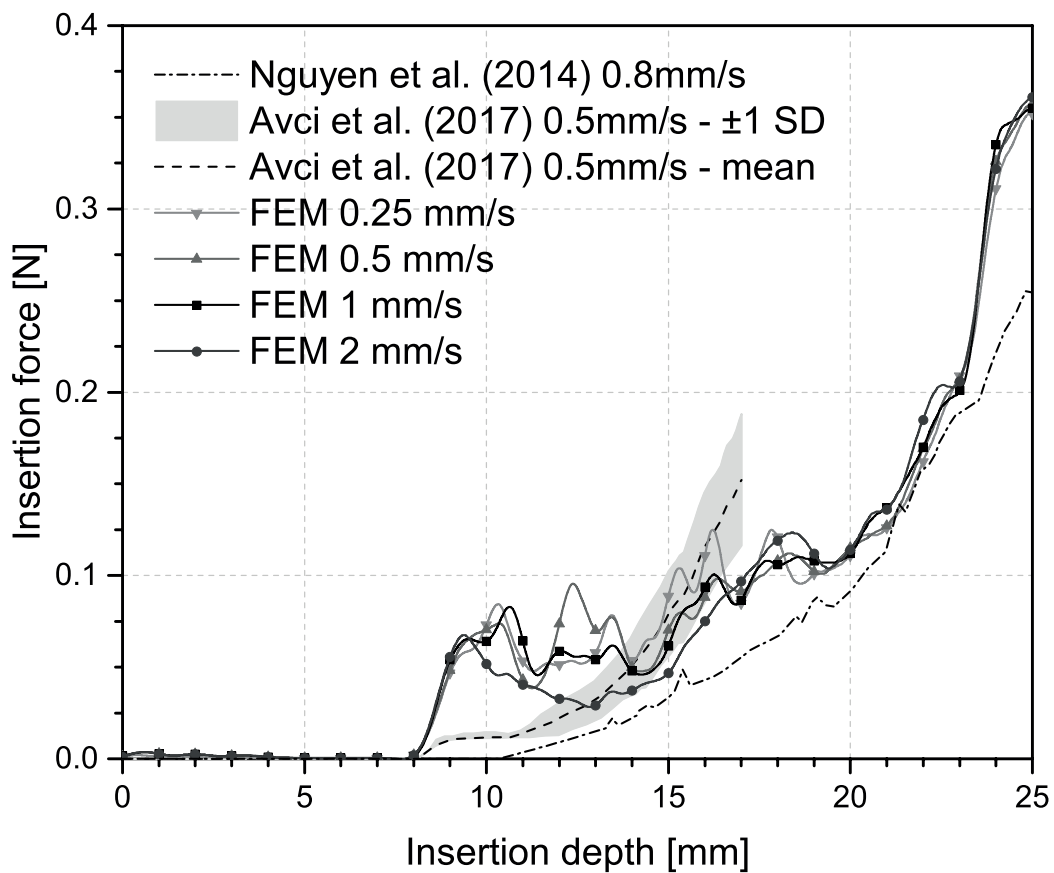


Figure 4.6: Insertion force during the insertion of 25 mm, for different insertion speeds ( $0.25$ ,  $0.5$ ,  $1$  and  $2 \text{ mm s}^{-1}$ ). Experimental data reported from Nguyen et al. [36] and Avci et al. [37] included in order to validate the model.

The differences observed in the responses, between the 8 mm and 12 mm, can be justified by a difference in the angle of insertion. The tangent insertion of the electrode array in relation to the lateral wall allows a decrease in the initial peak

force, however this type of procedure usually require the drilling of the round window or a cochleostomy. Our study considered the extraction of the round window, thus the insertion angle was not perfectly tangent to the cochlear walls, thus causing the sharp increase of the insertion force.

Among the different speeds tested, no major differences in the insertion force were found. In the study of Kontorinis et al. [29] a proportional correlation of the cochlear implant insertion speed with the insertion force was obtained. In contrast, Rau et al. [38], showed higher values of insertion force when implants were inserted with lower speeds. Some controversy exists in the literature, therefore the speeds usually used are very small to involve inertial effects.

The matrix presented in Figure 4.7 shows the influence of the friction coefficient on the von Mises stress distribution in the cochlear implant, for different insertion depths and for an insertion speed of  $1 \text{ mm s}^{-1}$ . The friction coefficients were based on the experimental data of Kha and Chen [39], which published values between 0.12 and 0.19 in conditions without lubricants and between 0.04 and 0.15 in conditions with glycerin and sorbelene. No major influence of the friction coefficient was verified on the von Mises stress distribution, along the cochlear implant. The higher differences appears for an insertion depth of 25 mm and for the higher friction coefficient used ( $\mu = 0.3$ ), where the cochlear implant started to buckle, near the round window. A decrease in the angular position of the cochlear implant, during insertion is also notorious as the friction coefficient increases. Outside the cochlear partition, on the cochlear implant an increase in the curvature as the friction increased is evident, thus showing the increasing resistance during insertion derived from the increasing friction coefficient (Figure 4.7, red arrows in the second row).

Frictional conditions are crucial in the evaluation of the contact stresses. As mentioned by Kha and Chen [39] small changes in the frictional coefficients can lead to large differences in the contact stresses. Figure 4.8 shows the relation between the mean contact pressure at the cochlear implant tip and the insertion depth, for different friction coefficients. An insertion speed of  $1 \text{ mm s}^{-1}$  was considered for all curves. As expected, the lowest mean contact pressure was obtained for the frictionless case. For the cases with friction, there is no notorious differences between an insertion depth of 5 mm ( $90^\circ$ ) and 15 mm ( $270^\circ$ ). However, a decrease of approximately 40% was

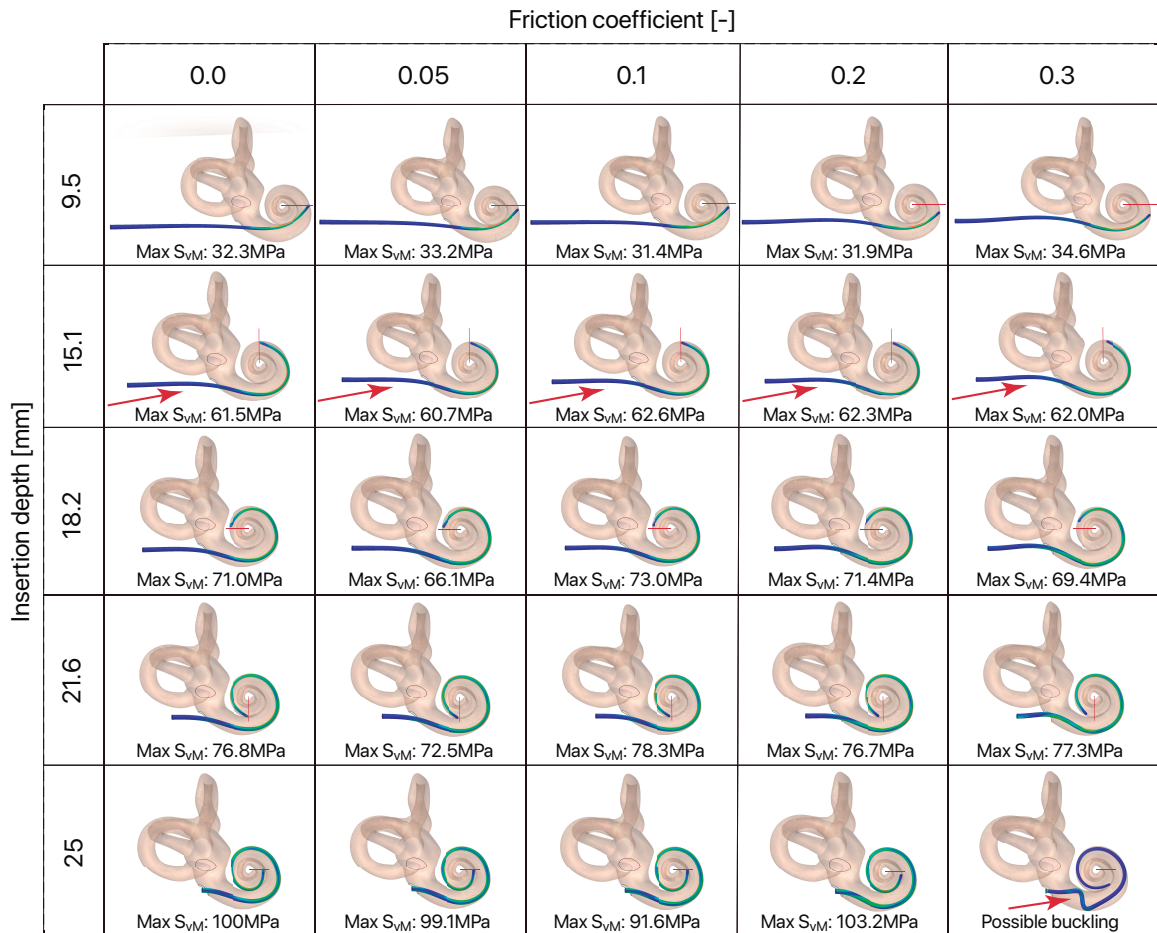


Figure 4.7: Influence of the friction coefficient between the cochlear implant and the scala tympani walls on the maximum von Mises stress ( $S_{vM}$ ) present on the cochlear implant, for different insertion depths.

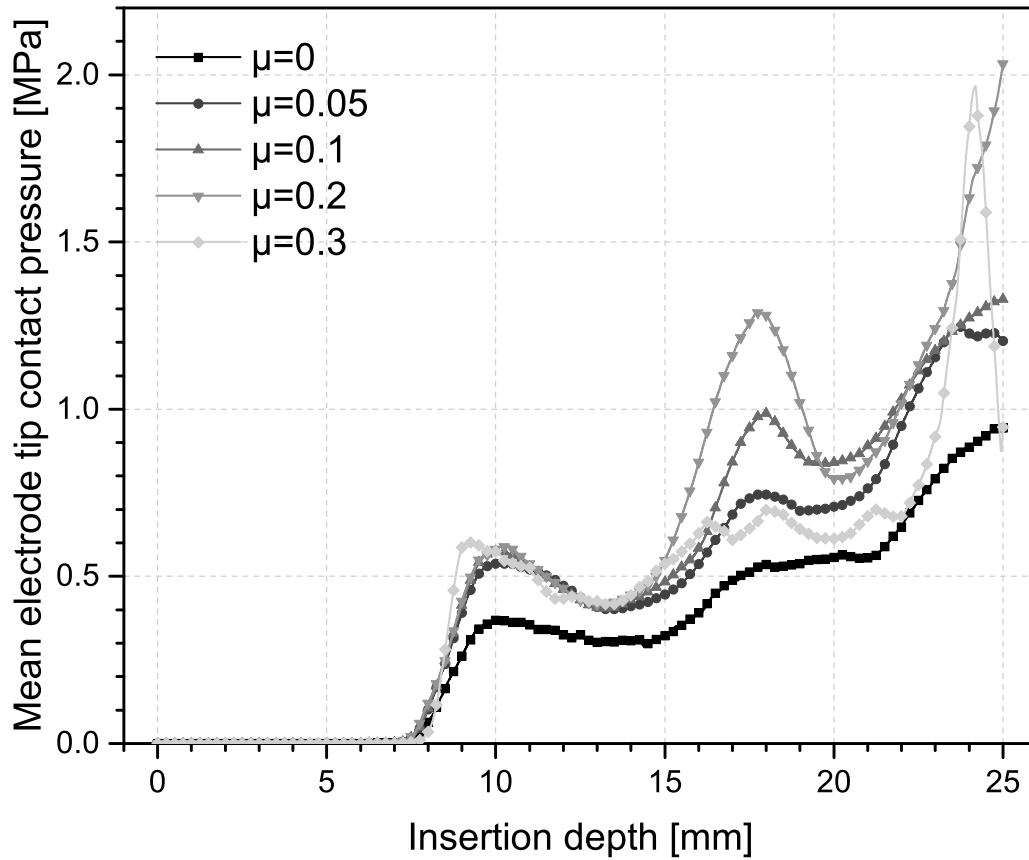


Figure 4.8: Mean electrode tip contact pressure during the insertion of 25 mm, for different friction coefficients (0, 0.05, 0.1, 0.2 and 0.3).

obtained between the frictionless case and all friction cases. After 15 mm, the mean contact pressure increases with friction, except for the case  $\mu = 0.3$ . In this case ( $\mu = 0.3$ ), the presence of the second peak (15 mm - 20 mm) was not evident. Such discrepancy can be related with the delay on the insertion of the cochlear implant due the friction between the electrode array and the endosteum lining, and also by the initiation of buckling which is visible in this case (Figure 4.7), which reduces the pressure on the tip. At the end of the cochlear implant insertion, the buckling of the electrode array causes an abrupt decrease of the mean contact pressure, for the higher friction coefficient.

Figure 4.9 shows the influence of the friction coefficient on the insertion force, for

an insertion speed of  $1 \text{ mm s}^{-1}$ . An increase in the insertion force for higher friction coefficients was obtained. Comparing with the frictionless case, there was an increase of the maximum insertion force in the order of 1.22 times with  $\mu = 0.05$ , of 1.67 times with  $\mu = 0.1$ , of 3.8 times with  $\mu = 0.2$  and of 9.4 times with  $\mu = 0.3$ . Therefore, an exponential increase of the maximum insertion force was obtained. Similarly, in Figure 4.8, the fast decrease of the insertion force for the higher friction coefficient ( $\mu = 0.3$ ) is a consequence of the electrode array buckling. Hence, for high friction coefficients ( $\mu > 0.2$ ), the buckling of electrode array may occur, thus damaging the cochlea near the round window.

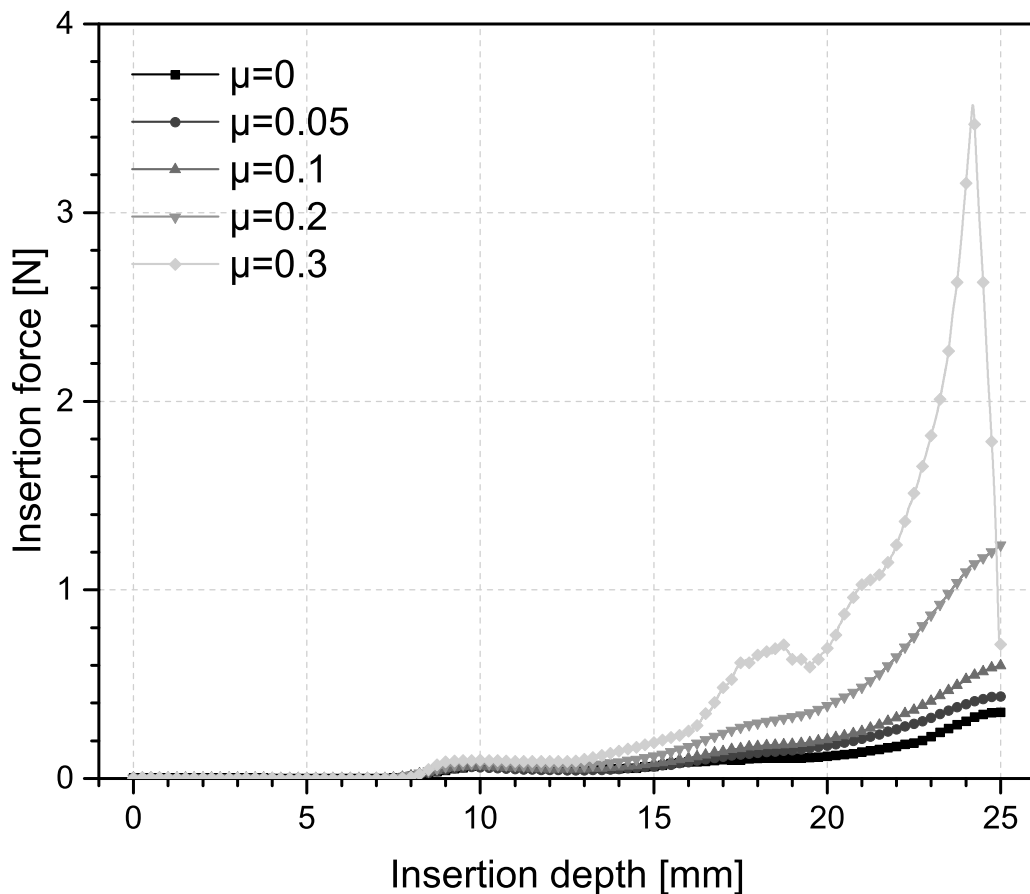


Figure 4.9: Insertion force during the insertion of 25 mm, for different friction coefficients (0, 0.05, 0.1, 0.2 and 0.3).

Figure 4.10 shows the mean contact pressure at the implant tip for different tip configurations. Overall, there was a decrease of the mean contact pressure as the Young's modulus of the tip decreased. No differences of the insertion trajectory were identified between all cases. The case with a Young's modulus of 250 MPa and a tip length of 5 mm shows an almost linear increase of the mean contact pressure, which can be correlated with fewer damages on the cochlear wall due to the smooth and progressive insertion. As mentioned by Dhanasingh and Jolly [40], damage of the cochlear wall can lead to the formation of new bone growth which could compromise the residual cochlear function. The case with a Young's modulus of 250 MPa and a tip length of 2.5 mm resulted in the lowest contact pressure with a reduction of 75 %

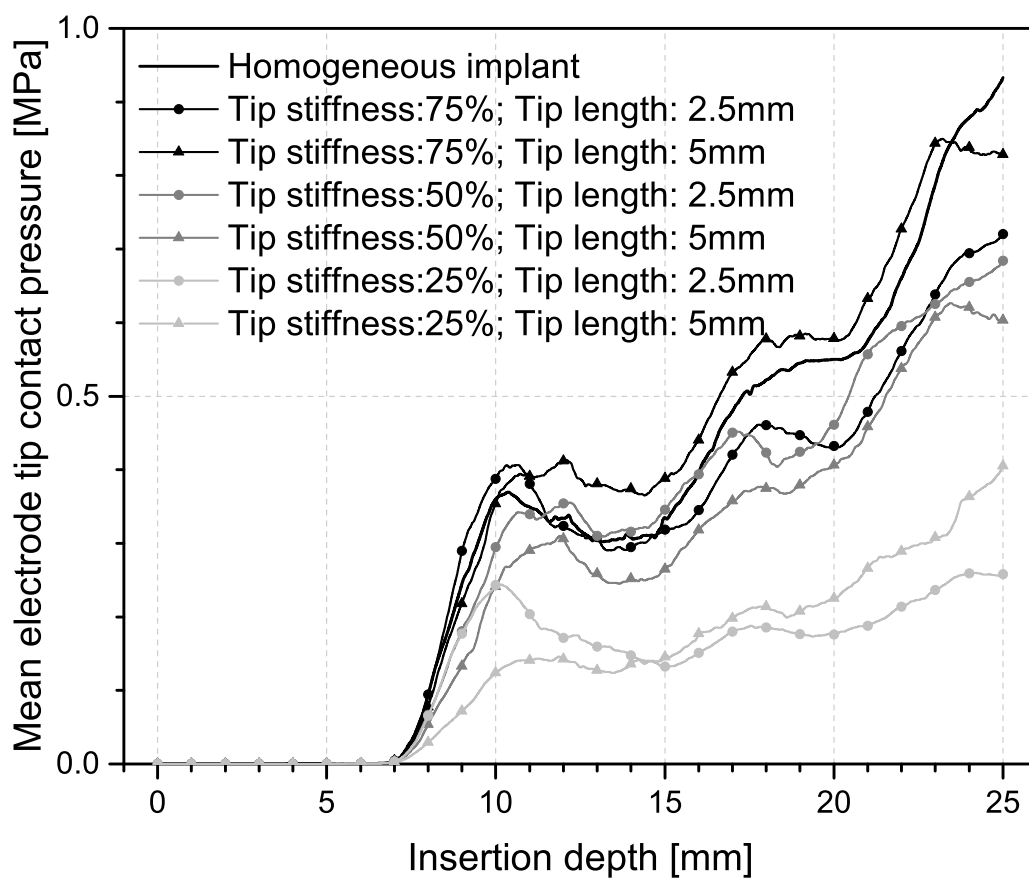


Figure 4.10: Mean electrode tip contact pressure during the electrode insertion, for different tip mechanical properties (Table 4.2).

when compared with the homogeneous case.

The insertion force for the different tip configurations is shown in Figure 4.11. No major differences were detected between all cases. Overall, a decrease in the maximum insertion force was obtained in all cases with modified tip when compared with the homogeneous implant case.

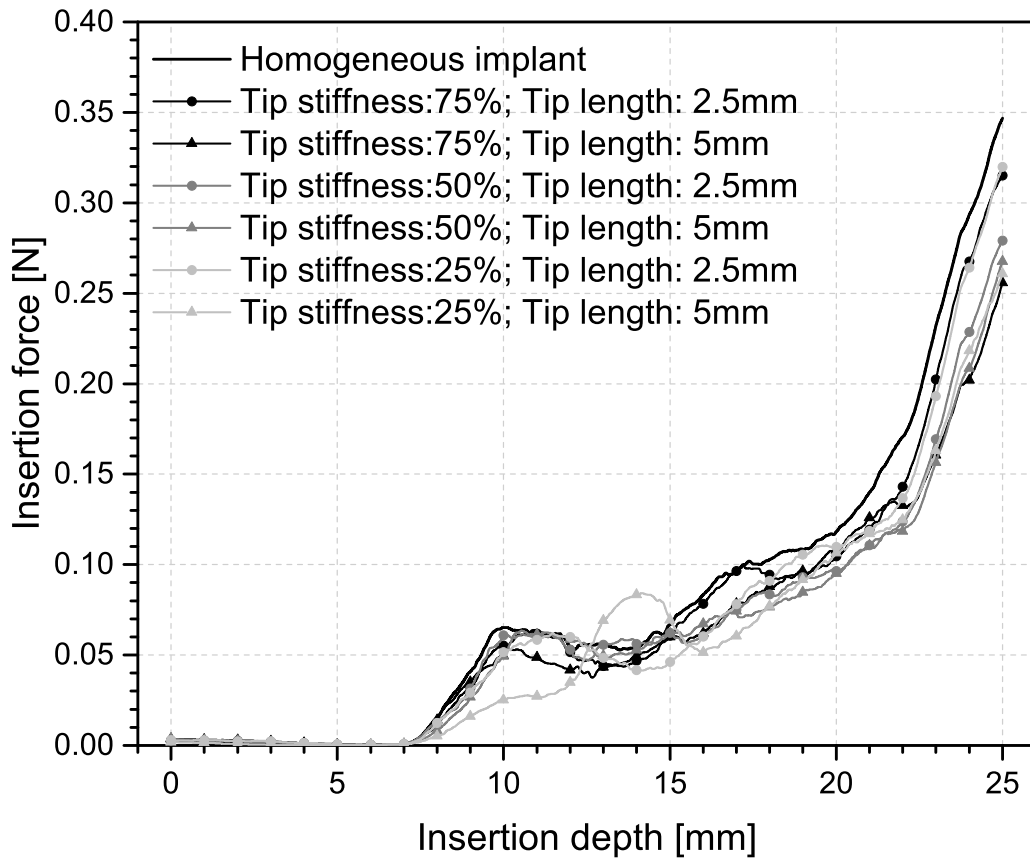


Figure 4.11: Insertion force during the electrode insertion, for different tip mechanical properties (Table 4.2).

## 4.6 Conclusions

Cochlear implant electrode insertion force and contact pressure between the implant tip and the cochlear wall can influence the intra-cochlear damage and the preservation of the residual hearing. A series of steps takes place during the cochlear

implant insertion. Such stages were investigated in this numerical study. The relation between the insertion depth and the angular position of the implant tip follows approximately a linear regression. For an insertion depth between 10 mm and 18 mm the initial contact was established and a consequent adaptation of the cochlear implant to the cochlear wall occurred.

The study involving different insertion speeds showed that lower speeds resulted in lower contact pressures at the implant tip. In relation to the friction coefficient, there was an abrupt decrease of the mean contact pressure and insertion force in the case of  $\mu = 0.3$ , thus showing a buckling of the electrode array. The friction coefficient exhibit no influence on the von Mises stresses along the electrode array. However, an increase in the insertion force as the friction coefficient increased was achieved. With respect to the study of the cochlear implant tip properties, a decrease in the mean contact pressure was obtained as the Young's modulus decreased. No differences in the electrode array trajectory were identified between all the studied cases. The homogeneous implant exhibited the highest insertion force compared with the modified tip cases.

In order to reduce the probability of buckling and increase the cochlear implant stability, a stiffer electrode array at the basal portion should be developed. The results showed that a soft tip can decrease the contact pressure, thus resulting in a less damage of the cochlear walls. It is therefore necessary to numerically study novel cochlear implants with gradual stiffness in order to avoid high contact pressures with the cochlear walls and the basilar membrane, which can lead to its perforation and consequently, the loss of the endo-cochlear potential and the loss of the residual hearing.



## **4.7 Conflict of interest statement**

The authors declare that there is no financial, professional or other personal interest of any nature or kind in any product, service and/or company that could be constructed as influencing the position.

## **4.8 Acknowledgements**

The authors truly acknowledge the funding provided by Ministério da Ciência, Tecnologia e Ensino Superior - Fundação para a Ciência e a Tecnologia (Portugal), under grant: SFRH/BD/129397/2017. This research was also supported by the Portuguese Foundation of Science and Technology under the research project UIDB/50022/2020.

## 4.9 References

- [1] Stilianos E. Kountakis. *Encyclopedia of otolaryngology, head and neck surgery*. Springer Reference, Heidelberg ; New York, 2013.
- [2] A. A. Eshraghi, R. Nazarian, F. F. Telischi, S. M. Rajguru, E. Truy, and C. Gupta. The cochlear implant: historical aspects and future prospects. *Anat Rec (Hoboken)*, 295(11):1967–80, 2012.
- [3] Anna Korver, Richard Smith, Guy Camp, Mark Schleiss, Maria Bitner-Glindzicz, Lawrence Lustig, Shin-ichi Usami, and An Boudewyns. Congenital hearing loss. *Nature Reviews Disease Primers*, 3:16094, 2017.
- [4] S. B. Allen and J. Goldman. Syndromic sensorineural hearing loss. In *StatPearls*, Treasure Island (FL), 2020.
- [5] H. Kha and B. Chen. Finite element analysis of damage by cochlear implant electrode array’s proximal section to the basilar membrane. *Otol Neurotol*, 33(7):1176–80, 2012.
- [6] T. Stover and T. Lenarz. Biomaterials in cochlear implants. *GMS Curr Top Otorhinolaryngol Head Neck Surg*, 8:Doc10, 2009.
- [7] A. Kral. Auditory critical periods: A review from system’s perspective. *Neuroscience*, 247:117–133, 2013.
- [8] I. Asimov. *Asimov’s biographical encyclopedia of science and technology: the lives and achievements of 1195 great scientists from ancient times to the present, chronologically arranged*. Doubleday, 1972.

- [9] A. Djourno and C. Eyries. Auditory prosthesis by means of a distant electrical stimulation of the sensory nerve with the use of an indwelt coiling. *La Presse medicale*, 65(63):1417, 1957.
- [10] Chong-Sun Kim, Dong-Kyu Kim, Myung-Whan Suh, Seung Ha Oh, and Sun O. Chang. Clinical outcomes of cochlear reimplantation due to device failure. *Clinical and experimental otorhinolaryngology*, 1(1):10–14, 2008.
- [11] N. L. Cohen and R. A. Hoffman. Complications of cochlear implant surgery in adults and children. *Ann Otol Rhinol Laryngol*, 100(9 Pt 1):708–11, 1991.
- [12] N. Loundon, M. Blanchard, G. Roger, F. Denoyelle, and E. N. Garabedian. Medical and surgical complications in pediatric cochlear implantation. *Arch Otolaryngol Head Neck Surg*, 136(1):12–5, 2010.
- [13] B. Terry, R. E. Kelt, and A. Jeyakumar. Delayed complications after cochlear implantation. *JAMA Otolaryngol Head Neck Surg*, 141(11):1012–7, 2015.
- [14] S. J. Dettman, D. Pinder, R. J. S. Briggs, R. C. Dowell, and J. R. Leigh. Communication development in children who receive the cochlear implant younger than 12 months: Risks versus benefits. *Ear and Hearing*, 28(2):11s–18s, 2007.
- [15] M. M. Cohen, C. B. Cameron, and P. G. Duncan. Pediatric anesthesia morbidity and mortality in the perioperative period. *Anesthesia and Analgesia*, 70(2):160–167, 1990.
- [16] A. Farinetti, D. Ben Gharbia, J. Mancini, S. Roman, R. Nicollas, and J. M. Triglia. Cochlear implant complications in 403 patients: Comparative study

- of adults and children and review of the literature. *European Annals of Otorhinolaryngology-Head and Neck Diseases*, 131(3):177–182, 2014.
- [17] I. K. Sefein. Surgical complications and morbidity in cochlear implantation. *Egyptian Journal of Otolaryngology*, 34(1):33–41, 2018.
- [18] P. Gibson and P. Boyd. Optimal electrode design: Straight versus perimodiolar. *European Annals of Otorhinolaryngology-Head and Neck Diseases*, 133:S63–S65, 2016.
- [19] A. A. Eshraghi, N. W. Yang, and T. J. Balkany. Comparative study of cochlear damage with three perimodiolar electrode designs. *Laryngoscope*, 113(3):415–419, 2003.
- [20] F. Risi. Considerations and rationale for cochlear implant electrode design - past, present and future. *Journal of International Advanced Otology*, 14(3):382–391, 2018.
- [21] Ahmed Khater and Mohammad Waheed El-Anwar. Methods of hearing preservation during cochlear implantation. *International Archives of Otorhinolaryngology*, 21:297–301, 2017.
- [22] Céline Richard, Jose N. Fayad, Joni Doherty, and Jr. Linthicum, Fred H. Round window versus cochleostomy technique in cochlear implantation: histologic findings. *Otology & Neurotology*, 33(7):1181–1187, 2012.
- [23] N. T. Jiam and C. J. Limb. The impact of round window vs cochleostomy surgical approaches on interscalar excursions in the cochlea: Preliminary results

- from a flat-panel computed tomography study. *World J Otorhinolaryngol Head Neck Surg*, 2(3):142–147, 2016.
- [24] K. Sikka, A. Kairo, C. A. Singh, T. S. Roy, S. Lalwani, R. Kumar, A. Thakar, and S. C. Sharma. An evaluation of the surgical trauma to intracochlear structures after insertion of cochlear implant electrode arrays: A comparison by round window and antero-inferior cochleostomy techniques. *Indian Journal of Otolaryngology and Head & Neck Surgery*, 69(3):375–379, 2017.
- [25] Cochlear Limited, 2019. Cochlear Limited. Available at <https://www.cochlear.com>. Accessed 10th February 2020.
- [26] Dassault Systemes. *ABAQUS analysis user's guide*. 2016.
- [27] G. P. Rajan, G. Kontorinis, and J. Kuthubutheen. The effects of insertion speed on inner ear function during cochlear implantation: a comparison study. *Audiol Neurootol*, 18(1):17–22, 2013.
- [28] I. Todt, P. Mittmann, and A. Ernst. Intracochlear fluid pressure changes related to the insertional speed of a ci electrode. *Biomed Research International*, 2014.
- [29] G. Kontorinis, T. Lenarz, T. Stover, and G. Paasche. Impact of the insertion speed of cochlear implant electrodes on the insertion forces. *Otology & Neurotology*, 32(4):565–570, 2011.
- [30] Bruno Areias, Carla Santos, Renato M Natal Jorge, Fernanda Gentil, and Marco P L Parente. Finite element modelling of sound transmission from outer to inner ear. *Proceedings of the Institution of Mechanical Engineers. Part H, Journal of engineering in medicine*, 230:999–1007, 2016.

- [31] Q. Sun, R. Z. Gan, K-H Chang, and K. J. Dormer. Computer-integrated finite element modeling of human middle ear. *Biomechanics and modeling in mechanobiology*, 1:109–22, 2002.
- [32] F Gentil, M Parente, P Martins, C Garbe, R N Jorge, A Ferreira, and João Manuel R S Tavares. The influence of the mechanical behaviour of the middle ear ligaments: a finite element analysis. *Proceedings of the Institution of Mechanical Engineers. Part H, Journal of engineering in medicine*, 225:68–76, 2011.
- [33] B. K. Chen, G. M. Clark, and R. Jones. Evaluation of trajectories and contact pressures for the straight nucleus cochlear implant electrode array - a two-dimensional application of finite element analysis. *Medical Engineering & Physics*, 25(2):141–147, 2003.
- [34] B. K. H. G. Franz and G. M. Clark. Refined surgical technique for insertion of banded electrode array. *Annals of Otology Rhinology and Laryngology*, 96(1):15–17, 1987.
- [35] D. De Seta, R. Torres, F. Y. Russo, E. Ferrary, G. Kazmitcheff, D. Heymann, J. Amiaud, O. Sterkers, D. Bernardeschi, and Y. Nguyen. Damage to inner ear structure during cochlear implantation: Correlation between insertion force and radio-histological findings in temporal bone specimens. *Hearing Research*, 344:90–97, 2017.
- [36] Y. Nguyen, G. Kazmitcheff, D. De Seta, M. Miroir, E. Ferrary, and O. Sterkers. Definition of metrics to evaluate cochlear array insertion forces performed with forceps, insertion tool, or motorized tool in temporal bone specimens. *Biomed Res Int*, 2014:532570, 2014.

- [37] E. Avci, T. Nauwelaers, V. Hamacher, and A. Kral. Three-dimensional force profile during cochlear implantation depends on individual geometry and insertion trauma. *Ear Hear*, 38(3):168–179, 2017.
- [38] T. S. Rau, A. Hussong, M. Leinung, T. Lenarz, and O. Majdani. Automated insertion of preformed cochlear implant electrodes: evaluation of curling behaviour and insertion forces on an artificial cochlear model. *International Journal of Computer Assisted Radiology and Surgery*, 5(2):173–181, 2010.
- [39] H. N. Kha and B. K. Chen. Determination of frictional conditions between electrode array and endosteum lining for use in cochlear implant models. *Journal of Biomechanics*, 39(9):1752–1756, 2006.
- [40] A. Dhanasingh and C. Jolly. An overview of cochlear implant electrode array designs. *Hear Res*, 356:93–103, 2017.





## Chapter 5

# Insertion of a cochlear straight electrode array with different wires arrangements: a numerical study



**Article 4 - Insertion of a cochlear straight electrode array  
with different wires arrangements: a numerical study**

B. Areias (1), M.P.L. Parente (1,2), F. Gentil (3), R.M. Natal Jorge (1,2)

1-INEGI, Institute of science and innovation in mechanical and industrial  
engineering, Porto, Portugal {bareias@fe.up.pt}

2-FEUP, Faculty of Engineering, University of Porto, Porto, Portugal  
{mparente@fe.up.pt, rnatal@fe.up.pt}

3-Escola Superior de Saúde - Politécnico do Porto; Clínica ORL – Dr. Eurico de  
Almeida; WIDEX {fernanda.fgnanda@gmail.com}

*Submitted to an international journal*

This chapter seeks to increase the knowledge on the best wires configuration within an electrode array. Three types of configuration are studied, including the straight, zigzag and helix configuration.



## 5.1 Abstract

A cochlear implant is a small and complex electronic device that can restore the sense of hearing in a person with severe to profound sensorineural hearing loss. Severe or profound hearing loss can be a consequence of the inability of the stereocilia to self-repair, which subsequently leads to hair cell death and permanent hearing loss. Until now, a cochlear implant is the only device which is able to help people with permanent hearing loss, giving a modified sense of hearing. One of the most important aspects when designing an cochlear implant is the minimization of the physical trauma caused by its insertion. This work intends to investigate three different arrangements in the platinum/iridium wires. Each configuration was designed with one parameter which was also studied. The results show that the helix configuration provides the lowest insertion force, minimizing the intra-cochlear damage during its insertion. The numerical simulations have shown that the helix  $p$ -parameter has reduced influence in the insertion force during implantation.

## 5.2 Keywords

cochlea, electrode array, wire arrangement, insertion force, finite element method

## 5.3 Introduction

According to the World Health Organization, approximately 466 million people worldwide suffer from some type of hearing loss. About ninety-three percent of them are adults, aged over 15 years of age [1]. Even with a low incidence in children, profound hearing loss in this group leads to a deficient development of spoken language, resulting in a negative impact on daily communication and later compromising their employment opportunities. Adults, on the other hand, which acquired the profound hearing loss after having developed spoken language and cognitive abilities are able to use these skills with the help of a cochlear implant, as stated by Jorgensen et al. [2].

The study of Ishiyama et al. [3] reports the incidence of a variety of complications associated with the surgical placement of cochlear implant electrode arrays. The incidence of incomplete electrode insertion and kinking is more prevalent in straight arrays and lower than 2% in patients with normal cochlear anatomy. Incidence of tip fold-over is lesser in straight arrays and is typically less than 5%. Scalar translocation or scala tympani–scala vestibuli crossover is more common with the cochleostomy approach and perimodiolar electrodes than with round window enlargement or round window techniques and straight electrode designs, as mentioned by Wanna et al. [4]. The consequences of such complications are associated with the preservation of residual acoustic hearing. Other common complication in straight electrodes is the electrode migration. Electrode migration may be due to inherent springiness of the array or to pulling forces external to the cochlea [3]. The cochlear anatomy, the surgeon experience, the type of material (metallic wires and embedding silicone) and the design of the electrode array are partly responsible for the complications

mentioned above.

Cochlear implant electrodes consist in platinum contacts and platinum-iridium 90/10 wires (isolated with Teflon coating) embedded in a non-conductive silicone carrier material. Electrode stiffness is mainly determined by the internal platinum-iridium wires. The wires arrangement configuration is the main influence on the electrode's mechanical properties, as stated by Stover and Lenarz [5].

Lim et al. [6], carried out a study based in six electrodes with different arrangements, each of which comprises sixteen metal wires. The numerical results obtained by the author, showed that low insertion forces and contact pressures at the cochlear implant tip are obtained when the wires are stacked vertically. The vertically plane was defined to be parallel with the central axis of the cochlea. However, the literature on this subject is scarce. Thus, this work seeks to increase the knowledge about the best wires configuration within the electrode array.

In this work, three types of configuration were studied, including the straight, zigzag and helix configuration. In each configuration, one parameter was also studied. The numerical results reached can serve as a basis for the future development of less traumatic electrode arrays.

## 5.4 Materials and Methods

The 3D anatomical geometry of the human bony labyrinth was obtained from a magnetic resonance imaging scan, of a male patient, 85 years-old, without cochlear pathologies. The images were manually segmented in order to obtain the 3D reconstruction.

The straight electrode array represented in Figure 5.1 was modelled in order to

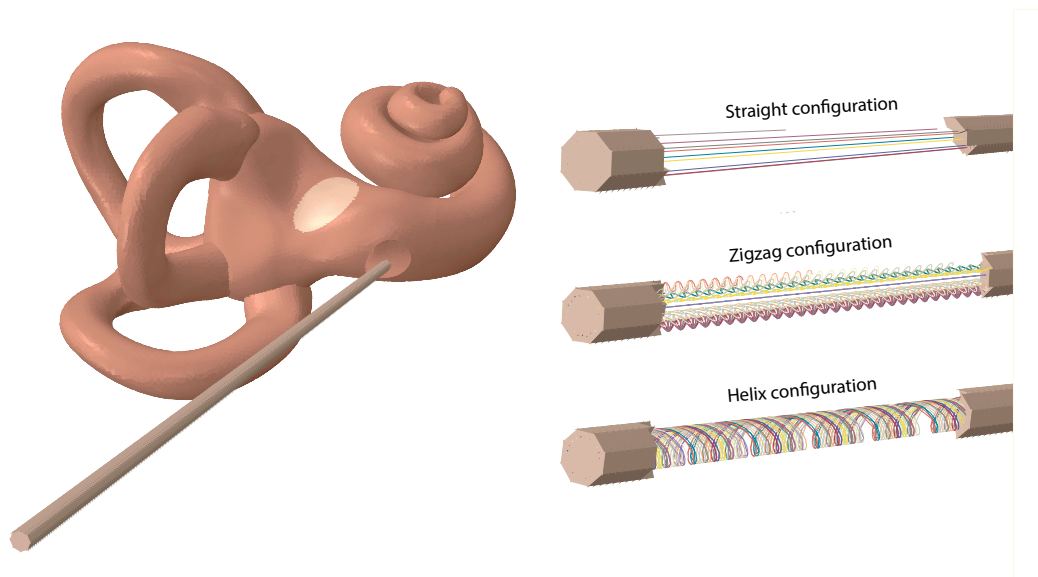


Figure 5.1: Bony labyrinth with the electrode array (left), Three different wires configurations, with the silicone partially removed (right).

simulate its insertion into the bony labyrinth. The geometry and dimensions of the straight electrode were based on a standard, commercially available, CI622 cochlear implant, manufactured by the Cochlear medical device company [7]. The CI622 electrode measures 25 mm in length and has 22 platinum electrode contacts along its length. The diameters at the basal end and hemispherical tip are 0.55 mm and 0.3 mm, respectively. The finite element model was simplified and the platinum contacts were not considered in the numerical simulations. The platinum/iridium wires were modelled with a diameter of 25  $\mu\text{m}$ . All 22 wires begin at the proximal end of the electrode array and end along the electrode array in such a way that all endings are equally spaced between them (the largest wire covers the total length of the electrode array). A radial distribution was applied to the platinum/iridium wires into the electrode array. The decrease of the electrode array's diameter towards the distal end result in a convergence angle of  $0.25^\circ$ , also imposed in the implant wires.

The mechanical properties of the electrode array are summarised in Table 5.1.



Table 5.1: Cochlear implant's mechanical properties

		$E$ [MPa]	$\nu$ [-]	$\rho$ [kg m <sup>-3</sup> ]	$\sigma_{pl1}$ [MPa]	$\varepsilon_{pl1}$ [-]	$\sigma_{pl2}$ [MPa]	$\varepsilon_{pl2}$ [-]
Cochlear implant	Implant matrix	180	0.45	1120				
	Implant wires	202300	0.378	21600	295	0	567	0.3

The bony labyrinth was assumed as a rigid body, being fixed in all degree of freedom. The matrix (silicone) and the wires (platinum/iridium - 90/10) of the electrode array were assumed with elastic and elasto-plastic properties, respectively. The mechanical behaviour of the electrode array components were based in the CES EduPack software [8], in the work of Merker et al. [9] and Kha et al. [10]. Plasticity data in Abaqus was defined using true stress and true strain. Two pairs of points ( $\sigma_{pl1}, \varepsilon_{pl1}; \sigma_{pl2}, \varepsilon_{pl2}$ ) were used to define the plastic behaviour of the wires. The first pair of points defines the yield point of the platinum/iridium alloy (90/10), whereas the second pair of points defines the ultimate strength point. Also, the Young's modulus,  $E$ , the Poisson's ratio,  $\nu$ , and the density,  $\rho$ , were defined for the electrode array components.

Three different wires arrangement were modelled. In each of them a different parameter was studied (straight  $d$ -parameter, zigzag  $c$ -parameter and helix  $p$ -parameter; see Figure 5.2). The straight  $d$ -parameter refers to the diameter of the circular arrangement of the set of wires at the proximal end of the electrode array (values:  $d=0.3$  mm and  $d=0.4$  mm). The zigzag configuration is composed by a sequence of semi-circles, therefore the zigzag  $c$ -parameter is then related with the diameter of the semi-circles (values:  $c=0.05$  mm and  $c=0.1$  mm). The helix  $p$ -parameter refers to the pitch of the helix (values:  $p=0.5$  mm and  $p=1$  mm). The diameter of the circular arrangement of the set of wires at the proximal end in both

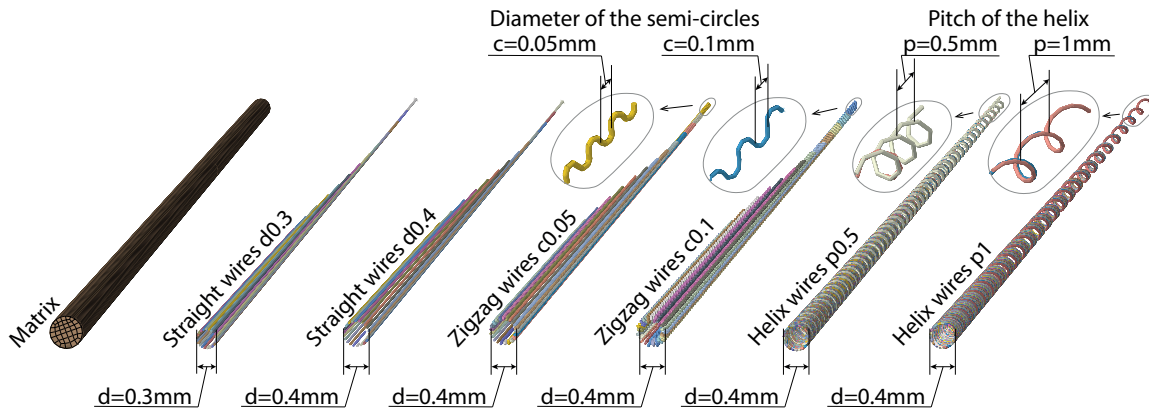


Figure 5.2: Dimensions of the three different electrode arrays configurations.

zigzag and helix configurations were considered with 0.4 mm.

The elements which discretizes the implant wires were embedded in the elements of the silicone matrix through an embedded element technique available in the Abaqus software [11]. This technique is used to specify that an element or group of elements is embedded in host elements. The geometric relationships between the nodes of the embedded elements and the host elements are automatically assigned by Abaqus. If a node of an embedded element lies within a host element, their translational degrees of freedom are eliminated becoming an embedded node.

The number of nodes and elements, and the type of element used in the electrode

Table 5.2: Mesh description of the electrode array

Parameter	Wires - Straight		Wires - Zigzag		Wires - Helix		Matrix
	$d$	$d$	$c$	$c$	$p$	$p$	
Nodes	0.3 mm	0.4 mm	0.05 mm	0.1 mm	0.5 mm	1 mm	20172
Elements	2293	2293	21485	10582	6065	3866	15942
Element type	B31						C3D8R
Element characteristic length	0.12 mm						0.06 mm

array are summarized in Table 5.2. A displacement of 25 mm at the proximal end of the electrode array was imposed in all case studies, resulting in a full electrode insertion. No friction was considered between the cochlear wall and the electrode array. The Software Abaqus Explicit [11] was used in order to conduct all numerical analysis.

## 5.5 Results

The insertion force, the mean contact pressure and the wire's plastic deformation for six case studies during the insertion process are shown in the next Figures. Figure 5.3 shows the insertion force during the implantation process. As shown in Figure 5.3, the straight d0.4 electrode array was the configuration with the highest insertion force at the end of the implantation process. The straight d0.3 electrode

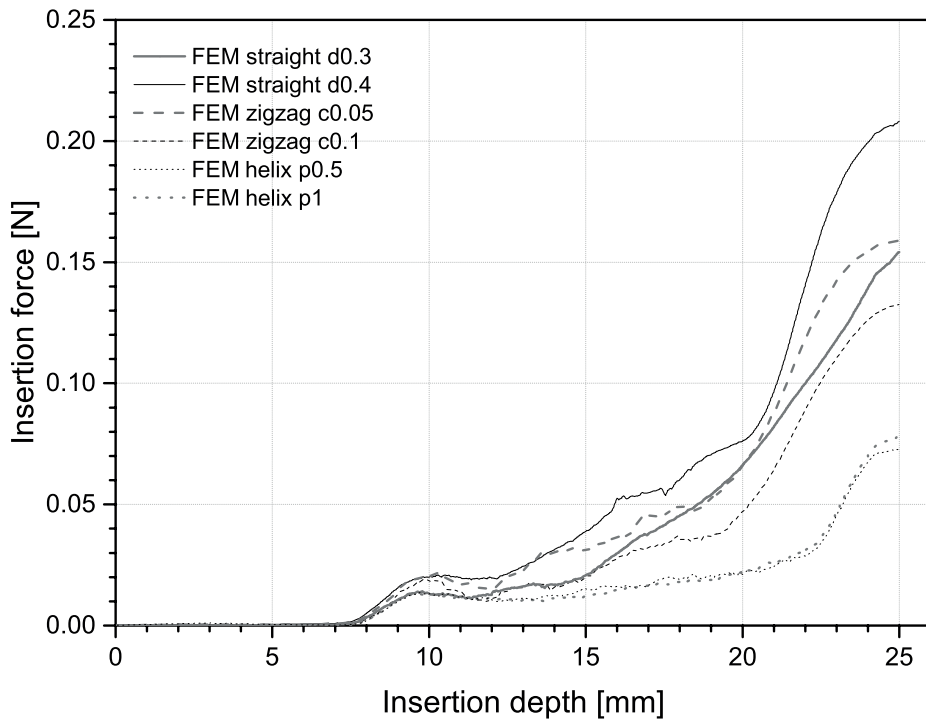


Figure 5.3: Insertion force vs insertion depth among the different wires configurations.

configuration shows a lower force in comparison with the electrode mentioned above. This demonstrates that the wires arrangement near the nucleus of the electrode array require a low insertion force, since the flexural modulus of the electrode array is smaller in this case.

On the other hand, the zigzag electrode array provided an intermediate insertion force, however, when the  $c$ -parameter is lowered, the force required for its insertion increases. Lastly, the helix electrode array showed a lower influence with the variation of the  $p$ -parameter. This configuration provided the lowest insertion force among all configuration studied. Comparing the maximum values, the helix configuration allowed a reduction of 36% in the maximum insertion force by comparison with the straight d0.4 electrode configuration. The Figure 5.4 shows the sequence of steps during the electrode array insertion for the helix p0.5 configuration.

Figure 5.5 shows the mean contact pressure at the electrode array tip during the cochlear implantation among the six configurations investigated. The maximum contact pressure at the electrode array tip was obtained for the helix configuration. Contrary to the insertion force graph, the straight model showed the lowest mean

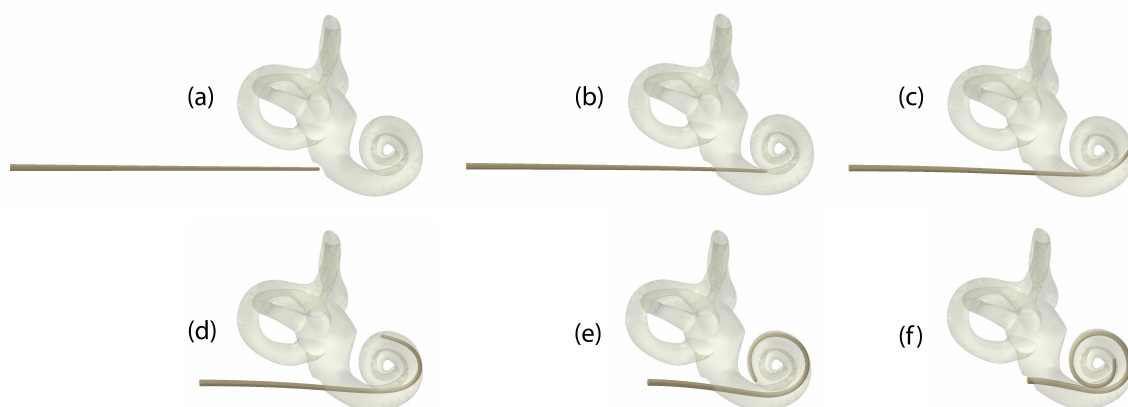


Figure 5.4: Steps during an electrode array insertion for the helix p0.5 configuration: (a) 0mm, (b) 5mm, (c) 10mm, (d) 15mm, (e) 20mm, (f) 25mm.

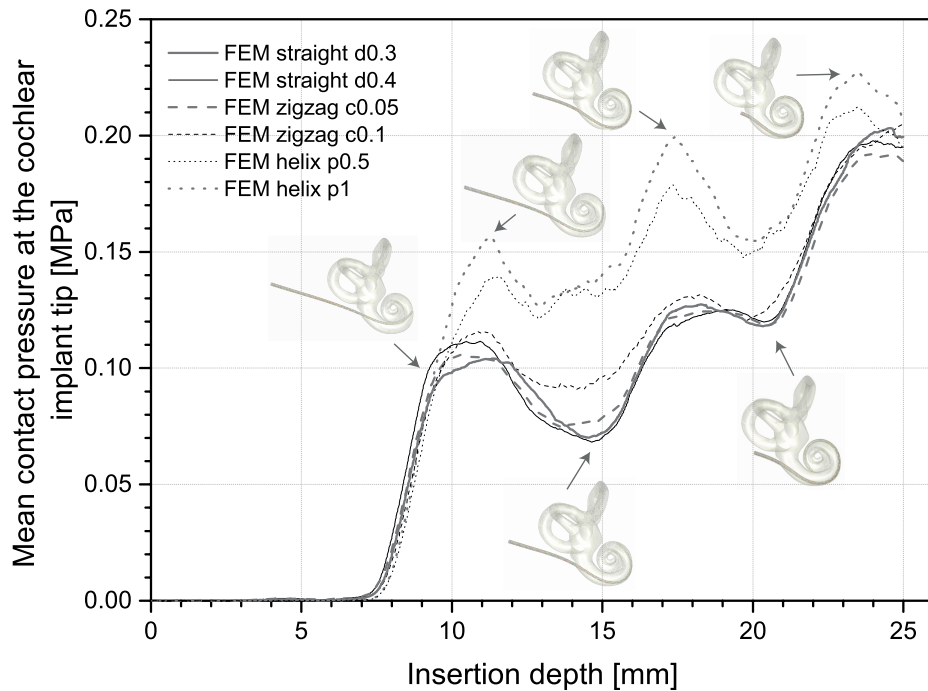


Figure 5.5: Mean contact pressure at the electrode array tip during the cochlear implantation among the different wires configurations.

contact pressure at the implant tip. This difference is due to the greater plastic deformation which the straight electrode showed during its insertion (see Figure 5.7). Such permanent deformation in the platinum/iridium wires along the electrode allows a reduction in the mean contact pressure at the implant tip. Further, the low plastic deformation in the helix configurations during its insertion can lead to an increase in mean contact pressure at the implant tip comparing to the other configurations studied. The fluctuation pattern in the mean contact pressure is notorious in all cases, this pattern is due to the relative position of the implant tip. When the velocity vector of the electrode tip is in the same direction of the velocity vector of the proximal end (where the displacement was applied), there is relief on the contact pressure.

The Figure 5.6 shows the mean contact pressure in two portions of the electrode array, the distal and the proximal portion. In contrast to Figure 5.5, we can verify that

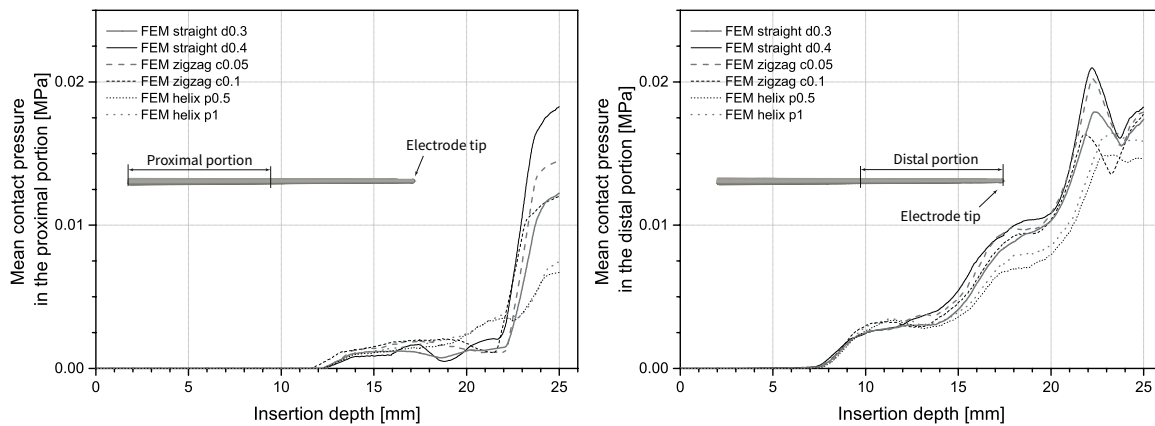


Figure 5.6: Mean contact pressure in the proximal and distal portion of the electrode array during the cochlear implantation among the different wires configurations.

the mean contact pressure in the helix configuration is almost always considerably inferior in comparison with others configurations, being obtained the maximum mean contact pressure in the straight configuration. Therefore, considering the entire surface of the electrode array, a greater plastic deformation of the implant wires lead to a greater mean contact pressure on the electrode array surface and a decrease at the implant tip.

Figure 5.7 shows the mean equivalent plastic strain (PEEK) in the implant wires during the electrode array insertion. The straight configurations provided the highest mean equivalent plastic strain in the implant wires. On the other hand, the helix configuration allowed to obtain the lowest plastic strain. The plastic deformation of the wires should be avoided since it increases the mean contact pressure along the electrode array (ver Figure 5.6).

Figure 5.8 shows the incidence rate of the location of the maximum PEEK in the implant wires during the cochlear implantation among the different wires configurations. The upper and lower right quadrants are the locations where the greatest plastic deformation is found. However, the zigzag and helix configurations

has a lower incidence rate in the lower right quadrant when compared with the straight configuration.

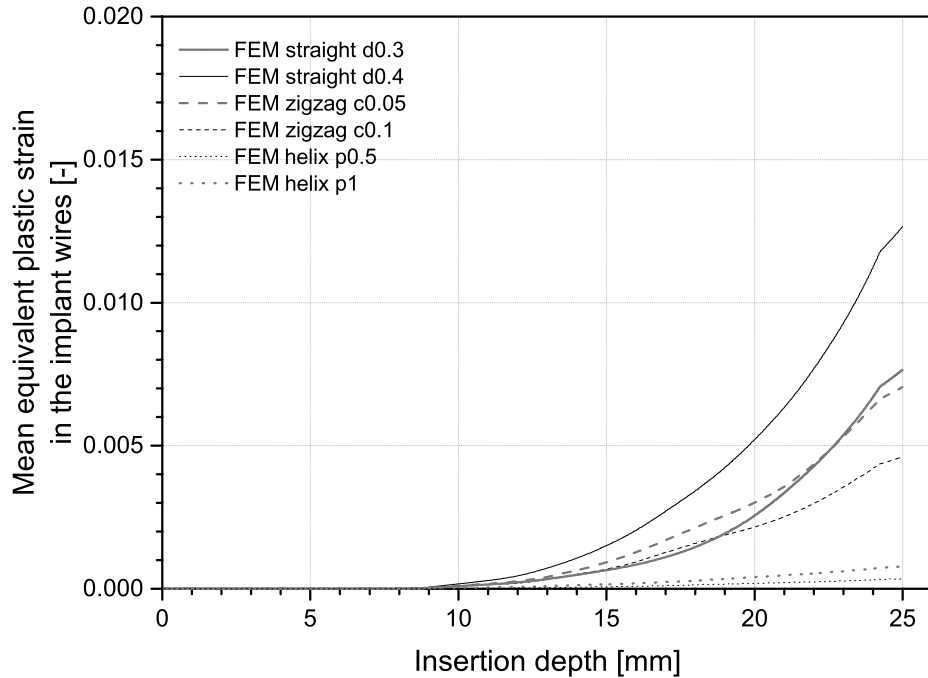


Figure 5.7: Mean equivalent plastic strain (PEEK) in the implant wires during the cochlear implantation among the different wires configurations.

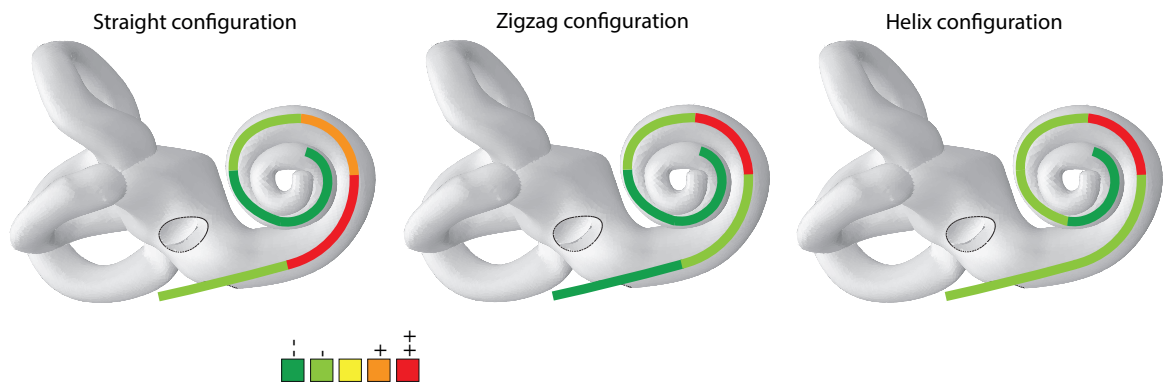


Figure 5.8: Incidence rate of the location of the maximum PEEK in the implant wires during the cochlear implantation among the different wires configurations.

## 5.6 Conclusions

The work developed allowed to evaluate the insertion force, the contact pressure during an electrode array insertion and, the plastic deformation in the electrode array

wires, in six different wires configurations. The helix wire configuration showed to be less aggressive with the lowest insertion force. Also, this configuration provides lower plastic deformation in the platinum/iridium wires and lower mean contact pressure at the distal and proximal portions of the electrode array. The  $d$ -parameter shown that when the wires arrangement are close to the nucleus of the electrode array, there is a decrease in the insertion force, facilitating the electrode insertion.

It is necessary to continue the search for less invasive electrodes, preserving the patient's residual hearing. The model developed has some limitations, including the lack of contacts in the platinum wires and the three scalae were reduced to one. A more realistic 3D finite element model will allow to study and, for example, to reduce basilar perforations.

## 5.7 Conflict of interest statement

The authors declare that there is no financial, professional or other personal interest of any nature or kind in any product, service and/or company that could be constructed as influencing the position.

## 5.8 Acknowledgements

The authors truly acknowledge the funding provided by Ministério da Ciência, Tecnologia e Ensino Superior - Fundação para a Ciência e a Tecnologia (Portugal), under grant: SFRH/BD/129397/2017. This research was also supported by the Portuguese Foundation of Science and Technology under the research project UIDB/50022/2020.



## 5.9 References

- [1] WHO. *Global estimates on prevalence of hearing loss*, 2018 (accessed January 5, 2021). Available at <http://www.who.int/deafness/Global-estimates-on-prevalence-of-hearing-loss-Jul2018.pptx>.
- [2] L. E. Jorgensen, E. A. Benson, and R. W. McCreery. Conventional amplification for children and adults with severe-to-profound hearing loss. *Semin Hear*, 39(4):364–376, 2018.
- [3] A. Ishiyama, F. Risi, and P. Boyd. Potential insertion complications with cochlear implant electrodes. *Cochlear Implants Int*, 21(4):206–219, 2020.
- [4] G. B. Wanna, J. H. Noble, M. L. Carlson, R. H. Gifford, M. S. Dietrich, D. S. Haynes, B. M. Dawant, and R. F. Labadie. Impact of electrode design and surgical approach on scalar location and cochlear implant outcomes. *Laryngoscope*, 124 Suppl 6:S1–7, 2014.
- [5] T. Stover and T. Lenarz. Biomaterials in cochlear implants. *GMS Curr Top Otorhinolaryngol Head Neck Surg*, 8:Doc10, 2009.
- [6] Y. S. Lim, S. I. Park, Y. H. Kim, S. H. Oh, and S. J. Kim. Three-dimensional analysis of electrode behavior in a human cochlear model. *Medical Engineering & Physics*, 27(8):695–703, 2005.
- [7] *Cochlear Limited*, 2019 (accessed February 10, 2021). Available at <https://www.cochlear.com/us/en/professionals/products/cochlear-implants/surgery/surgical-guides>.

- [8] *Granta EduPack 2020*. Granta Design Limited 2020, 2020.
- [9] Jürgen Merker, David Lupton, Michael Topfer, and Harald Knake. High temperature mechanical properties of the platinum group metals: Elastic properties of platinum, rhodium and iridium and their alloys at high temperatures. *Platinum Met. Rev.*, 45, 2001.
- [10] H. N. Kha, B. K. Chen, G. M. Clark, and R. Jones. Stiffness properties for nucleus standard straight and contour electrode arrays. *Medical Engineering & Physics*, 26(8):677–685, 2004.
- [11] Dassault Systemes. *ABAQUS analysis user's guide*. 2016.

## Chapter 6

# Thesis considerations



## 6.1 Conclusions

Hearing loss is considered a significant disability, affecting communication and impacting quality of life. The main causes of sensorineural hearing loss are the degenerative processes associated with aging, noise exposure, genetic mutations, among others. Treatments for hearing loss depends of the etiology and severity, however, it consists largely in amplification devices, which do not correct the damage of the auditory system, but help overcome the hearing loss. Patients with severe or profound sensorineural hearing loss do not typically benefit from hearing aids, since the hair cells are not able to stimulate the auditory nerve in response to an external stimuli. In these cases, cochlear implants, that bypass the hair cells to electrically stimulate the auditory nerve, permit partial restoration of hearing, improving the speech perception and the vocational, social, and psychological functioning. However, these devices need to be surgically implanted and require an auditory rehabilitation program that includes auditory training sessions.

In the context of the work developed, the first contribution shows that both the straight and spiral FEM provides a good definition of the cochlear mapping when the BM was considered with transversely isotropic properties. However the 3D model has some limitations such as, the use of an inviscid fluid and the non consideration of the scala media and the Reissner's membrane.

The second contribution studies the consequences of endolymphatic hydrops in the normal hearing, caused by a disorder of the inner ear that is characterized by a set of unpleasant and painful symptoms, the Ménière's disease. This disease affects the dynamic behaviour of the BM, but not equally along its length, thus representing a higher hearing loss at specific audible frequencies. Our FEM shows

that the endolymphatic hydrops affects mainly the lower frequencies. As expected, the static pressure leads to greater deformations near the apex of the cochlea, where the BM stiffness is lower.

In the third contribution, the influence of the insertion speed, the friction coefficient between the cochlear wall and the electrode array, and several configurations of the cochlear implant tip were studied. The insertion force and contact pressure between the electrode tip and the cochlear wall can influence the intra-cochlear damage and the preservation of the residual hearing. The results showed that lower speeds result in lower contact pressures at the implant tip. An abrupt decrease of the mean contact pressure and insertion force with a friction coefficient ( $\mu$ ) of 0.3 was obtained, thus showing a buckling of the electrode array. With respect to the study of the cochlear implant tip mechanical properties, a decrease in the mean contact pressure was obtained with lower Young's modulus.

The fourth contribution investigates three different arrangements in the platinum/iridium wires within the electrode array. Each configuration was designed with one parameter which was also studied. The results showed that the spiral configuration provides the lowest insertion force, probably minimizing the intra-cochlear damage during its insertion.

In conclusion to the thesis, the proposed aims and challenges were successfully achieved, leading to a knowledge improvement in the cochlear field.

## 6.2 Future works

The results in this thesis provides a strong foundation for future work in the cochlear field. This section briefly describes some interesting research topics, which

are worth investigating further. These points are elaborated below.

- The inclusion of the organ of Corti in the 3D FEM will allow to study the relative motion between the tectorial membrane and BM. Indeed, such displacement causes the deflection of the stereocilia and the modulation of the open probability of their transduction channels;
- The outer hair cells amplify the sound-induced vibrations in the mammalian inner ear through an active process. In conjunction with the first point, a detailed 3D FEM allows to simulate the active process and the consequences of the damage in each row of outer hair cells. Damaged outer hair cells leads to hearing loss, this point pretends to develop a direct relation between the source and consequence of this impairment;
- Develop an experimental work in order to study the cochlear implant insertion process. It would therefore be possible to validate the numeric model developed; Among the complications associated with the insertion of cochlear implants, the damage of the cochlea's internal tissues resulting from the cochlear implant insertion is one of the most relevant complication which should be minimised, in order to maintain the patient's residual hearing;
- Other types of cochlear implants are available on the market. A relevant work would be based on the comparison between the straight and perimodiolar electrodes, in order to find the least aggressive.





# Appendix A



## 6.3 Permission 1

### Autorização de compilação

Marco Paulo Lages Parente, Maria Fernanda Gentil Costa e Renato Manuel Natal Jorge na qualidade de co-autores do artigo "*Influence of the basilar membrane shape and mechanical properties in the cochlear response: a numerical study*" publicado na revista *Part H: Journal of Engineering in Medicine*, declaram que aceitam a inclusão do mesmo na tese de doutoramento do candidato Bruno André Faria Areias intitulada "*Numerical modelling of the human inner ear: associated pathologies and therapies*".

Porto, 19 de Julho de 2021



---

Marco Paulo Lages Parente



---

Maria Fernanda Gentil Costa



---

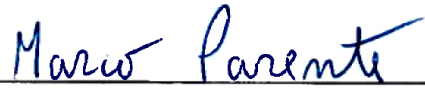
Renato Manuel Natal Jorge

## 6.4 Permission 2

### Autorização de compilação

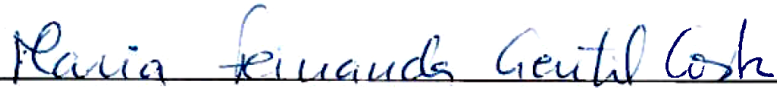
Marco Paulo Lages Parente, Maria Fernanda Gentil Costa, Cristina Maria de Paiva Chaves Lopes Carocha Tomé de Jesus, João Carlos Lopes Simões Paço e Renato Manuel Natal Jorge na qualidade de co-autores do artigo "*A finite element model to predict the consequences of endolymphatic hydrops in the basilar membrane*" publicado na revista *International Journal for Numerical Methods in Biomedical Engineering*, declaram que aceitam a inclusão do mesmo na tese de doutoramento do candidato Bruno André Faria Areias intitulada "*Numerical modelling of the human inner ear: associated pathologies and therapies*".

Porto, 19 de Julho de 2021



---

Marco Paulo Lages Parente



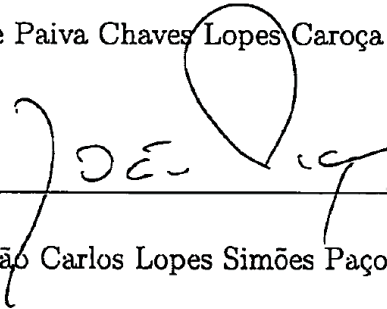
---

Maria Fernanda Gentil Costa



---

Cristina Maria de Paiva Chaves Lopes Caroça Tomé de Jesus



---

João Carlos Lopes Simões Paço



---

Renato Manuel Natal Jorge

## 6.5 Permission 3

### Autorização de compilação

Marco Paulo Lages Parente, Maria Fernanda Gentil Costa e Renato Manuel Natal Jorge na qualidade de co-autores do artigo "*Finite element modelling of the surgical procedure for placement of a straight electrode array: mechanical and clinical consequences*" publicado na revista *Journal of Biomechanics*, declaram que aceitam a inclusão do mesmo na tese de doutoramento do candidato Bruno André Faria Areias intitulada "*Numerical modelling of the human inner ear: associated pathologies and therapies*".

Porto, 19 de Julho de 2021



---

Marco Paulo Lages Parente



---

Maria Fernanda Gentil Costa



---

Renato Manuel Natal Jorge



## 6.6 Permission 4

### Autorização de compilação

Marco Paulo Lages Parente, Maria Fernanda Gentil Costa e Renato Manuel Natal Jorge na qualidade de co-autores do artigo "*Insertion of a cochlear straight electrode array with different wires arrangements: a numerical study*" submetido em uma revista internacional, declaram que aceitam a inclusão do mesmo na tese de doutoramento do candidato Bruno André Faria Areias intitulada "*Numerical modelling of the human inner ear: associated pathologies and therapies*".

Porto, 19 de Julho de 2021



---

Marco Paulo Lages Parente



---

Maria Fernanda Gentil Costa



---

Renato Manuel Natal Jorge

